Charles University in Prague
Faculty of Mathematics and Physics

DOCTORAL THESIS

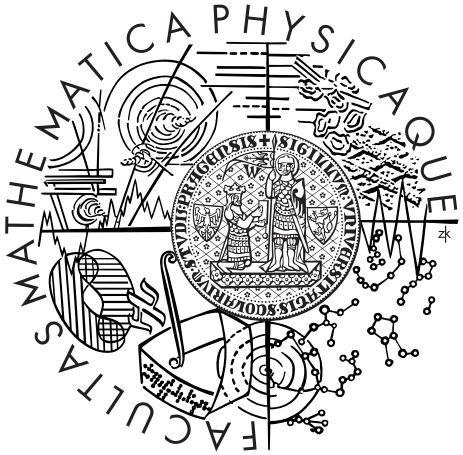

Miroslav Frost

Modeling of phase transformations in shape memory materials

Mathematical Institute of Charles University

Supervisor of the doctoral thesis:	Prof. Ing. František Maršík, DrSc.
Study programme:	Physics
Specialization:	Mathematical and Computer Modelling

Prague 2012

I would like to thank my supervisor, prof. Ing. František Maršík, DrSc., for his help and support throughout my Ph.D. study.

I wish to thank my colleague Ing. Petr Sedlák, Ph.D., who has continuously encouraged, motivated and supported me at that time. I am obliged to him and also to Mgr. Barbora Benešová, Ph.D., for their helpful and inspiring comments on the manuscript of this thesis.

I wish to thank them and all other colleagues at LUM (IT ASCR, Prague) for a friendly and enjoyable atmosphere and for many inspiring discussions. I thank colleagues in DFM (IP ASCR, Prague) for sharing their knowledge of shape memory alloys with me.

My thanks also belong to prof. Tarak Ben Zineb for his helpful advise on the numerical implementation of the model. I thank dr. Boris Piotrowski, who has helped me to utilize the computational cluster. I wish to thank them and other members of LEMTA (UL Nancy) and LEM3 (UL Metz) that I met during my research stay in France in 2010 for the very pleasant time I spent there.

I wish to express my deep gratitude to my family and Eva; this thesis would not have been possible without their constant support, love and understanding.

This work was performed as an activity within the Nečas center LC06052 (MŠMT) and was supported through the grant No. 41110 (GAUK ČR). The support of the New Technologies – Research Center in Plzeň is also acknowledged: this work was developed within the CENTEM project, Reg. No. CZ.1.05/2.1.00/03.0088, that is co-founded from the ERDF within the OP RDI programme of the Ministry of Education, Youth and Sports and was partly supported by the Czech Science Foundation through the project No. 201/10/0357.

I declare that I carried out this doctoral thesis independently, and only with the cited sources, literature and other professional sources.

I understand that my work relates to the rights and obligations under the Act No. 121/2000 Coll., the Copyright Act, as amended, in particular the fact that the Charles University in Prague has the right to conclude a license agreement on the use of this work as a school work pursuant to Section 60 paragraph 1 of the Copyright Act.

In Prague, October 17, 2012 Miroslav Frost

Název práce: Modelování fázových transformací v metriálech s tvarovou pamětí
Autor: Miroslav Frost
Katedra: Matematický ústav Univerzity Karlovy
Vedoucí disertační práce: Prof. Ing. František Maršík, DrSc., Matematický ústav Univerzity Karlovy
Abstrakt: Disertační práce představuje nový termomechanický třídimenzionální konstitutivní model slitin s tvarovou pamětí založených na NiTi. Model byl formulován v rámci konceptu tzv. zobecněných standardních modelů a vyznačuje se novou formu dissipační funkce, která kombinuje příspěvek fázové transformace mezi austenitem a martenzitem a příspěvek reorientace martenzitu. V modelu jsou také zachyceny jevy spojené s fázovým přechodem mezi austenitem a R-fází, materiálová anizotropie a asymetrie odezvy v tahu a tlaku. Evoluční úloha kvazistatického mechanického zatěžování tělesa z NiTi s předepsaným vývojem teploty byla formulována a analyzována v rámci konceptu tzv. energetických řešení. Minimalizační problém odvozený z časové diskretizace motivoval postup použitý při numerickém řešení problému. Konstitutivní model byl následně implementován do konečněprvkového prostředí Abaqus. Bylo provedeno několik numerických simulací, které byly porovnány s experimenty.
Klíčová slova: slitiny s tvarovou pamětí, konstitutivní model, zobecněné standardní modely, martenzitická fázová transformace

Title: Modeling of phase transformations in shape memory materials
Author: Miroslav Frost
Department: Mathematical Institute of Charles University
Supervisor: Prof. Ing. František Maršík, DrSc., Mathematical Institute of Charles University
Abstract: This thesis presents a new thermomechanical three-dimensional constitutive model of NiTi-based shape memory alloys. The model was formulated within the framework of generalised standard models and it features a novel form of the dissipation function, which combines contributions stemming from the phase transformation between austenite and martensite and from the reorientation of martensite. The change in the material response associated with the phase transformation between austenite and R-phase as well as material anisotropy and tension-compression asymmetry are also covered. The time-evolutionary problem of a quasistatic mechanical loading of a NiTi body with prescribed temperature evolution was formulated and analyzed within the framework of energetic solutions. The corresponding time-incremental minimization problem provided a conceptual algorithm utilized in the numerical treatment. The constitutive model was implemented into the finite element package Abaqus. Several numerical simulations were performed and compared with experiments.
Keywords: shape memory alloys, constitutive model, generalized standard models, martensitic phase transformation

Contents

Preface

Shape memory alloys (SMA) are metallic materials exhibiting unusual properties of being able to sustain and recover large strains and to "remember" the initial configuration and return to it with temperature change. These properties arise from a rearrangement of the crystal lattice associated with the so-called martensitic phase transformation, which can be induced by variation of temperature and/or variation of the applied mechanical load. Moreover, specific types of internal structure of the martensitic phase can develop depending on the loading conditions. These phenomena give rise to a very complex thermomechanical behavior, which classifies SMA into the group of so-called smart materials and makes them attractive for utilization in applications. Many products made of SMA polycrystals are already used or developed; they can be found, for instance, in aerospace industry (e.g. self-erecting space antennae, helicopter blades), in medicine (e.g. surgical tools, reinforcement for arteries and veins), in automotive industry (e.g. mirror actuators), in civil engineering (e.g. tightening rings, seismic dampers), in textile industry (adaptive textiles), or as devices of the everyday life (e.g. thermostatic valves, thermal switches), etc. For reliable performance of such products, a proper post-processing treatment and design is essential.

If computational models are employed in the process of products development and testing, they can substantially reduce costs and time. Commercially available finite element packages are particularly suitable for simulations of whole products with complex geometries. However, constitutive models provided by them cover only a limited number of types of materials. Particularly, none of them is designed for simulations of SMA under *complex* thermomechanical loading conditions.

A number of macroscopic constitutive models was proposed in literature to fill this gap. Performance of several of them was compared within a unique activity called "Roundrobin SMA modeling". Assessment of the results revealed that there exist particular phenomena which are still not satisfactorily covered in these models when they are applied to the NiTi alloy. Here should be emphasized that the most commercially successful types of SMA are based on this alloy.

First, pronounced imperfections were identified in simulations of the response of the material during a general (non-proportional) thermomechanical loading involving phase transformation and deformation in martensite. Since multiple deformation mechanisms come into play, their interaction leads to a "puzzling" behavior very sensitive to changes in loading conditions. Another troublesome phenomena is the presence of the so-called R-phase, which is actually another phase occurring specifically in NiTi-based SMA. If it is neglected, substantial deviations of predicted thermal and mechanical response from reality occur. Last but not least, influence of the anisotropy associated with strong texture was stressed. Texture is induced in the materials during processing and it is inherited

by final industrial products, thus, it must be inevitably considered when realistic simulations of such products are to be performed.

All these findings have highlighted a need for development of a computational model which would be tailored for polycrystalline NiTi-based SMA and which would be easily implementable into a finite element package. Naturally, *thermodynamical consistency* and *mathematical rigor* are essential requirements for such a model. However, practical reasons impose further, often contradictory demands on its form. On the one hand, the constitutive model should be simple enough to be *effective*, on the other hand it should be accurate enough in *reflecting the key physical phenomena* to reliably predict response of SMA in various operation modes. The *number of input parameters* should be *minimized* in order to facilitate the experimental effort prior to simulations, but the model should still provide freedom for *adaptation to the properties of the material* which can differ due to variation in composition or processing. Last but not least, the numerical implementation of the model should provide *fast computational response*, thus being time-effective, still it should be *reliable* from the point of view of numerical stability and robustness.

Development of a computational model capable to deal with the sketched obstacles became a challenge for the modeling community and the main motivation for this work.

Aims of the thesis

Reflecting the motivation above, the particular aims of this thesis are formulated as follows:

- To formulate a three-dimensional, thermodynamically consistent, rate-independent constitutive model for NiTi-based SMA which covers both the common shape memory effects and also the two-stage phase transformation with intermediate R-phase, anisotropy of transformation properties due to texture and tension-compression asymmetry.
- To express the general problem of a quasistatic mechanical loading of a NiTi-based SMA body with prescribed temperature evolution as a mathematical time-evolutionary problem within a suitable framework and establish properties of its solutions.
- To develop a ready-to-use software suitable for implementation into commercially available finite element package taking the results of mathematical analysis into account. The implementation should allow for easy modification of input the parameters in order to adjust the model to any particular NiTi-based alloy.

Overview of the thesis

Let us briefly characterize the main parts of this thesis:

Chapter 1 In the first chapter, we introduce the shape memory effects and their roots at the microscopic level – martensitic phase transformation and

reorientation. Furthermore, based on a review of experimental findings on NiTi-based SMA polycrystals, we identify the key phenomena which should be covered in the constitutive model.

Chapter 2 We present the concept of so-called generalized standard models (GSM), which provides a suitable framework for a systematic development of constitutive models within continuum thermodynamics. If the described approach is followed, it assures thermodynamical consistency of the model (the second law of thermodynamics is automatically satisfied), albeit providing enough freedom for proposing novel types of models.

Chapter 3 The chapter exposes the state of the art in the field of macroscopic modeling of SMA polycrystals. It provides an overview of some tools and approaches utilized so far and helps to identify the most successful and effective of them.

Chapter 4 In the crucial part of the thesis, we finally develop the constitutive model by defining the Helmholtz free energy and dissipation functions as required by GSM. A novel form of the dissipation function is formulated based on a careful analysis of experimentally determined phase diagrams. An alternative approach for derivation of dissipation function, which is based on a set of modeling assumptions, is also presented. Let us note that the chapter is mostly based on results already published in (Sedlák et al., 2012).

Chapter 5 We utilize the mathematical concept of energetic solutions to analyze the time-evolutionary problem of quasistatic mechanical loading of a NiTi SMA body with prescribed temperature evolution. Existence of solutions to the constitutive model is established in several steps imposing only natural restrictions on basic physical parameters of the model, which makes the model rather appealing from the experimental point of view. Due to the temperature dependence of the dissipation function, a slight modification of the approach presented in (Francfort and Mielke, 2006) is needed. The approach also provides a conceptual algorithm for numerical treatment of the model in a form of a constrained minimization problem.

Chapter 6 The last chapter of the thesis deals with the numerical implementation of the model into the finite element package Abaqus. A script written in C++ programming language solves a part of the aforementioned constrained minimization problem by the Nelder-Mead minimization method and establishes a transfer of the results to the main program, where the the solving procedure is completed. A comparison of experimental and simulated results of the "Roundrobin SMA modeling" activity show exceptionally good agreement confirming predictive abilities of the proposed model. Let us note that this chapter is also mostly based on results published in (Sedlák et al., 2012).

Conclusions We summarize the main achievements of the thesis.

Appendix A In the Appendix, a short overview of basic concepts of convex analysis can be found.

Overview of further activities related to this thesis

The present work originates in development of a constitutive model applicable for simulations of NiTi wires. Their thermomechanical behavior in applications as intervascular stents, adaptive textiles or actuating elements embedded in composites is under study within a long-term extensive research on SMA conducted at the Institute of Physics and the Institute of Thermodynamics of the Czech Academy of Science.

Initially, a one-dimensional phenomenological constitutive model was formulated. It covered the full two-stage phase transformation sequence between austenite, R-phase and reorientation of martensite. It addressed particular type of hierarchical hysteretic behavior and captured also the non-linear hyperelastic response observed in experiments. Differences in properties of the material in tension and compression reflected in the model allowed to apply it also to simple planar wire-structures deformed in bending. Such an approach was utilized in simulations of deformation of microhooks employed in SMA fasteners published in (Vokoun et al., 2009, 2011). The model itself was published in the work (Frost et al., 2010).

Analysis of the extensive set of experimental data obtained within 'Roundrobin SMA modeling" activity has motivated a simple extension of the concept to combined tension-torsion type of loading. Simulations of the experiments revealed a significant influence of the texture on the thermomechanical response, since it gives rise to anisotropy of some material properties. This was reflected in the modified model and described in papers (Frost and Sedlák, 2009; Sedlák and Frost, 2009).

In addition, practical experience acquired when martensite stabilization effect was studied by means of thermal and mechanical experiments was useful for considerations in the present stage of modeling. The results were published in (Frost and Rudajevová, 2009).

List of publications

- Sedlák, P., Frost, M. (2009), *Two-dimensional thermomechanical model for combined loading of NiTi wire structures*, in Proceeding of ASME 2009 Conference on Smart Materials, Adaptive Structures and Intelligent Systems, **1**, 101–109.

- Frost, M., Sedlák, P. (2009), *Modeling of Two-dimensional Thermomechanical Loading of NiTi Wires* in ESOMAT 2009 - The 8th European Symposium on Martensitic Transformations, 08002, edited by P. Šittner, L. Heller and V. Paidar, EDP Sciences

- Vokoun, D., Majtás, M., Frost, M., Sedlák, P., Šittner, P. (2009), *Shape memory hooks employed in fasteners*, J. Mater. Eng. Perform. **18**, 706–710.

- Frost, M., Rudajevová, A. (2009), *Strain release from pre-deformed* $Ni_{53.6}Mn_{27.1}Ga_{19.3}$ *shape memory alloy during thermal cycle*, Int. J. Mater. Res. **6**, 898–900.

- Frost, M., Sedlák, P., Sippola, M., Šittner, P. (2010), *Thermomechanical model for NiTi shape memory wires*, Smart. Mater. Struct. **19**, 094010.

- Vokoun, D., Sedlák, P., Frost, M., Pilch, J., Majtás, D., Šittner, P. (2011), *Velcro-like fasteners based on NiTi micro-hook arrays*, Smart. Mater. Struct. **20**, 085027.

- Sedlák, P., Frost, M., Benešová, B., Ben Zineb, T., Šittner, P. (2012), *Thermomechanical model for NiTi-based shape memory alloys including R-phase and material anisotropy under multi-axial loadings*, Int. J. Plast., **39**, 132–151.

Chapter 1

Introduction to Shape Memory Alloys

Intermetallic alloys exhibiting the unique shape memory effects (e.g. superelasticity, one-way shape memory effect) are known as shape memory alloys (SMA). Although these effects were firstly observed at AuCd alloy in 1951, the research has intensified after 1963, when the commercially most successful NiTi shape memory alloys were discovered (Otsuka and Wayman, 1998). In this section, we will briefly introduce martensitic phase transformation, which is the key physical phenomenon for SMA, describe the basic shape memory effects and provide more details for NiTi-based SMA, the particular type of SMA on which this work focuses.

1.1 Martensitic phase transformation

The key physical process for understanding of all shape memory effects is the *martensitic phase transformation* (MT): a first-order solid-to-solid phase transition from the parent phase, which is referred to as *austenite*, to the less-ordered product phase, *martensite*. The mechanism of this type of transformation consists of a regular rearrangement of the crystal lattice in such a way that relative displacement of neighboring atoms does not exceed the interatomic distances and the atoms do not interchange places. This "shearing of the parent lattice into the product" is sometimes referred as *lattice-distortive* transformation.[1]

In general, MT is *diffusionless* and *athermal*, i.e. the amount of martensite formed during cooling is a function only of temperature and not of length of time at which the alloy is held at that temperature. Furthermore, MT is *thermoelastic* phase transformation in the case of SMA, which indicates that (Otsuka and Ren, 2005):

i. the thermodynamic driving force for the phase transformation is rather small, which prevents introduction of irreversible process such as slip,

ii. phase boundaries are very mobile and their motion is reversible,

[1] Let us recall that the first-order phase transitions exhibit a discontinuity in the first derivative of the thermodynamic potential with respect to the thermodynamic variable, e.g. a discontinuity in strain, in entropy, etc.

iii. the product phase stays coherent with the parent phase,

iv. the group of symmetry of the product phase is a sub-group of the group of symmetry of the parent phase.

Thus, in an ideal case, the transformation as a crystal lattice distortion is fully reversible.

MT in SMA can be initiated and driven either by change of temperature, either by change of external stresses or by simultaneous change of stresses and temperature. Usually, the transformation is nucleated heterogeneously by formation of thin plates of parent/product phase in the matrix of product/parent phase forming a two-phase austenite-martensite zone. If there is no "preferred direction", martensite forms in a series of crystallographically equivalent variants. The product phase growing into a platelet shape is then termed *twinned* or *self-accommodated martensite* and is characterized by a twinned microstructure, which minimizes the misfit between the martensite and surrounding austenite. On the other hand, if there is a "preferred direction", e.g. imposed by stress, growing martensite tends to be formed into the favorable variant(s) with respect to the external condition. The product phase is then termed *detwinned* or *fully oriented martensite*. See (Bhattacharya, 2003) for details.

Microstructure observation reveals (Liu et al., 1999), that several types of structure rearrangement may be involved in evolution of martensite under applied stress. All such processes are related to existence of twins within the material and all of them contribute to change of the total strain of the specimen. Since this work focuses on description on the macroscopic scale, if there is no special concern in distinguishing between them, all such microstructural processes will be referred to as *reorientation of martensite* and the correspondig structure will be termed *reoriented martensite*, hereinafter.

Let us emphasise that, apart from the thermoelastic nature of MT, twinning as a deformation mode of martensite is a necessary condition for shape memory effects to occur. In fact, strain attained by twinning/detwinning is easily recovered upon the reverse transformation which makes the shape memory effects possible (see the next section).

As briefly sketched, crystallographic considerations play a key role in understanding of MT and martensite structure evolution at the microstructural scale. Mathematical theories allowing rigorous determination of twinning modes or conditions of compatibility for a phase interface in single crystals have been presented in (e.g. Ball and James, 1987; Bhattacharya, 2003).

As experimentally observed, MT and martensitic structure evolution are accompanied by a dissipation of energy, which gives rise to *hysteretic properties* of SMA. For instance, due to dissipation, the temperature of the forward phase transformation (austenite to martensite) is different from the temperature of the reverse one. The essential contributions to dissipation are associated with interfacial friction, defect production and acoustic emission caused by nucleation and growth of martensite structure and interaction of interface with defects during transformation and reorientation (Bekker and Brinson, 1997; Sun and Li, 2002). Generally, several dissipative mechanisms can operate at different time (intrinsic relaxation time scale, the time scale of external loading) and length scales (interface thickness, grain size, sample dimension) and contribute to macroscopic

hysteresis of a real polycrystalline SMA material (see e.g. Ortín and Delaey, 2002; Petryk and Stupkiewicz, 2010; Sun and He, 2008).[2]

1.2 Shape memory effects

Nowadays, SMA applications are already used or developed in aerospace industry (Hartl et al., 2009) (e.g. self-erecting space antennae, helicopter blades), in automotive industry (Williams and Elahinia, 2008)(e.g. mirror actuators), in medicine (Machado and Savi, 2003) (e.g. surgical tools, reinforcement for arteries and veins), in civil engineering (Wilson and Wesolowsky, 2005) (e.g. self-locking valves, seismic dampers), or as devices of the everyday life (Otsuka and Wayman, 1998)(e.g. thermostatic valves, thermal switches), etc. These applications make profit from the unique properties of SMA, sometimes generally called shape memory effects.

To briefly introduce them, let us restrict ourselves to combined thermal and mechanical loading in one dimension. In that case, the *generic* stress-strain response of a polycrystal is, at least from the macroscopic point of view, very similar to the one of a single crystal. The initiation and propagation of a phase boundary and formation and evolution of internal martensitic structure in a single crystal have been very well experimentally examined (Ball et al., 2011) and theoretical explanation of the basic shape memory effects is generally accepted (Otsuka and Ren, 2005). However, the issue is much more complex in *polycrystal specimens* because of mutual interaction between phase interfaces, martensitic variants, grain boundaries and other crystallographic defects, and the situation is "far from being fully understood and quantified" (Sun and Li, 2002). Thus, for easier understanding of the microstructural background of observed polycrystalline sample response, the single crystal terminology is often adopted. We will follow that approach keeping the aforementioned applicability limitations in mind.

In the range of mechanical loading frequencies, where the isothermality assumption is valid, SMA behave in a *rate-independent* manner (Sadjadpour and Bhattacharya, 2007*b*). Indeed, based on set of sophisticated experiments performed for complex loading paths and complex NiTi SMA specimen geometries, Grabe and Bruhns (2008) confirmed that "the material shows no strain rate dependence within the regime of quasi-static processes". Evolution of stress for strain loading at various strain rates coincided under isothermal conditions in their experiments and different, rate-dependent responses reported by some authors, e.g. (Nemat-Nasser et al., 2005), were attributed to temperature effects[3], which are absent for isothermal tests. Throughout this work we will strictly adhere to the assumption of rate-independence of isothermal response of SMA

[2] An interesting property of hysteresis in SMAs is so-called *return point memory (or property)*. After a cyclic variation of the driving, the system follows exactly the same trajectory that it would have followed if the cyclic variation had not taken place. In this way, a hierarchy of "subloops" within hysteretic loops may be formed. This feature was studied and discussed in author's previous works (Frost, 2007; Frost et al., 2010).

[3] If latent heat of a phase transformation is not absorbed by environment completely, it increases temperature of a specimen, which then conversely changes transformation conditions within the specimen.

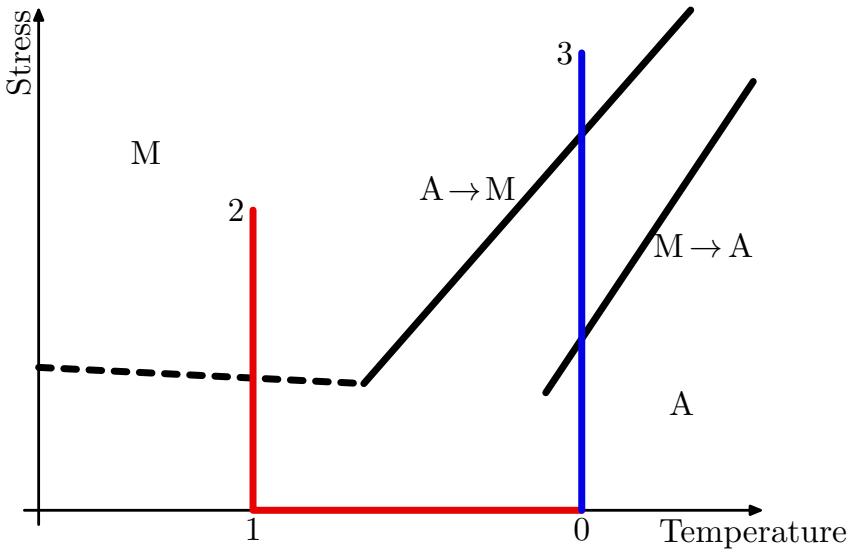

Figure 1.1: A simplified generic stress-temperature phase diagram of SMA. See text for details.

and, particularly, results of all experiments introduced here are supposed to be rate-independent, too.

The phase space parameterized by stress and temperature is commonly used to introduce shape memory effects. A generic form of such a diagram is depicted in Fig. 1.1. Regions of austenite and martensite denoted by A and M, respectively. Full black lines mark increasing dependence of stress needed for initialisation of forward and reverse phase transformation on temperature (stress induced transformation at constant temperature), so-called *phase boundaries*. Approximate linearity of this dependence is related to the Clausius-Clapeyron relationship (see below). Dashed line marks stress level at intensive reorientation initiates when martensite is loaded at constant temperature.

Depending upon the path within the phase diagram, various types of response is observed. If austenite is cooled to low enough temperature at zero applied stress (path $0 \rightarrow 1$ in Fig. 1.1), austenite transforms into martensite with zero net macroscopic shape change of the specimen (neglecting thermal expansion) since emerging variants of martensite tend to average the overall deformation to zero by formation of a twinned microstructure. If the material is subsequently mechanically stressed (path $1 \rightarrow 2$), the twinned microstructure will reorient into an arrangement which is preferred by the direction of applied loading. This process is manifested by a plateau-like response in stress-strain dependence. However, based on microstructural observations in NiTi polycrystals, Liu et al. (1999) pointed out that martensite structure reorientation may start even before the onset of this plateau, i.e. during the initial stage of deformation. Upon removal of the mechanical load (path $2 \rightarrow 1$), a permanent deformation is retained in the specimen. This is usually called *pseudoplasticity* or *quasiplasticity*.

If the material is now heated above a particular temperature (path $1 \rightarrow 0$), it completely reverts to austenite and fully recovers its original shape. The whole cycle is the so-called *one-way shape memory effect*, see the red curve in Fig. 1.2.

When the specimen is kept at a temperature at which austenite is a stable phase under stress-free condition and then loaded mechanically above a certain

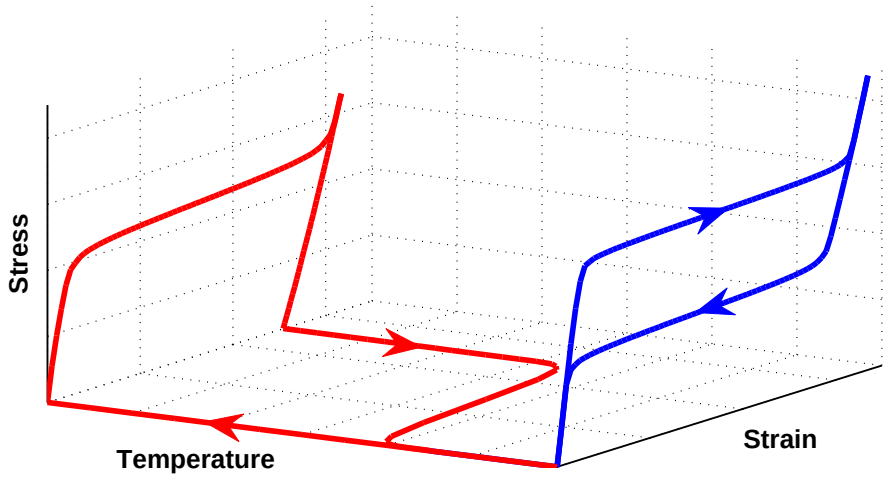

Figure 1.2: A simplified generic stress-strain-temperature phase diagram of SMA. See text for details.

critical stress level (path $0 \rightarrow 3$), austenite starts to transform into martensite. With respect to the direction of loading, a large macroscopic strain, so-called *transformation strain*, is induced. It originates in lattice deformation due to formation of reoriented martensite in the material and leads to a plateau in stress-strain response. The dependence of the critical stress inducing the phase transformation on temperature may be determined with the Clausius-Clapeyron-type equation in a very good approximation. In one-dimensional setting, it has the form:

$$\frac{\mathrm{d}\sigma}{\mathrm{d}T} = \frac{\Delta s^{AM}}{\varepsilon^{\mathrm{tr}}} = \frac{h}{T\varepsilon^{\mathrm{tr}}}, \tag{1.1}$$

where σ denotes (one-dimensional) stress, T is temperature, Δs^{AM} denotes specific entropy change per unit volume due to phase transition, $\varepsilon^{\mathrm{tr}}$ is the transformation strain in the loading direction and transformation latent heat is denoted $h := T\Delta s^{AM}$. When the entropy change and transformation strain are assumed to be temperature independent, then relation between the critical stress and temperature is linear. However, more general considerations may be done, see e.g. (Frost, 2007; Liu et al., 2008).

Now, if the mechanical load is removed in a reverse process (path $3 \rightarrow 0$), the strain of the specimen is recovered, since martensite is not stable at low stress and high temperatures and it transforms back into austenite. Typically, this type of process is called *superelasticity* (or *pseudoelasticity*), since the behavior is similar to elasticity—the material returns to its initial configuration upon removal of the loading, see the blue curve in Fig. 1.2.

Although Clausius-Clapeyron relation predicts the same slope of the phase boundary both for forward and reverse phase transformation, it is often not the case in experiments (see e.g. Shaw and Kyriakides, 1995, or results in Section 6.4). As stated by Lagoudas et al. (2012), different dissipation could be associated with transformation induced at different stress and temperature conditions. Moreover, temperature induced transformation usually occurs in a temperature

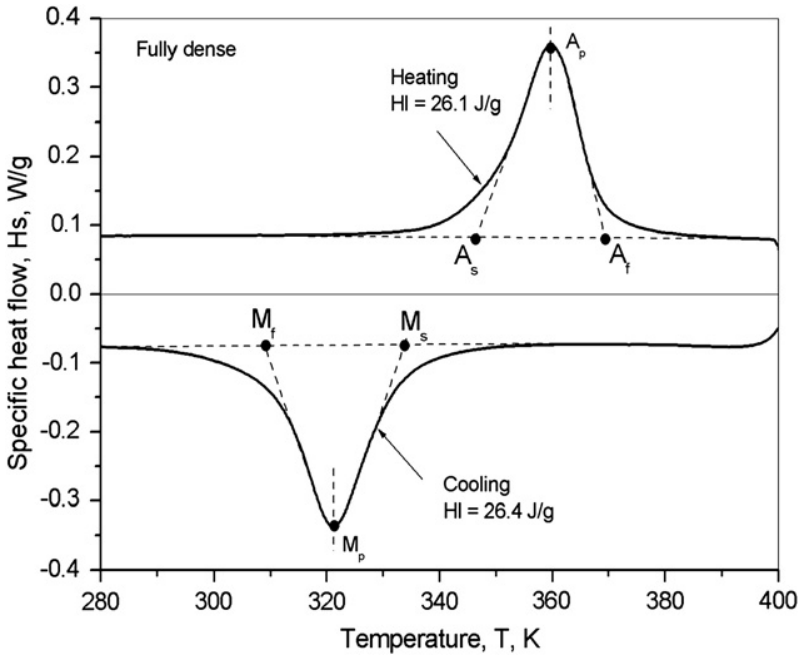

Figure 1.3: An example of determination of transformation temperatures from the measurement of the heat flow in NiTi SMA by Differential Scanning Calorimetry. (HI denotes transformation latent heat.) Reprinted from (Zanotti et al., 2010).

interval rather than in a single temperature instance. For transformation from austenite to martensite under stress-free condition, limiting temperatures between which (most of) transformation occurs are usually denoted M_s and M_f, with subscripts denoting "start" and "finish" of the process. Analogous meaning for transformation from twinned martensite to austenite have the symbols A_s and A_f. These temperatures can be determined by the Differential Scanning Calorimetry (DSC) measurements, see Fig. 1.3, where the phase transformation manifests itself by pronounced peaks.

Superelastic and pseudoplastic responses exhibit "hardening-like" effect in the sense that the plateaux are "inclined" with respect to constant stress lines as schematically sketched in Fig. 1.2. We will address this issue in Section 3.2.

Of course, more complex loading paths combining temperature and general stress states are possible which leads to a broad variety of responses combining the aforementioned types. For instance, when reoriented martensite is present in a specimen with fixed elongation, very large macroscopic stress upon heating commonly called the *recovery stress* can develop (see Šittner et al., 2000, for instance).

An interesting phenomenon called *martensite stabilization effect* has also been observed both in single crystals and in polycrystals of SMA, e.g. (Frost and Rudajevová, 2009; Liu and Favier, 2000; Liu and Tan, 2000; Piao et al., 1993). Liu and Favier (2000) systematically investigated the influence of transformation strain on the transformation behaviour of a polycrystalline NiTi sample. The sample was deformed up to different levels of deformation in martensitic state, then unloaded to a stress-free state and thermally cycled, i.e. heated and cooled to induce MT. A simple shear deformation was chosen in order to avoid localised deformation behaviour. The following phenomena were observed for deformation

up to the end of the reorientation plateau ($\sim 6\%$ strain):

1. Both the critical temperature and the endothermic heat of the first reverse transformation (i.e. transformation of deformed martensite to austenite) increased as compared to an undeformed specimen. Such behaviour may be viewed as a "stabilisation" of martensite, which is more "resistant" to induction of phase transformation.

2. With increasing deformation the shift of the reverse transformation temperature and corresponding transformation heat increased.

3. During subsequent thermal cycles, the deformed specimen was found to behave practically in the same manner as an undeformed specimen.

Although a complete explanation of the effect has not been reached yet, Liu and Favier admit that different martensitic structure induced by different deformation level may be responsible for the observed effects through its influence on both the energy stored in the specimen and the energy dissipated during the reverse transformation. They also note that the quantitative analysis seems to suggest the change in stored energy is insufficient for explanation of observed results. In this work, we will formulate a specific function determining dissipation which will be able to explain the results of the experiments not only qualitatively, but also quantitatively.[4]

Finally, let us mention so-called *two-way shape memory effect*. It is a phenomenon of spontaneous direct and backward change of the sample shape with thermal cycling in the temperature range of martensitic transformation, even if no loading or constraint are applied on the specimen. The sample then exhibits two "natural" configurations, one at low temperatures, the other at high temperatures. It is believed that dislocation arrays, retained martensite and residual stress fields are necessary to obtain some two-way shape memory effect, but the details about the internal mechanism are still not clear (Otsuka and Ren, 2005). Because of the necessity of permanent internal structure changes to occur in the material in that case two-way shape memory effect is not covered in this work.

Let us further note that since we will restrict ourselves to modeling of (ideal) thermoelastic MT within this work, process connected to plastic slip, creep, long-term cycling microstructure evolution, fatigue, etc. will be also not taken into account. Therefore, they are not described herein, even though they are also of high importance in material research on SMA.

Many alloys exhibiting shape memory effects due to MT have been discovered since 1950s. With respect to type of crystal lattice of martensite, we can distinguish SMA with tetragonal lattice (e.g. Ni_2MnGa[5], NiAl, FePt), with orthorombic lattice (e.g. AuCd, CuNiAl), with monoclinic lattice (e.g. CuAlZn, NiTi) or with rhomboedral lattice (e.g. R-phase in NiTi). Only some of these can be easily produced and manufactured and, hence, are suitable for commercial applications. Most of SMA products are based on NiTi-based alloy at the present time.

[4]We will restrict ourselves to strain levels where the influence of plastic deformation may be neglected, i.e. we will not try to explain the phenomena obtained for deformations behind the transformation plateau in (Liu and Favier, 2000).

[5]Recent results by Straka et al. (2011) indicate that this alloy could have the monoclinic lattice.

1.3 NiTi-based shape memory alloys

NiTi SMA was discovered in 1963 at the Naval Ordnance Laboratory (NOL), hence the often referred acronym NiTiNOL.

Although reversibility of MT in NiTi is essentially guaranteed for the alloy of nominally stoichiometric composition, small additional increase in nickel is admissible and it has an important effect of decreasing the temperature at which MT is initiated Otsuka and Wayman (1998). Moreover, the effective behavior of NiTi binary alloy can be modified by substituting some amount of one of constituent elements by another element producing a ternary alloy. As an example, substitution of manganese, aluminium for titanium or cobalt or iron for nickel lowers the transformation temperatures (see Otsuka and Wayman, 1998, and references therein). If such modified alloys still preserve the basic shape memory characteristics, they are sometimes broadly termed as NiTi-based SMA.

For a NiTi single crystal, the maximum value of recoverable strain has been computed theoretically and it was found that it strongly depends on crystallographic orientation of the specimen with respect to loading direction. For instance, the value for reversible elongation varies between 10.7% and 2.7% as has been also experimentally confirmed (Otsuka and Wayman, 1998). The direct relation between transformation strain (and some other transformation features) in NiTi polycrystals and crystallography of MT at a single crystal level has been demonstrated by simulations of Šittner and Novák (2000). However, transformation strain is usually considered as a material parameter in macroscopic models of SMA polycrystals and the same approach will be adopted in this work. For full MT the usual maximum recoverable strain reachable in experiments on NiTi polycrystals is about 8% (Shu and Bhattacharya, 1998). It shall be also noted that, as reported by Brinson et al. (2004), martensitic plates formation at microscopic scale can occur in NiTi polycrystal both before and after the "macroscopic" transformation stage conventionally defined by presence of plateau in stess-strain dependence. Such effects have been phenomenologically addressed in (Frost et al., 2010) by introduction of a particular hysteresis operator, but it will be neglected in this work.

NiTi-based SMA may transform from (cubic) austenite into (monoclinic) martensite either directly or via an intermediate phase. For some specific composition and metallurgical treatment, an intermediate (rhomboedral) phase known as R-phase occurs (Otsuka and Ren, 2005). The associated transformation process between austenite and R-phase will be called *R-phase transformation* hereinafter. Since this transformation is thermoelastic and R-phase is prone to twinning, shape memory and superelasticity effects are exhibited. The transformation can occur in a possibly wide temperature range (Olbricht et al., 2011). Nevertheless, small hysteresis is observed indicating low associated dissipation. Also a quite small transformation strain ($\sim 0.8\%$) is associated with the transformation between austenite and R-phase. Since the changes in transformation strain occur gradually in a wide interval of transformation temperatures it is usually difficult to detect the presence R-phase directly from measured stress-strain dependency. However, the transformation may be characterized, e.g., by detection of associated latent heat and/or sharp change of electrical resistivity in experiments (Novák et al., 2008). The latent heat associated with austenite-to-R-phase

transformation was found to be about $1/5 \sim 1/3$ of the latent heat of direct austenite-to-martensite transformation (Airoldi and Rivolta, 1988).

It shall be noted that a lattice distortion also accompanies R-phase-to-martensite transformation and usually no R-phase occurs when martensite transforms back to austenite in experiments. R-phase appears in most of the commercially available cold worked/annealed NiTi wires (Šittner et al., 2006) and affects considerably the mechanical response of particular structures as springs, stents and knitted NiTi textiles since large macroscopic changes occur in them even for small strains accompanying the transformation from austenite to R-phase. This is mainly the reason why R-phase transformation is covered in this work.

Due to the lattice-distortive origin of MT, elasticity of SMA plays an important role in understanding of microscopic background of the transformation phenomena (Ren and Otsuka, 1998). The elastic properties of austenite have been experimentally investigated in many works, see the references in the paper of Ren and Otsuka (1998).

The elastic properties of NiTi undergoing R-phase transformation were experimentally examined by ultrasound measurements and neutron diffraction methods by Šittner et al. (2006). It was observed that Young and shear moduli substantially decrease during that transformation.

Due to experimental difficulties, the coefficients of elasticity tensor of martensite single crystal has not been measured yet. However, based on results of theoretical study performed by Wagner and Windl (2008) and recent research on elastic properties of polycrystalline NiTi specimen by Qiu et al. (2011), it seems that martensite exhibits elastic anisotropy. In addition, comparison of results in the former work with those in (Šittner et al., 2006) suggests that the value of bulk moduli of all the phases are very close to each other. Findings of Qiu et al. (2011) confirmed that reorientation processes in pseudoplasticity occur even at low stresses where macroscopic stress-strain dependence appears linear, which results in more than 50% difference between (macroscopically) apparent and real Young's moduli of martensite.

Let us now summarize some further experimental findings on NiTi polycrystals which have to be taken into account when a macroscopic constitutive model is developed. The relative volume change associated with MT in thermoelastic alloys is usually small, according to theoretical calculation of order 10^{-3} for both austenite-to-martensite and austenite-to-R-phase transformation in case of NiTi (Otsuka and Ren, 2005). Experimental data confirmed these estimates (Funakubo and Kennedy, 1987; Jacobus et al., 1996). The assumption of zero net relative volume change, sometimes termed as *volume preserving property* of MT, is thus often made in SMA modelling and it is also the case for the model introduced in this work.

The difference between heat capacity of martensite and austenite at constant volume are also found negligibly small in the literature (Lagoudas and Bo, 1999). Regarding coefficient of thermal expansion, although the values for the three phases considerably differ, the highest value of them is of order $10^{-5}\,\mathrm{K}^{-1}$ (Uchil et al., 1999) which represents strain about 10^{-3} for temperature variation within a range of 100 K, i.e. one order less than typical maximum transformation strain which is the salient contribution to thermomechanical response that SMA models concentrate on. In other words, thermal expansion becomes relevant only for

thermal loading at zero or rather small applied stress which is not a mode that SMA application are usually constructed to operate on. That is the reason why it will be neglected here, albeit its adoption does not pose any obstacle.

In a typical superelastic loading-unloading experiment under tension and compression, so-called *tension-compression asymmetry* demonstrates itself: under compression, the transformation strain induced by phase transformation is lower and the absolute value of stress level required to start the forward phase transformation is higher than in experiments in tension[6] (Gall et al., 1999; Grolleau et al., 2011; Liu et al., 1998; Mao et al., 2010; Orgéas and Favier, 1999). When a full hysteresis loop is exhibited, it is shorter along the strain axis and wider along the stress axis in compression than in tension. Let us note that more explanations of such phenomena at microscopic level were suggested.

Many applications utilize SMA wires or plates, since they are generally the least expensive and most readily available form. Since a strong texture[7] is usually induced during manufacturing of these products, a pronounced dependence of transformation characteristics on mechanical loading direction is observed. The transformation strain anisotropy (Sedlák et al., 2010; Sun and Li, 2002) was observed experimentally in NiTi textured polycrystalline material. Based on crystallographic and microstructural calculations, Shu and Bhattacharya (1998) have shown that in NiTi alloy, the texture developed by rolling, extrusion or drawing is favourable for large transformation strains. They pointed up that in wires, rods and tubes, the maximum value of transformation strain in torsion is typically significantly lower than in tension and it may further decrease with increasing, simultaneously applied uniaxial tension for some textures. We will introduce material anisotropy and tension-compression asymmetry into the model.

A particular type of processing (e.g. the combination of cold-working and subsequent annealing) has been explored as a way to further improve NiTi characteristics (Otsuka and Wayman, 1998). Depending on composition and heat treatment, it is possible to obtain NiTi alloy for which the properties associated with the transformation stabilize after few training cycles. For example, Delville et al. (2010) utilized non-conventional pulsed electric current method to yield heat-treated NiTi wires with various microstructures and functional superelastic properties. At specific conditions, nanosized microstructure with optimal grain size may be developed. After about 10 cycles-training, the wire exhibited high transformation strain and excellent stability (negligible irreversible strains). Such a stability of the material is highly desired in applications, thus it is reasonable to assume it also in development of a constitutive model in next chapters.

For sake of completeness, let us note that NiTi-based alloys exhibit excellent corrosion-resistance and fulfil severe biocompatibility requirements (Machado and Savi, 2003; Shabalovskaya, 1995), which makes them suitable for medical applications.

[6]Note that the Clausius-Clapeyron relation predicts the latter fact if the former one is accepted.

[7]Texture is the distribution of crystallographic orientations of a polycrystalline sample. If the crystallographic orientations are not random, but exhibit pronounced preferred orientation, the texture is termed strong.

Chapter 2

Framework of Generalized Standard Models

As described in the previous chapter, during general response of SMA, mutual interaction between multiple dissipative processes may be awaited. Continuum thermodynamics together with the concept of *generalised standard models* (also called generalised standard materials) (GSM) developed by Halphen and Nguyen (1975) provide a powerful framework for description and modeling of thermomechanical response of SMA. In this chapter, this framework will be briefly introduced in a way which allows to utilize it successfully for development of the model introduced in Chapter 4. Our starting point will be the continuum thermodynamics.

2.1 Elements of continuum thermodynamics

In order to fully determine a system of equations describing the time evolution of a thermodynamical system (e.g. solid body), the balance laws must be completed by a proper constitutive relation. From the point of view of continuum thermodynamics, construction of a constitutive relation is essentially restricted by the laws of thermodynamics.

An elementary term of the theory of continuum is a material point, a small enough elementary particle of solid or fluid, whose state represents the local state of material. A basic assumption of the (local equilibrium) thermodynamics of continuum is then that "the (continuum mechanical) system is composed of infinitesimal sub-systems in slow evolution such that each sub-system can be always considered as almost in thermodynamic equilibrium at any time" (cf. e.g. Nguyen (2000)). Any material point is then assumed to be composed of one of these infinitesimal subsystems. The internal physical state of a material point in equilibrium can be characterized by the present value of a set of variables called as *state variables*. The set of state variables includes the temperature, T, and other physical variables suitable for the investigated system. The above postulate allows to introduce locally the entropy and thermodynamic potentials as functions of state variables, even in a case when the system as a whole is not necessary in equilibrium.

Important examples of state variables come from description of kinetics of continuum. Having now a body occupying a domain $\Omega \subset \mathbb{R}^3$ in a reference configura-

tion, a smooth injective vector function $y(t) : \Omega \to \mathbb{R}^3$ satisfying $\det \nabla y(x,t) > 0$ is then called *deformation*; t and x denote time and space coordinates. The tensor $\nabla y(x)$ is called *deformation gradient* and it is of high importance in solid mechanics. We omit the explicit dependence on time and space in notation for simplicity in the rest of this chapter, since all variables introduced in what follows are time- and space-dependent.

Defining the right Cauchy-Green deformation tensor as

$$C := (\nabla y)^\top \nabla y, \tag{2.1}$$

one possible measure of *strain* is then given by the (Green-)Lagrangian strain tensor in the form:

$$G := \frac{1}{2}(C - I), \tag{2.2}$$

where I is the identity tensor.

By geometric linearization of G we obtain the *small strain tensor*

$$\boldsymbol{\varepsilon} := \frac{1}{2}[\nabla u + (\nabla u)^\top], \tag{2.3}$$

where u denotes displacement of a material point. A direct relation between deformation and displacement is given by

$$u(x) = y(x) - x. \tag{2.4}$$

Since we aim to formulate a constitutive model in the *small strain setting*, we restrict ourselves to this setting in what follows.

The local version of *the first law of thermodynamics*, i.e. conservation of the overall (total) energy, may be written in the following form Nguyen (2000):

$$\boldsymbol{\sigma} : \dot{\boldsymbol{\varepsilon}} - \operatorname{div}(q) = \dot{u}^X, \tag{2.5}$$

where u^X is the internal energy of material per unit volume, which, in line with the local state postulate, is supposed to be a function of the entropy (considered per unit volume), s, and strain, $\boldsymbol{\varepsilon}$. The Cauchy stress tensor[1] is denoted by $\boldsymbol{\sigma}$, whereas q denotes the heat flux.[2]

The local form of the *second law of thermodynamics* states that the production of entropy in time is always non-negative Nguyen (2000):

$$\dot{s} - \operatorname{div}\left(\frac{q}{T}\right) \geq 0, \tag{2.6}$$

Equivalently,

$$T\dot{s} + \operatorname{div}(q) - \frac{q}{T}\nabla T \geq 0. \tag{2.7}$$

Combining inequality (2.7) with the local form of the first law of thermodynamics (2.5) we obtain an equivalent form of the second law, which is sometimes referred to as the Clausius-Duhem inequality:

$$T\dot{s} - \dot{u}^X + \boldsymbol{\sigma} : \dot{\boldsymbol{\varepsilon}} - \frac{q \cdot \nabla T}{T} \geq 0. \tag{2.8}$$

[1] Let us note that since we are working in the small strain setting, the Cauchy stress tensor is equivalent to the Piola-Kirchhoff stress tensors, which are the primary measures of stress state in Lagrangian setting commonly used in modeling of solids.

[2] We omitted change of energy due to radiation for simplicity

We also introduce the Helmholtz free energy, f, more convenient for further development, as a Legendre transformation of internal energy:

$$f(T, \boldsymbol{\varepsilon}) := u^X(s, \boldsymbol{\varepsilon}) - sT. \tag{2.9}$$

Thus, the Clausius-Duhem inequality takes the form:

$$\boldsymbol{\sigma} : \dot{\boldsymbol{\varepsilon}} - \dot{f} - s\dot{T} - \frac{q \cdot \nabla T}{T} \geq 0. \tag{2.10}$$

Let us investigate a process for which equality is imposed in the previous equation:

$$\sigma : \dot{\boldsymbol{\varepsilon}} - \frac{\partial f}{\partial \boldsymbol{\varepsilon}} : \dot{\boldsymbol{\varepsilon}} - \frac{\partial f}{\partial T}\dot{T} - s\dot{T} - \frac{q}{T} \cdot \nabla T = 0. \tag{2.11}$$

Such a process is called *reversible*. Introducing the following notation:

$$\boldsymbol{\sigma}_{\text{el}} := \frac{\partial f}{\partial \boldsymbol{\varepsilon}}, \tag{2.12}$$

and applying standard thermodynamic arguments, i.e. mutual independence of state variables (and also ∇T), we arrive at a set of equations:

$$\boldsymbol{\sigma} - \boldsymbol{\sigma}_{\text{el}} = \mathbf{0}, \tag{2.13}$$

$$s + \frac{\partial f}{\partial T} = 0, \tag{2.14}$$

$$q = 0. \tag{2.15}$$

Let us note that (2.14) is often called the Gibbs relation and the system describes so-called hyperelastic behavior. However, many inelastic processes can be found in the nature (viscosity, plasticity, etc.), thus, it is beneficial not to limit the theory to be able to capture such effects, too.

2.2 Irreversible processes in solids

We introduce a possibility to describe a wider class of materials than only hyperelastic ones, i.e. where non-zero dissipation occurs. To do so, lets turn our attention to the Clausius-Duhem inequality (2.10) once again. The term

$$\mathfrak{D}_{\text{mech}} := \boldsymbol{\sigma} : \dot{\boldsymbol{\varepsilon}} - \dot{f} - s\dot{T} \tag{2.16}$$

is called a *mechanical dissipation*, the last term on the left-hand side of (2.10) is often called a *thermal dissipation* in the literature Houlsby and Puzrin (2000); Nguyen (2000). It is usually reasonable to adopt the Fourier law for the heat conduction, i.e. to assume the heat flux density, q, is proportional to a negative gradient of temperature, $-\nabla T$, with an appropriate proportionality coefficient so that the thermal dissipation is always non-negative. Requiring the mechanical dissipation itself be non-negative (Nguyen, 2000)

$$\dot{s}T + \operatorname{div}(q) = \mathfrak{D}_{\text{mech}} = \boldsymbol{\sigma} : \dot{\boldsymbol{\varepsilon}} - \dot{f} - s\dot{T} \geq 0 \tag{2.17}$$

together with the Fourier law is a slightly more stringent condition than formula (2.10). However, it is a widely accepted assumption in the literature on constitutive modelling (Helm and Haupt, 2003; Houlsby and Puzrin, 2000; Nguyen, 2000), thus it will be applied within this work.

We now introduce the concept that the thermodynamic state of the material depends, together with strain and temperature, on further, internal variables to capture dissipative processes. With respect to the model introduced in Chapter 4, let us restrict ourselves to one additional scalar, ξ, and one additional tensor, $\boldsymbol{\kappa}$, as additional internal variables, albeit more internal variables of various types are possible, see (Houlsby and Puzrin, 2001).

Introducing $f(\boldsymbol{\varepsilon}, \boldsymbol{\kappa}, \xi, T)$ into (2.17) we obtain

$$\boldsymbol{\sigma} : \dot{\boldsymbol{\varepsilon}} - \frac{\partial f}{\partial \boldsymbol{\varepsilon}} : \dot{\boldsymbol{\varepsilon}} - \frac{\partial f}{\partial T}\dot{T} - \frac{\partial f}{\partial \xi}\dot{\xi} - \frac{\partial f}{\partial \boldsymbol{\kappa}} : \dot{\boldsymbol{\kappa}} - s\dot{T} \geq 0. \tag{2.18}$$

Motivated by (2.12), we introduce the decomposition $\boldsymbol{\sigma}_{\text{dis}} := \boldsymbol{\sigma} - \boldsymbol{\sigma}_{\text{el}}$ in order to include strain rate-dependent processes (Nguyen, 2000). Applying a strategy known as the Coleman-Noll procedure (Coleman and Noll, 1963) to (2.18), one obtains the following system:

$$\boldsymbol{\sigma} - \boldsymbol{\sigma}_{\text{dis}} - \frac{\partial f}{\partial \boldsymbol{\varepsilon}} = \mathbf{0}, \tag{2.19}$$

$$s + \frac{\partial f}{\partial T} = 0, \tag{2.20}$$

$$\boldsymbol{\sigma}_{\text{dis}} : \dot{\boldsymbol{\varepsilon}} - \frac{\partial f}{\partial \boldsymbol{\kappa}} : \dot{\boldsymbol{\kappa}} - \frac{\partial f}{\partial \xi}\dot{\xi} \geq 0. \tag{2.21}$$

The equation (2.18) may be understood as a restriction imposed by the second law of thermodynamics on time-evolution of state variables, particulary to the (so far) formally introduced additional internal variables. System (2.19)–(2.21) may be viewed as a set of sufficient condition to satisfy that restriction[3], useful for construction of a constitutive model.

We define $A := (\boldsymbol{\sigma}_{\text{dis}}, -\partial f/\partial \boldsymbol{\kappa}, -\partial f/\partial \xi)$ and $\alpha := (\boldsymbol{\varepsilon}, \boldsymbol{\kappa}, \xi)$. It is common to refer to any member of the vector A as a *generalized force* and to corresponding member of $\dot{\alpha}$ as a *generalized flux* in irreversible thermodynamics literature (Nguyen, 2000). The entropy production equation (2.21) then takes the form:

$$A \cdot \dot{\alpha} \geq 0. \tag{2.22}$$

For meaningful utilization of the concept, it is necessary to choose appropriate internal variables with respect to the nature of the involved physical processes. Usually, internal variables are introduced to account for microscopic phenomena at the macroscopic level, where they manifest themselves by dissipation.[4] Then, it remains to prescribe *the relation between generalized forces and fluxes* such that (2.22) is satisfied, i.e. to establish the constitutive law. Such a relation then

[3] Coleman and Noll (1963) even argue that these conditions are necessary.

[4] However, this is not necessarily always the case. As will be demonstrated on the example of the volume fraction of R-phase in Chapter 4, it is also possible to introduce non-dissipative variables in order to distinguish different microscopic contributions to reversible processes at the macroscopic level, for instance.

defines the irreversible behavior of the material under study and together with balance laws characterise its time-evolution.

Various methods how to establish the constitutive relations can be found in the literature Ziegler (1983). They are often based on an extremum principle applied to a physical entity related to entropy production.[5] Among the most well-known are the *principle of maximum dissipation (rate)*, whose roots may be dated back to Onsager, and the *minimum principle for the dissipation potential*. Although there can be often found appropriate forms of extremalized entities such that both principles lead to the same evolution equations for the internal variables, e.g. in case of rate-independent processes, as shown by Hackl and Fischer (2008), such an equivalence is not valid generally. In the following, we will introduce a simple concept based on the work of Nguyen (see e.g. Nguyen, 2000) with is most cases equivalent to the minimum principle for the dissipation potential.[6]

2.3 Generalised standard model

"By definition, a model of material behaviour is a *generalized standard model* if it is defined by two potentials, the energy potential, f, and the dissipation potential, d. The energy is a function of state variables and the dissipation potential is a convex function of flux and may eventually depend on the present state" (Nguyen, 2000). Moreover, the dissipation potential is supposed to be nonnegative and to be zero for zero fluxe and the relation between the generalised flux and the dissipation potential is established by the following inclusion:

$$A \in \partial_{\dot{\alpha}} d(T, \alpha, \dot{\alpha}). \tag{2.23}$$

Since d is considered not necessarily smooth, the sub-differential notation of a convex function is used, see Appendix A. Let us note the nomenclature "potential" is motivated by the fact that its derivative[7] corresponds to the generalized force (Nguyen, 2000). The term dissipation function is also used in the literature as a synonym and will be mostly utilized in this work.

A GSM framework automatically ensures satisfaction of the inequality (2.22) related to the second law of thermodynamics, since

$$A \cdot \dot{\alpha} \geq d(T, \alpha, \dot{\alpha}) - d(T, \alpha, 0) = d(T, \alpha, \dot{\alpha}) \geq 0, \tag{2.24}$$

where we used in turn convexity, "zero in zero" and nonnegativity properties of d.

A simple scheme for a formal construction of a constitutive model[8] within the GSM framework may be summarised as follows (Nguyen, 2000):

[5] The question on conceptual relation between such principles is still open in some cases (Svoboda et al., 2005).

[6] Particularly it is the case if the free energy function is convex in state variables and the dissipation function is convex in their rates.

[7] Or, generally, "one of its subderivatives".

[8] Of course, there are other conditions a physically relevant model should satisfy; e.g. the so-called axioms of constitutive theory Coleman and Noll (1963), which express some "natural" requirements as frame indifference, material symmetry, casuality, etc., and which are satisfied for common models of solids.

$\boldsymbol{\sigma}_{\text{dis}}$	$\boldsymbol{\kappa}$	ξ	f	d	Constraint(s), comments
Maxwell visco-elasticity					
1	0	0	$\frac{1}{2}\boldsymbol{\varepsilon} : \mathbb{C} : \boldsymbol{\varepsilon}$	$\frac{1}{2}\dot{\boldsymbol{\varepsilon}} : \mathbb{D} : \dot{\boldsymbol{\varepsilon}}$	$\Rightarrow \boldsymbol{\sigma}_{\text{dis}} = \mathbb{D} : \dot{\boldsymbol{\varepsilon}}$
Kelvin-Voight visco-elasticity					
0	1	0	$\frac{1}{2}(\boldsymbol{\varepsilon} - \boldsymbol{\kappa}) : \mathbb{C} : (\boldsymbol{\varepsilon} - \boldsymbol{\kappa})$	$\frac{1}{2}\dot{\boldsymbol{\kappa}} : \mathbb{D} : \dot{\boldsymbol{\kappa}}$	$\boldsymbol{\kappa}$ represents viscous strain
Perfect Von-Mises plasticity					
0	1	0	$\frac{1}{2}(\boldsymbol{\varepsilon} - \boldsymbol{\kappa}) : \mathbb{C} : (\boldsymbol{\varepsilon} - \boldsymbol{\kappa})$	$Y\|\dot{\boldsymbol{\kappa}}\|$	$\text{dev}(\boldsymbol{\kappa}) = 0$, $\boldsymbol{\kappa}$ represents plastic strain
Very simple one-dimensional SMA superelasticity					
0	0	1	$\frac{1}{2}E(\varepsilon - \xi\Lambda)^2$ $+C(T) + \frac{1}{2}k\|\xi\|^2$	$Y\|\dot{\xi}\|$	$0 \leq \xi \leq 1$, ξ represents volume fraction of martensite

Table 2.1: Simplified examples of mechanical constitutive models within GSM for isothermal evolution. The simplified superelasticity model in tension is based on (Auricchio and Sacco, 1997). The first three columns indicate if the correpondig type of internal variable is employed. The fourth-order tensors $\mathbb{C}$ and $\mathbb{D}$ represent the tensor of elastic constants and the tensor of viscous moduli, respectively. Y and k are constants reflecting the onset of dissipation process and the "rate of hardening" of the mechanical response, respectively. The constant Λ denotes the maximum transformation strain in the direction of loading, E is the Young modulus and $C(T)$ is a positive constant depending linearly on temperature. Further restrictions may apply to these constants due to their physical meaning.

A. Choice of the set of state variables with respect to the nature of the system and behavior to be modeled.

B. Definition of the energy function.

C. Dissipation analysis, i.e. definition of dissipation function as a function of flux and, possibly, of the present state.

As pointed up in (Nguyen, 2000), a good knowledge of both reversible and irreversible mechanisms operating within the considered material is needed to construct a physically meaningful model.

Examples of some types of very simple material models can be found in Table 2.1.[9] As widely discussed in (Collins and Houlsby, 1997; Houlsby and Puzrin, 1999), by a suitable choice of free energy and/or dissipation functions, further types of common models, e.g. visco-plasticity, kinematic or isotropic hardening plasticity, models of soils, etc., may be derived.

The final form of governing equations for the introduced class of models based on GSM framework when neglecting inertia, assuming small strain setting and

[9] In that table we utilize the common mechanical engineering notation for matrix products, i.e. it holds $\boldsymbol{x} : \boldsymbol{M} : \boldsymbol{x} := \boldsymbol{M}x \cdot x$ with respect to our standard notation.

positivity of thermal dissipation, follows:

$$\begin{aligned} \operatorname{div}(\partial_{\boldsymbol{\varepsilon}} f + \partial_{\dot{\boldsymbol{\varepsilon}}} d) &\ni 0, && (2.25)\\ \partial_{\alpha} f + \partial_{\dot{\alpha}} d &\ni 0, && (2.26)\\ \partial_{\dot{\boldsymbol{\varepsilon}}} d : \dot{\boldsymbol{\varepsilon}} + \partial_{\dot{\alpha}} d \cdot \dot{\alpha} = \mathfrak{D}_{\text{mech}} &= T\dot{s} + \operatorname{div}(q), && (2.27) \end{aligned}$$

where f is assumed to depend on $T, \boldsymbol{\varepsilon}$ and a set of internal state variables α. The first relation corresponds to the balance of momentum and the third to the entropy balance. The second one provides relation between forces and fluxes due to (2.23).

2.3.1 Rate-independent processes within GSM

A special class of dissipative processes represent rate-independent processes as plasticity or dry friction. They are associated with a particular type of dissipation function, which is *positively homogeneous of degree one* with respect to fluxes, i.e.

$$d(T, \alpha, C\dot{\alpha}) = C d(T, \alpha, \dot{\alpha}) \qquad \forall\, C > 0. \tag{2.28}$$

The force-flux relationship (2.23) is in the rate-independent setting equivalent to the relation[10]

$$\dot{\alpha} \in \partial_A \mathcal{I}_K(T, \alpha, A). \tag{2.29}$$

where K is a convex set called the domain of admissible forces (Nguyen, 2000). With respect to Example A.0.5, we then obtain so-called "normality law" for $A \in \partial K$:

$$\dot{\alpha} \in N_K(T, \alpha, A), \tag{2.30}$$

which states that $\dot{\alpha}$ must be an external normal to the admissible domain at the present state of the force A (Nguyen, 2000). This formulation is widely used in "generalized standard models of plasticity" in small strain setting (Nguyen, 2000), where the set K is referred to as an elasticity domain, d^* is called yield function and the relation (2.29) is known as so-called flow rule.[11] Moreover, it can be shown[12] that

$$d(T, \alpha, \dot{\alpha}) + \mathcal{I}_K(T, \alpha, A) = A \cdot \dot{\alpha}. \tag{2.31}$$

Then, we obtain[13]

$$A \cdot \dot{\alpha} = d(\alpha, \dot{\alpha}). \tag{2.32}$$

Hence, (2.27) gives in that case

$$d = \mathfrak{D}_{\text{mech}}, \tag{2.33}$$

i.e. value of (prescribed) dissipation function is equal to the (real) mechanical part of dissipation of energy.

[10] Actually, (2.23) is equivalent to the dual relation $\dot{\alpha} \in \partial_A d^*(T, \alpha, A)$, where the dual dissipation potential, d^*, is given by the Legendre-Fenchel transform of d, see Appendix A. It is also shown there (see Lemma A.0.10), that, in the rate-independent setting, the dual dissipation potential is equal to the indicator function of a convex set, K.

[11] In perfect plasticity setting, stress $\boldsymbol{\sigma}$ plays the role of the force A.

[12] One utilizes the Lemma A.0.10 and relation (A.9) in Appendix A.

[13] We suppose that A is the admissible force, i.e. it is "inside" or on "the boundary" of the elasticity domain.

Chapter 3

Modeling of Shape Memory Alloys

In the last three decades, continuously increasing effort in modeling of shape memory effects can be observed. The modeling is attractive both for physicists, who are interested in confirmation of the proposed explanation of some underlying phenomena, for engineers, demanding accurate prediction of SMAs thermomechanical behavior needed in new products development, and even for mathematicians, who are motivated by further development of advanced mathematical concepts. However, due to the different objectives, these groups usually elaborate their modeling concepts at various levels compromising rigor with phenomenology. A scale transition between neighbouring modelling levels often poses a challenge in mathematical modeling (Benešová, 2012; Patoor, 2009; Roubíček, 2004).

One of possible classification motivated by Roubíček (2004) is the following one, see also Fig. 3.1:

1. Atomic level: the description counts barycenter of particular atoms and inter-atomic potentials, tools of the quantum mechanics or the molecular dynamics are employed (e.g. Entel et al., 2000)

2. Microscopic level: continuum mechanics is used to describe deformation, stress, strain, temperature field, etc. at material points, microstructure inside the specimen is fully resolved (e.g. Stupkiewicz and Petryk, 2010)

3. Mesoscopic level: the state of the material is described by "averaged" deformation gradients and volume fractions of phases or phase variants, the system is treated by tools of continuum mechanics (e.g. Benešová, 2012)

4. Macroscopic level: macroscopic deformation and volume fractions of phases are used to describe configuration at given material point, information about the microstructure is encompassed by so-called internal variables

Let us note that especially the second and the third levels are used for single crystals modelling, whereas the last one is used for polycrystalline models. A number of models based on various approaches at all the levels has appeared, see e.g. following review papers (Khandelwal and Buravalla, 2009; Lagoudas et al., 2006; Patoor et al., 2006; Roubíček, 2004).

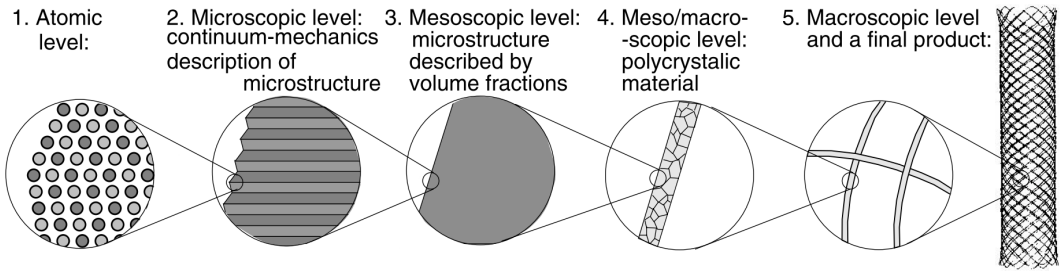

Figure 3.1: A schematic representation of the different scales of an SMA. Reprinted from (Roubíček, 2004).

Thanks to simple numerical implementation, less time-consuming calculations and the possibility to be adjusted for the particular material easily, macroscopic thermodynamics-based models appear to be a very powerful tools for simulation of behavior of polycrystalline SMA applications. Derivation of such a type of models in case of SMAs may be summarized into three fundamental steps similar to those introduced in Section 2.3:

A. Choice of internal kinematic variable(s).

   Physical motivation usually leads to the introduction of volume fraction of martensite for description of proceeding phase transformation and a tensorial variable for description of inelastic deformation processes in martensite. Such a strongly simplified description of complicated martensitic microstructure is motivated by the aim to obtain fast, efficient models with a low number of fitting parameters. Several authors extend the simplified description by using additional variables as volume fraction of twinned/detwinned martensite[1] (Leclercq and Lexcellent, 1996; Panico and Brinson, 2007; Popov and Lagoudas, 2007), twins accommodation strain (Chemisky et al., 2011), plastic strain (Auricchio et al., 2007; Hartl et al., 2010; Zaki et al., 2010), various "material memory variables" (Chemisky et al., 2011; Rajagopal and Srinivasa, 1999; Saint-Sulpice et al., 2009), etc.

B. Choice of a suitable energy function.

   Both prescription of the Helmholtz and the Gibbs free energies can be found in derivation of constitutive equations of SMAs, see the review of Khandelwal and Buravalla (2009). The free energy has two fundamental contributions – the (thermo)elastic energy and the chemical energy related to the change of entropy associated with the phase transformation. Elastic isotropy of phases is mostly assumed in the models, different material parameters for austenite and martensite are considered only in some of them (e.g. Moumni et al., 2008; Popov and Lagoudas, 2007). The mechanical and chemical contributions are commonly supplemented by interaction or interfacial energies (Chemisky et al., 2011; Moumni et al., 2008; Peultier et al., 2006).

C. Formulation of the dissipation mechanism.

[1] Often the terminology "stress-induced" and "temperature-induced" martensite is used.

A proper formulation of the dissipation mechanism, which describes how much energy the system should "pay" for the change of internal variables, is a crucial, and often the least developed, part of SMA-model formulation. The main peculiarities of SMA behavior as path-dependent response, switching between transformation-reorientation processes, etc. are related to dissipation. Insufficiently captured dissipation could lead to incorrect simulations of path-dependent material responses under general multiaxial loadings.

In a common approach a yield surface is constructed as a function of the generalized stress and separates the thermoelastic and trans-for-ma-tion/reo-rien-ta-tion regions (e.g. Auricchio and Petrini, 2004; Hartl and Mooney, 2010; Popov and Lagoudas, 2007; Qidwai and Lagoudas, 2000*b*). A closely related approach (see Section 2.3.1) starting by prescription of a rate-independent dissipation function is used in works (Chemisky et al., 2011; Moumni et al., 2008; Souza et al., 1998; Zaki et al., 2010), for instance. However, there are also models combining the rate-independent and rate-dependent types of response in order to extend the applicability of the model to high-frequency loading or elevated temperature when viscosity effects are not negligible, e.g. (Hartl et al., 2010; Sadjadpour and Bhattacharya, 2007*a*; Saleeb et al., 2011).

Also, there is a subgroup of macroscopic models, often referred to as phenomenological in literature, which differs from the above approach by establishing the transformation kinetics separately and focuses on mechanical loading in one dimension. The phase evolution and transformation conditions are derived using empirically determined stress-temperature phase diagrams and the phase fraction, derived out of the explicit evolution kinetics, is incorporated into a simple constitutive relation. Although there are many examples of this approach (e.g. Bekker and Brinson, 1997; Gao et al., 2007; Zhou and Yoon, 2006), possibilities of its extension to general loading cases seems to be limited. Hence, such models are not considered in what follows.

3.1 Overview of macroscopic thermodynamics-based models

Three-dimensional *rate-independent* continuum thermodynamics-based models for polycrystalline SMAs represent a salient subgroup of SMA models. With respect to the final aim of this work, in following review, we will focus on the most prominent models, which represent a distinct directions in the SMA modeling field. We will mainly try to pinpoint their features that are relevant for the ability to reliably simulate NiTi-based SMA response to general thermomechanical loadings involving complex loading paths.

Thus, we will omit models intended *only* for superelastic temperature range modelling. Those are usually the pioneering works (Boyd and Lagoudas, 1996; Liang and Rogers, 1990; Raniecki and Lexcellent, 1998), which served as a basis for recent, more developed models, or works, which have traded universality for elaboration of particular, interesting phenomena of the SMA response in more

detail, e.g. internal loops evolution (Bouvet et al., 2004; Saint-Sulpice et al., 2009), cycling behavior (Saint-Sulpice et al., 2009), temperature effects (Thiebaud et al., 2007), etc.

The type and the number of internal variable(s) will be chosen as an auxiliary classifying criterion, since it provides a hint for discovering common features of models. Further, we will mention the particular form of dissipation function. Importance of both aspects for constitutive model construction was sketched in Chapter 2. Throughout this section, we will use a unified notation for the most common parameters utilised in modeling of SMA, i.e. the (total) strain, $\boldsymbol{\varepsilon}$, the stress, $\boldsymbol{\sigma}$, the temperature, T, and a simplified notation of particular parameters, whose exact form can be found in referred works.

In all following models a general assumption of additivity of strains is adopted (i.e. small strain setting), $\boldsymbol{\varepsilon} = \boldsymbol{\varepsilon}^{\mathrm{el}} + \boldsymbol{\varepsilon}^{\mathrm{in}}$, where $\boldsymbol{\varepsilon}^{\mathrm{el}}$ denotes the (thermo)elastic contribution to the total strain of the material and $\boldsymbol{\varepsilon}^{\mathrm{in}}$ represents an inelastic strain related to changes of martensitic structure which can be fully released by completed transformation back to austenite.

In simple models, only a single bounded scalar internal variable representing the volume fraction of martensite, ξ, is introduced. By relating the transformation induced strain with the volume fraction of martensite through a constant, e.g. $\dot{\boldsymbol{\varepsilon}}^{\mathrm{in}} = \boldsymbol{\Lambda}\dot{\xi}$, where $\boldsymbol{\Lambda}$ denotes a constant material parameter called transformation direction tensor, it would not be possible to capture the temperature induced transformation, i.e. transformation with zero net macroscopic shape change. Thus, some three-dimensional models, e.g. (Hartl and Mooney, 2010; Qidwai and Lagoudas, 2000*b*), force $\boldsymbol{\Lambda}$ to depend on stress, i.e. $\boldsymbol{\Lambda}(\boldsymbol{\sigma})$. If disappearance of martensite is appropriately treated, this simple approach covers both proportional loading in pseudoelasticity and the one-way shape memory effect, therefore, it is efficient for many practical applications. However, it is not sufficient for general loadings leading to more complex evolution of martensite.

In an attempt to extend the applicability of such a type of models, some authors (e.g. Leclercq and Lexcellent, 1996; Lexcellent et al., 2006; Popov and Lagoudas, 2007) introduce two "types" of martensite.[2] Popov and Lagoudas (2007) conceptually distinguish twinned martensite, which is assigned zero transformation strain, and detwinned martensite, which exhibits non-zero macroscopic strain. In the model, they use three scalar internal variables describing the amount of twinned and detwinned martensite transformed from austenite, ξ_1, ξ_2, and the amount of detwinned martensite produced from twinned one, ξ_3. By introduction of two different transformation surfaces for transition between twinned/detwinned martensite and austenite, the effect of martensite stabilisation is captured. The formulation inherits problems with absence of the transformation strain evolution for general mechanical loading after complete transformations to detwinned martensite, i.e. if

$$\dot{\xi}_2 = \dot{\xi}_3 = 0, \tag{3.1}$$

it is necessarily

$$\dot{\boldsymbol{\varepsilon}}^{\mathrm{in}} = \boldsymbol{\Lambda}^{\mathrm{t}}(\boldsymbol{\sigma})\dot{\xi}_2 + \boldsymbol{\Lambda}^{\mathrm{d}}(\boldsymbol{\sigma})\dot{\xi}_3 = \mathbf{0} \tag{3.2}$$

[2] It should be noted this idea is widely used in one-dimensional modeling of SMAs (Lagoudas et al., 2006).

and, thus, the model does not reflect change of external mechanical loading mode (tension-shear-compression for instance). $\boldsymbol{\Lambda}^{\mathrm{t}}(\boldsymbol{\sigma}), \boldsymbol{\Lambda}^{\mathrm{d}}(\boldsymbol{\sigma})$ denote the transformation direction tensors. Moreover, the two independent transformation surfaces may lead to a two-step reverse transformation demonstrated by two distinguishable peaks at differential calorimetry measurements, which is actually in not observed in experiments investigating martensite stabilisation by reorientation (Liu and Favier, 2000; Popov and Lagoudas, 2007).[3]

Souza et al. (1998) chose a single traceless tensorial internal variable, which is interpreted as the mean strain of the mixture of a generic parent phase, i.e. austenite or temperature-induced martensite, and a generic product phase, i.e. martensite formed in a non-zero stress field. Following this interpretation and physical limitation of transformation strain, the tensorial internal variable is defined as symmetric tensor with bounded norm. The chosen dissipation potential is prescribed in a very simple form: $R\|\dot{\boldsymbol{\varepsilon}}^{\mathrm{in}}\|$, where R is a positive material parameter. As a consequence, total dissipation in a full mechanical loading cycle is constant, independent on temperature. The original model was refined and numerically implemented by Auricchio and Petrini (2002) and further modified to cover tension-compression asymmetry in papers (Auricchio and Petrini, 2004; Evangelista et al., 2009).

Recently, Arghavani et al. extended the previous concept. In their work (Arghavani et al., 2010), the measure of the amount of stress-induced martensite is chosen ro be a scalar internal variable, q, while the average direction of different variants (or preferred direction of variants) is chosen as a tensorial internal variable, $\boldsymbol{N}$. The tensor is considered to be traceless and have a constant norm ($\|\boldsymbol{N}\| = 1$). The evolution of q and $\boldsymbol{N}$ are treated independently, which brings more flexibility to the model. The transformation strain tensor is obtained as a product of the internal variables, $\boldsymbol{\varepsilon}^{\mathrm{in}} = q\boldsymbol{N}$, which implies $\|\boldsymbol{\varepsilon}^{\mathrm{in}}\| = q$. Thus, in fact, the situation effectively corresponds to only one tensorial internal variable, $\boldsymbol{\varepsilon}^{\mathrm{in}}$, in the model. It describes the state of martensite and its evolution is driven by two contributions: a "transformation one" due to evolution of q and a "reorientation one" due to evolution of $\boldsymbol{N}$. Since there is no representation of twinned martensite, absence of dissipation in the transition between austenite and martensite in absence of a stress field still remains an inherent disadvantage of the aforementioned approach. As the authors admit, both physically distinguishable phases (austenite, twinned martensite) correspond to one generic parent phase in the model. Based on given standard yield functions (Arghavani et al., 2010), the dissipation function can be derived:

$$d = r_1(q)\|\dot{q}\| + r_2(q)\|\dot{\boldsymbol{N}}\|, \tag{3.3}$$

with r_1, r_2 being positive functions of q.

A direct relation between the martensite volume fraction and the norm of the internal tensorial variable $\boldsymbol{\varepsilon}^{\mathrm{in}}$ can be also found in the work of Panico and Brinson (2007). The evolution of $\boldsymbol{\varepsilon}^{\mathrm{in}}$ is driven, similarly to Arghavani et al. (see an interesting comparison of simulations there), by two driving forces related

[3]For the sake of completeness, we should mention experiments on martensite stabilisation due to *deformation via stress-induced transformation* conducted by Liu and Tan (2000) where a two-step transformation to austenite was observed. They suggest that this effect may be related to the altering of the variant structure within martensite due to localisation.

to two transformation surfaces. A scalar variable is added for description of twinned martensite, but, as far as also thermal loading is concerned, the model was formulated only for the case of pure thermal loading at constant stress.

Zaki and Moumni (Moumni et al., 2008; Zaki and Moumni, 2007*b*) utilised one traceless tensorial and one scalar internal variables. Since the scalar, ξ, represents volume fraction of martensite and the tensor, $\boldsymbol{\varepsilon}^{\mathrm{tr}}$, represents the local martensite orientation strain tensor, the following term for the inelastic strain is obtained:

$$\boldsymbol{\varepsilon}^{\mathrm{in}} = \xi \boldsymbol{\varepsilon}^{\mathrm{tr}}. \tag{3.4}$$

Authors define dissipation potentials separately: $p(\xi)|\dot{\xi}|$ for dissipation related to evolution of martensite volume fraction and $Y\xi^2\|\dot{\boldsymbol{\varepsilon}}^{\mathrm{tr}}\|$ for dissipation related to changes of martensite orientation. $p(\xi)$ is a linear function and Y is a positive constant. No explicit motivation is provided for the particular (quadratic in volume fraction of martensite) form of the latter part of the dissipation function. In later works, the model was extended to capture cyclic behaviour (Zaki and Moumni, 2007*a*), tension-compression asymmetry (Zaki, 2010) or plasticity (Zaki et al., 2010).

The same definition of internal variables was used by (Peultier et al., 2006, 2008) and their work was then substantially extended by Chemisky et al. (2011). Dissipation related to the increase of martensite volume fraction in a full transformation cycle is defined via

$$\dot{\xi} \geq 0: \quad d^{\mathrm{tr}} = \left(h_1(T) - H\|\boldsymbol{\varepsilon}^{\mathrm{tr}}\|\right)\dot{\xi}, \tag{3.5}$$

and for decrease of volume fraction of martensite via

$$\dot{\xi} < 0: \quad d^{\mathrm{tr}} = \left(h_2(T) - H\|\boldsymbol{\varepsilon}^{\mathrm{tr}}\|\right)\dot{\xi}, \tag{3.6}$$

where $h_1(T), h_2(T)$ are temperature dependent functions and H is a positive constant. A novel term, $H\|\boldsymbol{\varepsilon}^{\mathrm{tr}}\|$, was added to capture the martensite stabilisation effect.[4] Dissipation related to changes of martensite orientation has the form $d^{\mathrm{reo}} = F\xi\|\dot{\boldsymbol{\varepsilon}}^{\mathrm{tr}}\|$ with a positive constant F. In contrast to the model of Zaki and Moumni (2007*b*), the dependence on ξ is linear. All together, the dissipation function can be rewritten in the following form

$$d^{\mathrm{Chem}}(T, \xi, \dot{\xi}, \boldsymbol{\varepsilon}^{\mathrm{tr}}, \dot{\boldsymbol{\varepsilon}}^{\mathrm{tr}}) = \begin{cases} h_1(T)\dot{\xi} - H\|\boldsymbol{\varepsilon}^{\mathrm{tr}}\||\dot{\xi}| + F\xi\|\dot{\boldsymbol{\varepsilon}}^{\mathrm{tr}}\| & \text{if } \dot{\xi} \geq 0, \\ h_2(T)\dot{\xi} + H\|\boldsymbol{\varepsilon}^{\mathrm{tr}}\||\dot{\xi}| + F\xi\|\dot{\boldsymbol{\varepsilon}}^{\mathrm{tr}}\| & \text{if } \dot{\xi} < 0. \end{cases} \tag{3.7}$$

Chemisky et al. (2011) also address the description of internal loops (partial transformation) by further modification of the dissipation terms (3.5) and (3.6) with incorporated internal memory variables. To sum up, to the author's knowledge, their model exhibits the most complex and the most elaborated form of dissipation function within the group macroscopic thermodynamics-base models of SMA.

Another novel feature of their work is the introduction of a tensorial variable representing the mean strain due to a specific process within twinned martensite

[4] However, its relevance to dissipation in the case of forward transformation is not clarified at least from the physical point of view.

variants (they call it "twin accommodation" referring to the work of Liu et al. (1999)). This variable is of hyperelastic nature, since the process is assigned no dissipation in the model. Such an approach is used for modification of deformation properties (apparent elasticity) of martensite at low stress.

Although a considerable influence of R-phase transformation on the mechanical behavior of certain NiTi structures is widely accepted, there have been only sparse attempts to tackle this issue in macroscopic models for NiTi so far. The models considering it usually adopt modeling techniques developed for single martensitic phase transition, therefore, they remain restricted only to phase transformation between austenite and R-phase (Langelaar and van Keulen, 2004; Lexcellent et al., 1994). The full transformation sequence between austenite, R-phase and martensite is covered by models of Chan et al. (2012) and Sengupta and Papadopoulos (2009). Nevertheless, the former one concentrates on localization behavior in one-dimensional setting, the latter one develops a constitutive model for stress-induced transformation in a single crystal and adopts a multiscale finite element-based method to simulate a textured NiTi polycrystal. Both models are formulated only for the superelasticity temperature range.

Macroscopic SMA models taking account of material anisotropy are also rare in the literature, e.g. the works Sadjadpour and Bhattacharya (2007*a*); Saleeb et al. (2011), even though, as shown by Taillard et al. (2008), isotropic approximation appears insufficient for textured materials. The anisotropy is captured by an appropriate form ("shape") of either the yield surface of the transformation or the transformation strain domain in the aforementioned works.

3.2 A remark on contributions to the energy function

The chosen forms of two dominant contributions to the energy function, i.e. the (thermo-)elastic and the chemical parts, do not differ much within the SMA models examined above. Most of them may be easily shown to be a specific case of a unified thermodynamical framework presented by Lagoudas et al. (2006). This general framework utilizes the rule of mixtures applied to the free energies of phases considered as linear thermoelastic materials.[5] Such an approach will be used in the next chapter, too.

In addition, there may be found other energy contributions related to the heterogenity of material caused either by its multiphase state and/or by its polycrystalline nature. Contributions associated with multiphase composition, sometimes generally called "energy of mixing" (Lagoudas et al., 2006), are of importance in SMA modeling since they influence transformation kinetics. Their general form depends on the chemical composition, heat treatment, mechanical training, etc. Hence, some authors follow rather phenomenological approach and choose a particular form to fit experimental observations (Hartl and Mooney, 2010; Lagoudas et al., 2012; Popov and Lagoudas, 2007).

[5] Actually, the conventional definition of *linear thermoelastic material* usually assumes entropy as a quadratic function of temperature Coleman and Noll (1963), whereas a logarithmic dependence is assumed in (Lagoudas et al., 2006) as well as many SMA models.

Other authors (Chemisky et al., 2011; Peultier et al., 2006) set out from micromechanical homogenisation considerations and arrive at energetic terms covering inter-granular, intra-granular and inter-variant strain incompatibilities. On the macroscopic scale, the resulting contributions also demonstrate themselves as a "hardening" during phase transformation and reorientation and also as a hyperelastic contribution considered in one-dimensional model of Frost et al. (2010).

Some examples of the generic terms (C denotes a generic constant which is ξ- and $\boldsymbol{\varepsilon}^{\mathrm{tr}}$-independent constant and can be temperature-dependent and whose physical meaning and unit differs in each particular case) include:

- $\frac{1}{2}C\xi(1-\xi)\|\boldsymbol{\varepsilon}^{\mathrm{tr}}\|^2$ accounts for interaction between austenite and martensite in models (Morin et al., 2011; Moumni et al., 2008) and also in (Leclercq and Lexcellent, 1996; Lexcellent et al., 2006) if the transformation strain is considered as a material constant. Note that the term is proportional to a product of volume fractions of the two interacting phases.

- $\frac{1}{2}C\xi^2$ measures the inter-variant interaction energy within martensite regardless of their orientation in (Chemisky et al., 2011; Moumni et al., 2008; Peultier et al., 2006).

- $\frac{1}{2}C\xi^2\|\boldsymbol{\varepsilon}^{\mathrm{tr}}\|^2$ represents interaction between oriented martensite variants in models (Moumni et al., 2008; Peultier et al., 2006). Note that considering $\boldsymbol{\varepsilon}^{\mathrm{in}} = \xi\boldsymbol{\varepsilon}^{\mathrm{tr}}$ in the kinematic hardening term in "classical" plasticity leads to the same type of expression. Based on such similarity, this kind of term is also introduced in works (Arghavani et al., 2010; Auricchio and Petrini, 2004; Souza et al., 1998).

- $\frac{1}{2}C\xi\|\boldsymbol{\varepsilon}^{\mathrm{tr}}\|^2$ corresponds to intergranular and intragranular incompatibilities in the material in (Chemisky et al., 2011). Note the difference in the power of ξ with respect to the previous term.

Let us make a note how these terms influence the macroscopic response of models. If one assumes a state-independent form of dissipation function, i.e. $d(\dot{\xi}, \dot{\boldsymbol{\varepsilon}}^{\mathrm{tr}})$, than all these types of terms except for the second one lead to a hardening type of behavior in superelastic and pseudoplastic responses. On the other hand, only the second one implies temperature intervals in stress-free phase transformation (and also the first one if $\boldsymbol{\varepsilon}^{\mathrm{tr}}$ is considered as a constant). However, the same type of behavior can be obtained if the dissipation function depends also on state of internal variables, i.e. $d(\xi, \boldsymbol{\varepsilon}^{\mathrm{tr}}, \dot{\xi}, \dot{\boldsymbol{\varepsilon}}^{\mathrm{tr}})$, and the free energy function consists only of (thermo-)elastic and chemical terms.[6] Such a situation will naturally appear in the next chapter.

Ultimately, with respect to variety of proposed forms, it should be emphasised that "the exact form of the interaction energy remains an open problem" (Lexcellent et al., 2006). It shall be also noted that, due to their physical origins, a change of any of them owing to a change of internal variables is relatively small in comparison with the change of the (thermo-)elastic and chemical terms in the energy function caused by the same change of internal variables.

[6]These consideration poses a natural question of the physical origins of (contributions to) the dissipation within the polycrystalline SMA material, which to the author's knowledge has not been fully resolved yet.

Chapter 4

Description of the Constitutive Model

In this chapter, we will formulate a three-dimensional thermoemchanical constitutive model of SMA. We will follow the framework of GSM, introducing in turn internal variables describing the material, Helmholz free energy function and dissipation function, all motivated by experimental observations. We will derive a set of governing equations and formulate a quasi-static time-evolutionary problem of an SMA specimen under mechanical and temperature loading. In the last section, we propose an alternative way, how to derive (a particular part of) the dissipation function from a set of assumptions based on a simplified notion of martensitic structure evolution.

4.1 Description of state of the material; choice of internal variables

Adopting the small strain continuum mechanics formalism, the total strain, $\boldsymbol{\varepsilon}$, representing the total deformation of the material, and temperature, T, are chosen as state variables in present formulation. A general assumption of additivity of strains is adopted in the form:

$$\boldsymbol{\varepsilon} = \boldsymbol{\varepsilon}^{\mathrm{el}} + \boldsymbol{\varepsilon}^{\mathrm{in}}, \tag{4.1}$$

where $\boldsymbol{\varepsilon}^{\mathrm{el}}$ denotes the elastic contribution to the total strain of the material and $\boldsymbol{\varepsilon}^{\mathrm{in}}$ represents the inelastic strain related to changes of martensite structure which *can be fully released* by complete transformation to austenite.[1]

We choose a common way for description of martensite at macroscopic level (see Section 3.1), by one scalar internal variable, ξ, representing the volume fraction of martensite in the material and one tensorial variable, $\boldsymbol{\varepsilon}^{\mathrm{tr}}$, describing the mean transformation strain of martensite.

The inelastic strain is then given by relation:

$$\boldsymbol{\varepsilon}^{\mathrm{in}} = \xi \boldsymbol{\varepsilon}^{\mathrm{tr}}, \tag{4.2}$$

[1] As mentioned before, we do not include plasticity processes in the present formulation of the model.

The scalar variable, ξ, is naturally constrained as follows:

$$0 \leq \xi \leq 1. \tag{4.3}$$

In a reasonable approximation, the martensitic phase transformation preserves volume of NiTi SMA, therefore we put

$$\mathrm{tr}(\boldsymbol{\varepsilon}^{\mathrm{tr}}) = 0, \tag{4.4}$$

where $\mathrm{tr}(\boldsymbol{x})$ denotes the trace of a tensor $\boldsymbol{x}$.[2] There exists a maximum value of attainable transformation strain stemming from crystallographic considerations. Thus, the value of the mean transformation strain is assumed to lie in a bounded convex set defined by the following inequality:

$$\langle \boldsymbol{\varepsilon}^{\mathrm{tr}} \rangle \leq 1, \tag{4.5}$$

for some, positively 1-homogenous convex function $\langle \cdot \rangle : \mathbb{R}^{3\times 3} \to \mathbb{R}_0^+$ satisfying the condition $\langle \boldsymbol{\varepsilon}^{\mathrm{tr}} \rangle = 0 \Rightarrow \boldsymbol{\varepsilon}^{\mathrm{tr}} = 0$. Its particular form will be specified later. Note that the transformation strain is allowed to take *all* values within this convex set, which allows to capture effects such as formation of twinned martensite. By a particular choice of the function in the model tension-compression asymmetry and anisotropy of the material behavior will be captured in Chapter 6.

For description of R-phase, we introduce only one scalar variable, η, representing the volume fraction of R-phase within the material. A natural constraint reads as follows:

$$0 \leq \eta \leq 1 - \xi. \tag{4.6}$$

As a result of the above definitions, the actual volume fraction of austenite within the material is given by the difference $(1 - \xi - \eta)$. Introduction of η allows to simulate two important phenomena associated with the phase transition between austenite and R-phase – the dramatic change of elastic behavior and the distinct entropy change. However, we neglect the R-phase transformation strain. This simplification still leads to reasonable results since

- during early stage of austenite-to-R-phase transformation the change of elasticity associated with the austenite-to-R-phase transformation has a larger impact on the overall strain than the transformation strain of R-phase itself (Šittner et al., 2006),
- the R-phase transformation strain increase with decreasing temperature reaching in maximum roughly only 1/10 of the transformation strain of martensite (Lexcellent et al., 1994), whereas the change of entropy in austenite-to-R-phase transformation is about 1/3 of entropy change in austenite-to-martensite transformation. Thus, for the transformation driving forces the entropy change is dominant.

[2] Models taking into account effects related to relative volume change associated with phase transformation were presented by Qidwai and Lagoudas (2000*b*).

4.2 Formulation of Helmholtz free energy

To establish the specific free energy of a polycrystalline SMA material, f, a mechanistic decomposition to two dominating contributions, elastic energy, f^{el} and chemical energy, f^{chem}, is used[3]:

$$f = f^{\text{el}} + f^{\text{chem}}. \tag{4.7}$$

Following the general scheme summarized by Lagoudas et al. (2006), the rule of mixtures is employed to determine the free energy contributions f^{el} and f^{chem}, i.e. we consider a mixture of austenite, R-phase and martensite and the total value of the free energy contribution is considered as a weighted sum of the contributions of all phases. The respective phases – austenite, R-phase and martensite – are denoted by superscripts – ^{A},^{R} and ^{M} – in following.

Elastic energy

To derive the elastic energy contribution, we assume the polycrystalline material is elastically isotropic[4] with a homogeneous distribution of stresses in austenite, R-phase and martensite. Motivated by the work of Wagner and Windl (2008), the same bulk modulus, K, for all three phases is assumed and the total shear modulus of mixture, $G(\xi, \eta)$, is determined from the Reuss model, i.e.:

$$K = K^A = K^R = K^M, \tag{4.8}$$

$$\frac{1}{G(\xi,\eta)} = (1-\xi-\eta)\frac{1}{G^A} + \eta\frac{1}{G^R} + \xi\frac{1}{G^M}. \tag{4.9}$$

Let us note that this approach results in additive decomposition of the elastic strain into three parts corresponding to elastic strains of the three aforementioned phases.

Neglecting thermal expansion and considering condition (4.4), the elastic energy term follows:

$$f^{\text{el}}(\boldsymbol{\varepsilon}, \boldsymbol{\varepsilon}^{\text{tr}}, \xi, \eta) = \frac{1}{2}K\text{tr}(\boldsymbol{\varepsilon})^2 + G(\xi,\eta)\|\text{dev}(\boldsymbol{\varepsilon}) - \xi\boldsymbol{\varepsilon}^{\text{tr}}\|^2, \tag{4.10}$$

where $\text{dev}(\boldsymbol{x})$ denotes the deviatoric part of a tensor $\boldsymbol{x}$.

Chemical energy

We assume the chemical energy contribution in the following form

$$f^{\text{chem}}(T, \xi, \eta) = (1-\xi-\eta)f^A(T) + \eta f^R(T) + \xi f^M(T), \tag{4.11}$$

where $f^A(T)$, $f^R(T)$ and $f^M(T)$ are specific free energies of pure phases at stress-free conditions, respectively. Utilizing a standard form (e.g. Lexcellent et al.,

[3] Actually, we are motivated by the form of the free energy for a linear thermoelastic material. However, we will neglect the thermal expansion contribution, see Section 1.3

[4] To the author's knowledge, very limited experimental data related to the form of possible elastic anisotropy of textured polycrystalline SMA materials are available in the literature. Extension of the model to elastic anisotropy is straightforward.

2006; Panico and Brinson, 2007), assuming constant heat capacities c^i of individual phases, we may write:

$$f^i(T) = u_0^i - s_0^i T + c^i \left[(T - T_0) - T \ln\left(\frac{T}{T_0}\right) \right] \tag{4.12}$$

for $i \in \{A, R, M\}$. u_0^i and s_0^i denote the specific internal energy and entropy of the corresponding phase at some fixed temperature T_0. In our case, T_0 is chosen such that $f^A(T_0) = f^M(T_0)$ holds, i.e. $T_0 = \Delta u^{AM}/\Delta s^{AM}$ where $\Delta u^{AM} = u_0^A - u_0^M$ and $\Delta s^{AM} = s_0^A - s_0^M$. Expanding the right-hand side of Eq. (4.11), f^{chem} reads:

$$\begin{aligned} f^{\text{chem}}(T, \xi, \eta) \;=\; & u_0^A - s_0^A T + c^A \left[(T - T_0) - T \ln\left(\frac{T}{T_0}\right) \right] \\ & \underbrace{- (\Delta c^{AM} \xi + \Delta c^{AR} \eta) \left[(T - T_0) - T \ln\left(\frac{T}{T_0}\right) \right]}_{(\star)} \\ & + \Delta s^{AM} (T - T_0) \xi + \Delta s^{AR} (T - T_0^R) \eta, \end{aligned} \tag{4.13}$$

where $\Delta s^{AR} = s_0^A - s_0^R$, $\Delta c^{AM} = c^A - c^M$ and $\Delta c^{AR} = c^A - c^R$. It is known that $\Delta c^{AM} \ll \Delta s^{AM}$. We make the same assumption on the relation between Δc^{AR} and Δs^{AR}, thus, we can neglect the term $(\star)$. In Eq. (4.13), $T_0^R = \Delta u^{AR}/\Delta s^{AR}$ is, due to the previous assumption, close to the equilibrium austenite-R-phase temperature. To account for a possibly wide temperature range in which the austenite-to-R-phase transformation takes place, T_0^R is considered to depend (in first approximation linearly) on the concentration of R-phase in austenite, $\eta/(1-\xi)$, i.e.

$$T_0^R(\xi, \eta) := R_{\text{s}} + \frac{\eta}{1 - \xi} \frac{R_{\text{f}} - R_{\text{s}}}{2}, \tag{4.14}$$

where R_{s} and R_{f} denote the initial and final temperature of the transformation from austenite to R-phase, i.e. $R_{\text{s}} > R_{\text{f}}$.

4.3 Derivation of dissipation function

As already mentioned, we consider the formulation of the dissipative mechanism to be of key importance in SMA model derivation and hence it is given a special attention here.

Since the phase transformation between austenite and R-phase has a very narrow hysteresis, we *neglect* the associated dissipation. Moreover, it is assumed that the same amount of energy is dissipated when austenite transforms to martensite through R-phase as when it transforms directly. Thus, the dissipation function will not depend on variables η and $\dot{\eta}$, i.e.

$$d = d(T, \boldsymbol{\varepsilon}^{\text{tr}}, \xi, \dot{\boldsymbol{\varepsilon}}^{\text{tr}}, \dot{\xi}). \tag{4.15}$$

In following, the dissipation function will be sequentially formulated by considering several loading cases. First, we consider special loading processes for which only one internal variable evolves. These findings are generalized to the coupled evolution, then.

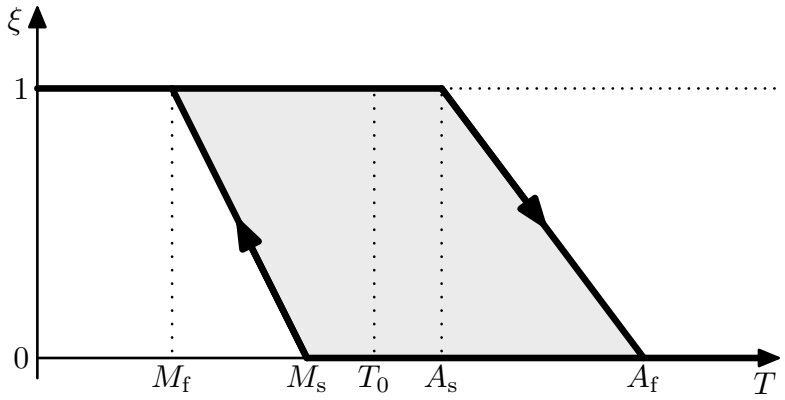

Figure 4.1: The evolution of volume fraction of martensite with temperature under stress-free condition when only the transformation dissipation is considered in the model.

Dissipation during stress free thermal cycles

During cooling, martensite phase transformation starts at temperature M_s and finishes at M_f. The reverse transformation occurs in a temperature range from A_s to A_f. To capture this transformation hysteresis, we propose a simple dissipation function in the form

$$\dot{\xi} \geq 0: \quad d^{\mathrm{tr}} = \Delta s^{AM}[(T_0 - M_s) + \xi(M_s - M_f)]\dot{\xi}, \tag{4.16}$$

$$\dot{\xi} < 0: \quad d^{\mathrm{tr}} = \Delta s^{AM}[(T_0 - A_f) + \xi(A_f - A_s)]\dot{\xi}. \tag{4.17}$$

Such a type of transformation dissipation was analytically studied by Bernardini and Pence (2002) (see the model M2 there). Proposed form sets the appropriate transformation temperatures for initialisation and termination of transformation process under stress-free condition and leads to a linear evolution of volume fraction of martensite in between, see Fig. 4.1.

Dissipation during mechanical loading in full martensite state

The dissipation by reorientation of martensite is related to moving of twin interfaces and can be described similarly as plastic deformation. Adapting von Mises plasticity-type term leads to:

$$d = \sigma^{\mathrm{reo}} \|\dot{\boldsymbol{\varepsilon}}^{\mathrm{in}}\|, \tag{4.18}$$

where σ^{reo} is the reorientation stress measured in tension multiplied by $\sqrt{\frac{3}{2}}$.

It is usually experimentally observed (see dash line in Fig. 4.2) that the stress needed for initialization of martensite reorientation decreases with increasing temperature; this is probably related to changes of mobility of twin boundaries with temperature. We included this phenomenon by assuming parameter σ^{reo} to be a decreasing linear function of temperature in the temperature range of interest, i.e.

$$\sigma^{\mathrm{reo}} \equiv \sigma^{\mathrm{reo}}(T) = \sigma_0^{\mathrm{reo}} + \Sigma^{\mathrm{reo}}\,(T - T_0), \tag{4.19}$$

where σ_0^{reo} and Σ^{reo} are material parameters.

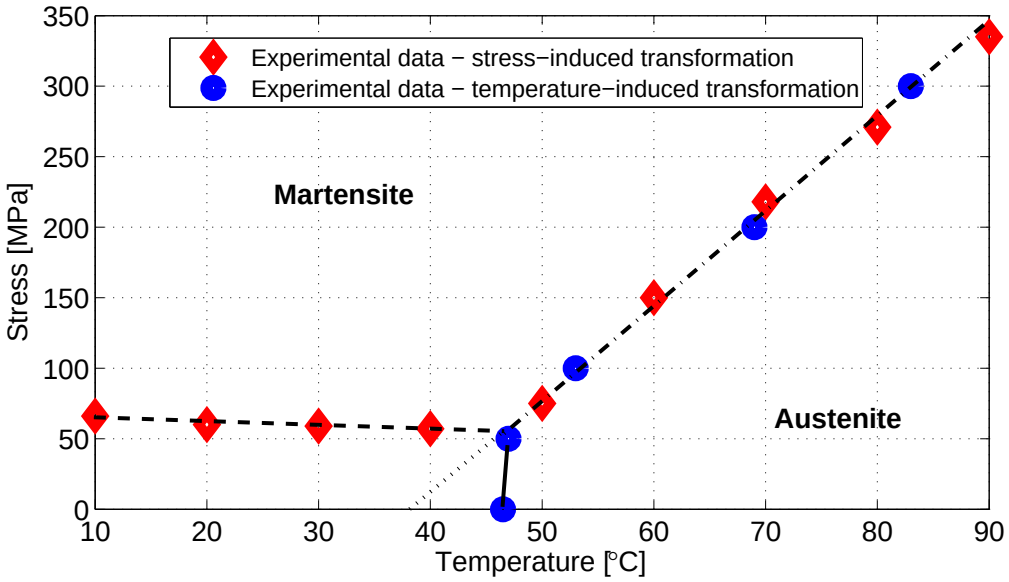

Figure 4.2: Stress-temperature phase diagram for forward transformation and martensite reorientation. Experimental transformation stresses obtained from results of loading at constant temperature are marked by diamonds, transformation temperatures obtained from results of cooling at constant load by circles. See text for details.

Dissipation during austenite-to-martensite transformation under general stress and temperature change

The description of the dissipation mechanism in forward transformation was motivated by several experimental stress-temperature phase diagrams on NiTi-based SMA.

A typical one is shown in Fig. 4.2 (compiled from results published by Frost et al., 2010, measurements were performed on a trained NiTiCu memory wire with $A_\mathrm{f} = 65\,^\circ\mathrm{C}$ and $M_\mathrm{s} = 47\,^\circ\mathrm{C}$). Note that from this phase diagram we may, in particular, deduce the following points:

1. We need not to distinguish between stress- and temperature-induced transformation. Indeed, assume that the material held at a constant temperature T^* transforms to martensite when the applied stress reaches the value σ^*. Then, when the material is held at the stress σ^*, it will transform to martensite at temperature T^*.

2. The transformation temperature of the forward transformation depends linearly (cf. dash-dot line in Fig. 4.2) on the external tensile stress provided this *stress is higher than* σ^{reo}. Moreover, in this case, the slope of the phase boundary is predictable from the Clausius-Clapeyron relation. Thus, we can assume that the dissipation during this process is independent or "weakly" linearly dependent on the applied temperature/stress.

3. For *stress lower than* σ^{reo}, the transformation temperature is almost independent of the applied stress (cf. solid line in Fig. 4.2). Martensite formed under such stress appears in a twinned form with negligible transformation

strain. Dissipation for transformation at a stress lower then σ^{reo} is thus described by Eq. (4.16).

4. There is no discontinuity of the transformation temperature *at stress* σ^{reo}. This observation is consistent with the assumption of existence of the so-called "triple point" in the stress-temperature phase diagram made by several authors (e.g. Juhasz et al., 2002; Lexcellent et al., 2006). This implies that the energy dissipated in forward transformation at stresses higher than σ^{reo} is raised only by a contribution due to martensite reorientation.

These observations are consistent with the following formulation of dissipation in forward transformation:

$$\begin{aligned} \dot{\xi} \geq 0 \;\Rightarrow\; d(T, \boldsymbol{\varepsilon}^{\mathrm{tr}}, \xi, \dot{\boldsymbol{\varepsilon}}^{\mathrm{tr}}, \dot{\xi}) &= \Delta s^{AM}[(T_0 - M_{\mathrm{s}}) + \xi(M_{\mathrm{s}} - M_{\mathrm{f}})]\dot{\xi} \\ &\quad + \sigma^{\mathrm{reo}} \|\dot{\boldsymbol{\varepsilon}}^{\mathrm{in}}\| \\ &= \Delta s^{AM}[(T_0 - M_{\mathrm{s}}) + \xi(M_{\mathrm{s}} - M_{\mathrm{f}})]\dot{\xi} \\ &\quad + \sigma^{\mathrm{reo}} \|\dot{\xi}\boldsymbol{\varepsilon}^{\mathrm{tr}} + \xi\dot{\boldsymbol{\varepsilon}}^{\mathrm{tr}}\| \end{aligned} \tag{4.20}$$

Indeed, note that in a process in which austenite transforms to self-accommodated martensite, during which the change of the inelastic strain is negligible, essentially only the term $\Delta s^{AM}[(T_0 - M_{\mathrm{s}}) + \xi(M_{\mathrm{s}} - M_{\mathrm{f}})]\dot{\xi}$ in (4.42) is important; this is consistent with point 3. above. If it is not the case, then the term $\sigma^{\mathrm{reo}}\|\dot{\boldsymbol{\varepsilon}}^{\mathrm{in}}\|$, corresponding to martensite reorientation, contributes to the dissipation as well (consistently with point 4 above).

Dissipation during martensite to austenite transformation under general stress and temperature change

Dissipation in the martensite-to-austenite transformation cannot be simply described by (4.17) because the dissipated energy must depend on the actual transformation strain of martensite. Direct experimental evidence of this fact is the "martensite stabilization", see Section 1.3. Experiments by Liu and Favier (2000) show that with increasing martensite deformation the reverse transformation temperature increases, too. Based on these results, we suggest to describe this additional dissipation by the term

$$d^{\mathrm{rev}} = \sigma^{\mathrm{reo}}|\dot{\xi}|\,\|\boldsymbol{\varepsilon}^{\mathrm{tr}}\|. \tag{4.21}$$

Note that, $\sigma^{\mathrm{reo}}\|\boldsymbol{\varepsilon}^{\mathrm{tr}}\|$ is the minimal energy needed for previous reorientation of the disappearing martensite. As shown in Fig. 4.3, simulations based on the assumption correspond well to experimental data by Liu and Favier (2000).

Therefore, in the general case of reverse transformation including stress-induced evolution of martensite, one obtains the following expression of dissipation:

$$\begin{aligned} \dot{\xi} < 0 \;\Rightarrow\; d(T, \boldsymbol{\varepsilon}^{\mathrm{tr}}, \xi, \dot{\boldsymbol{\varepsilon}}^{\mathrm{tr}}, \dot{\xi},) &= \Delta s^{AM}[(T_0 - A_{\mathrm{f}}) + \xi(A_{\mathrm{f}} - A_{\mathrm{s}})]\dot{\xi} \\ &\quad + \sigma^{\mathrm{reo}} \left[|\dot{\xi}|\,\|\boldsymbol{\varepsilon}^{\mathrm{tr}}\| + \xi\,\|\dot{\boldsymbol{\varepsilon}}^{\mathrm{tr}}\| \right], \\ &= \Delta s^{AM}[(T_0 - A_{\mathrm{f}}) + \xi(A_{\mathrm{f}} - A_{\mathrm{s}})]\dot{\xi} \\ &\quad + \sigma^{\mathrm{reo}} \left[\|\frac{\dot{\xi}}{\xi}\boldsymbol{\varepsilon}^{\mathrm{in}}\| + \|\dot{\boldsymbol{\varepsilon}}^{\mathrm{in}} - \frac{\dot{\xi}}{\xi}\boldsymbol{\varepsilon}^{\mathrm{in}}\| \right], \end{aligned} \tag{4.22}$$

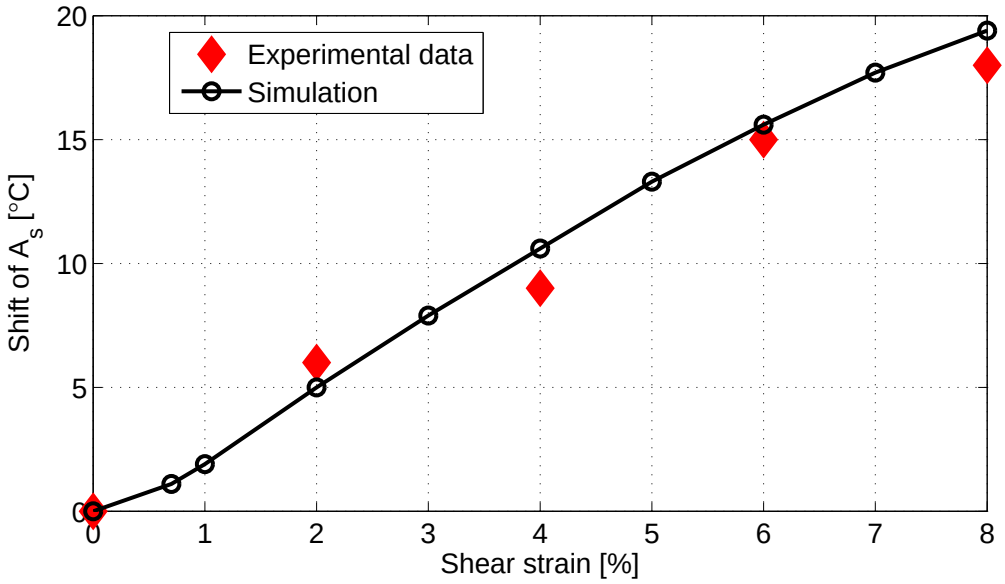

Figure 4.3: Data from simulation and experiment of the martensite stabilization effect induced by shear predeformation. The shift of A_s temperature was computed with respect to A_s of the undeformed specimen. Input parameters for simulations adopted from (Liu and Favier, 2000).

where term $\sigma^{\mathrm{reo}}|\dot{\xi}|\,\|\boldsymbol{\varepsilon}^{\mathrm{tr}}\|$ corresponds to the martensite stabilization (as described above), whereas term $\sigma^{\mathrm{reo}}\xi\,\|\dot{\boldsymbol{\varepsilon}}^{\mathrm{tr}}\|$ captures the dissipation due to possible reorientation of the remaining (not yet transformed) martensite (cf. Eq. (4.18)).

Final remarks on the dissipation function

(a) The form of proposed dissipation function was developed based on experimental stress-strain-temperature records reflecting the progress of transformation in dependence on temperature and stress. An possible alternative view on it is introduced in Section 4.5.

(b) The dissipation function is *asymmetric* from the point of view of the forward/reverse relation (cf. (4.45) and (4.42)). Moreover, due to coupling of internal variables in forward transformation (see (4.42)) it is *in general* not possible to split the dissipation potential into two additive terms corresponding to time evolution of variables $\dot{\xi}$ and $\dot{\boldsymbol{\varepsilon}}^{\mathrm{tr}}$, respectively. This is in a pronounced contrast to separation of the two processes commonly used in SMA modeling.

(c) It is apparent that the derived dissipation function is non-negative, 1-homogeneous in the rate of internal variables $(\dot{\boldsymbol{\varepsilon}}^{\mathrm{tr}}, \dot{\xi})$ and it is equal to zero, when the rates are zero. Since it is also convex in the rate variables (see proof of Proposition 5.2.2), we may employ the result in Section 2.3 and conclude that the *Clausius-Duhem inequality* is fulfilled.

4.4 Governing equations

A standard formulation of the model is finished by explicit specification of the governing equations, which are usually used in numerical procedures.

Making use of relation (4.2), the derived free energy function and dissipation function take the form:

$$\begin{aligned} f(T,\boldsymbol{\varepsilon},\boldsymbol{\varepsilon}^{\mathrm{in}},\xi,\eta) &= \frac{1}{2}K\mathrm{tr}(\boldsymbol{\varepsilon})^2 + G(\xi,\eta)\|\mathrm{dev}(\boldsymbol{\varepsilon}) - \boldsymbol{\varepsilon}^{\mathrm{in}}\|^2 \\ &\quad + \Delta s^{AM}(T-T_0)\xi + \Delta s^{AR}(T - T_0^R(\xi,\eta))\eta \\ &\quad + u_0^A - s_0^A T + c^A\left[(T-T_0) - T\ln\left(\frac{T}{T_0}\right)\right] \end{aligned} \tag{4.23}$$

$$d(T,\boldsymbol{\varepsilon}^{\mathrm{in}},\xi,\dot{\boldsymbol{\varepsilon}}^{\mathrm{in}},\dot{\xi}) = \begin{cases} \Delta s^{AM}[T_0 - M_{\mathrm{s}} + \xi(M_{\mathrm{s}} - M_{\mathrm{f}})]\dot{\xi} \\ \quad + \sigma^{\mathrm{reo}}(T)\|\dot{\boldsymbol{\varepsilon}}^{\mathrm{in}}\| & \text{if } \dot{\xi} \geq 0 \\ \Delta s^{AM}[T_0 - A_{\mathrm{f}} + \xi(A_{\mathrm{f}} - A_{\mathrm{s}})]\dot{\xi} \\ \quad + \sigma^{\mathrm{reo}}(T)\left[\|\frac{\dot{\xi}}{\xi}\boldsymbol{\varepsilon}^{\mathrm{in}}\| + \|\dot{\boldsymbol{\varepsilon}}^{\mathrm{in}} - \frac{\dot{\xi}}{\xi}\boldsymbol{\varepsilon}^{\mathrm{in}}\|\right] & \text{if } \dot{\xi} < 0 \end{cases} \tag{4.24}$$

In order to satisfy constraints (4.3), (4.5) and (4.6), one may introduce the indicator function $\mathcal{I}(\boldsymbol{\varepsilon}^{\mathrm{in}},\xi,\eta)$:

$$\mathcal{I}(\boldsymbol{\varepsilon}^{\mathrm{in}},\xi,\eta) = \begin{cases} 0 & \text{if} \quad 0 \leq \xi \leq 1,\ 0 \leq \eta \leq 1-\xi \quad \text{and} \quad \langle\boldsymbol{\varepsilon}^{\mathrm{in}}\rangle \leq \xi, \\ +\infty & \text{else,} \end{cases} \tag{4.25}$$

and subsequent reformulation of the free energy function as follows:

$$\mathcal{F}(T,\boldsymbol{\varepsilon},\boldsymbol{\varepsilon}^{\mathrm{in}},\xi,\eta) = f(T,\boldsymbol{\varepsilon},\boldsymbol{\varepsilon}^{\mathrm{in}},\xi,\eta) + \mathcal{I}(\boldsymbol{\varepsilon}^{\mathrm{in}},\xi,\eta). \tag{4.26}$$

Repeating standard thermodynamic arguments introduced in Chapter 2, the generalized thermodynamic forces π, P and $\boldsymbol{X}$ associated to the internal variables ξ, η and $\boldsymbol{\varepsilon}^{\mathrm{in}}$, respectively, may be derived:

$$\boldsymbol{\sigma} = \frac{\partial\mathcal{F}}{\partial\boldsymbol{\varepsilon}} = K\mathrm{tr}(\boldsymbol{\varepsilon})\boldsymbol{I} + 2G(\xi,\eta)(\mathrm{dev}(\boldsymbol{\varepsilon}) - \boldsymbol{\varepsilon}^{\mathrm{in}}), \tag{4.27}$$

$$s = -\frac{\partial\mathcal{F}}{\partial T} = s_0^A + c^A\ln\left(\frac{T}{T_0}\right) - \Delta s^{AM}\xi - \Delta s^{AR}\eta, \tag{4.28}$$

$$\boldsymbol{X} = -\frac{\partial\mathcal{F}}{\partial\boldsymbol{\varepsilon}^{\mathrm{in}}} = 2G(\xi,\eta)(\mathrm{dev}(\boldsymbol{\varepsilon}) - \boldsymbol{\varepsilon}^{\mathrm{in}}) - \partial_{\boldsymbol{\varepsilon}^{\mathrm{in}}}\mathcal{I}(\boldsymbol{\varepsilon}^{\mathrm{in}},\xi,\eta), \tag{4.29}$$

$$\begin{aligned} \pi = -\frac{\partial\mathcal{F}}{\partial\xi} &= -2\frac{\partial G(\xi,\eta)}{\partial\xi}\|\mathrm{dev}(\boldsymbol{\varepsilon}) - \boldsymbol{\varepsilon}^{\mathrm{in}}\|^2 - \Delta s^{AM}(T-T_0) \\ &\quad + \Delta s^{AR}\frac{\partial T_0^R(\xi,\eta)}{\partial\xi}\eta - \partial_\xi\mathcal{I}(\boldsymbol{\varepsilon}^{\mathrm{in}},\xi,\eta), \end{aligned} \tag{4.30}$$

$$\begin{aligned} P = -\frac{\partial\mathcal{F}}{\partial\eta} &= -2\frac{\partial G(\xi,\eta)}{\partial\eta}\|\mathrm{dev}(\boldsymbol{\varepsilon}) - \boldsymbol{\varepsilon}^{\mathrm{in}}\|^2 + \Delta s^{AR}\frac{\partial T_0^R(\xi,\eta)}{\partial\eta}\eta \\ &\quad - \Delta s^{AR}(T - T_0^R(\xi,\eta)) - \partial_\eta\mathcal{I}(\boldsymbol{\varepsilon}^{\mathrm{in}},\xi,\eta), \end{aligned} \tag{4.31}$$

$\partial_\alpha\mathcal{I}$ denoting the subderivative of the indicator function with respect to the variable α, see Appendix.

Now let us consider an SMA body occupying a domain $\Omega \subset \mathbb{R}^3$ in space. Our aim is to determine the evolution of the system in time t within a time interval $[0,\mathcal{T}]$. We suppose

- the influence of inertia may be neglected, i.e. quasistatic approximation, and
- temperature field $T(t)$ is prescribed within all the body over the whole time interval, i.e. approximation of isothermal processes.

Next,

- volume forces, $F_{\mathrm{vol}}(t)$, acting within the body,
- surface forces, $F_{\mathrm{surf}}(t)$, acting over a body surface Γ_{N},
- displacement, $U(t)$, on the rest of the body surface, Γ_{D},

are also supposed to be prescribed within the time interval as well as

- initial values of internal variables, $\boldsymbol{\varepsilon}^{\mathrm{in}}(0), \xi(0), \eta(0)$, and displacement, $u(0)$, prescribed within the whole body.

Under this conditions, we assume the evolution is fully resolved if time evolution of displacement, $u(t)$, and internal variables, $\boldsymbol{\varepsilon}^{\mathrm{in}}(t), \xi(t), \eta(t)$, are known.

Utilizing constitutive relations developed within the framework of GSM in Section 2.3, the problem can be formulated as follows (cf. (2.25) and (2.26)):

$$
\begin{aligned}
-\mathrm{div}\,(\boldsymbol{\sigma}(t)) &= F_{\mathrm{vol}}(t) && \text{in } \Omega, && (4.32)\\
\boldsymbol{\sigma}(t)n &= F_{\mathrm{surf}}(t) && \text{on } \Gamma_{\mathrm{N}}, && (4.33)\\
u(t) &= U(t) && \text{on } \Gamma_{\mathrm{D}}, && (4.34)\\
\boldsymbol{X}(t) &\in \partial_{\dot{\boldsymbol{\varepsilon}}^{\mathrm{in}}} d(t) && \text{in } \Omega, && (4.35)\\
\pi(t) &\in \partial_{\dot{\xi}} d(t) && \text{in } \Omega, && (4.36)\\
N(t) &= 0 && \text{in } \Omega, && (4.37)
\end{aligned}
$$

along with initial conditions

$$
u(0) = u_0,\ \boldsymbol{\varepsilon}^{\mathrm{in}}(0) = \boldsymbol{\varepsilon}^{\mathrm{in}}_0,\ \xi(0) = \xi_0,\ \eta(0) = \eta_0 \text{ in } \Omega, \qquad (4.38)
$$

where we remind the relation $\boldsymbol{\varepsilon}(t) = \frac{1}{2}(\nabla u(t) + (\nabla u(t))^{\top})$.

An natural discrete analogy to dissipation function in case of rate-independent framework of energetic solutions (e.g. Francfort and Mielke, 2006; Mielke et al., 2002, see the next chapter for details) is *dissipation distance*, δ. It measures the dissipated energy between two arbitrary chosen physical states of a material in the following sense: Let us consider a time increment with a small change between an initial and a final internal variables state denoted by α_A and α_B, respectively. Then the dissipated energy between α_A and α_B is given by dissipation distance $\delta(\alpha_A, \alpha_B)$.

When we introduce the dissipation distance as follows

$$
\delta(T, \boldsymbol{\varepsilon}^{\mathrm{in}}_A, \xi_A, \boldsymbol{\varepsilon}^{\mathrm{in}}_B, \xi_B) = \begin{cases} \Delta s^{AM}[T_0 - M_{\mathrm{s}} + \xi(M_{\mathrm{s}} - M_{\mathrm{f}})]|\xi_B - \xi_A| \\ \quad + \sigma^{\mathrm{reo}}(T)\|\boldsymbol{\varepsilon}^{\mathrm{in}}_B - \boldsymbol{\varepsilon}^{\mathrm{in}}_A\| & \text{if } \xi_B \geq \xi_A, \\ \Delta s^{AM}[A_{\mathrm{f}} - T_0 + \xi(A_{\mathrm{s}} - A_{\mathrm{f}})]|\xi_B - \xi_A| \\ \quad + \sigma^{\mathrm{reo}}(T)\left[\|\frac{\xi_B}{\xi_A}\boldsymbol{\varepsilon}^{\mathrm{in}}_A\| + \|\boldsymbol{\varepsilon}^{\mathrm{in}}_B - \boldsymbol{\varepsilon}^{\mathrm{in}}_A - \frac{\xi_B}{\xi_A}\boldsymbol{\varepsilon}^{\mathrm{in}}_A\|\right] & \text{if } \xi_B < \xi_A, \end{cases} \qquad (4.39)
$$

then, making profit of following relation (see Mielke, 2006)

$$d(\alpha, \dot{\alpha}) = \lim_{\epsilon \to 0} \frac{1}{\epsilon} \delta(\alpha, \alpha + \epsilon \dot{\alpha}), \tag{4.40}$$

it is easy to verify, that the dissipation distance actually correspond to the dissipation functions defined in previous sections.

Prior to mathematical treatment of the model, where the dissipation distance will be employed, we introduce an alternative approach for its derivation.

4.5 Alternative approach to derivation of the proposed dissipation function

In this section, we introduce a set of assumptions which may be used to derivation of explicit forms of dissipated energy when the material transits between two states with a different phase fraction and/or a different state of martensite structure. The assumptions are based on a simplified modeling notion of evolution of the internal structure of the material during the transformation processes. However, it should be emphasised that the real situation in polycrystals is very complex, since many different physical phenomena on various levels come into the play. Thus, proposed modeling notion must be considered as a useful, albeit not rigorous enough (in the sense of physics) approximation.

There are two main reasons, why such an approach is introduced in this work:

- based on the proposed notion, we may formulate a set of several modeling assumptions which lead to a an explicit form of the energy dissipated between two different material states,
- the link between the assumptions and the resulting formulas is clear and easy to understand,
- we directly obtain the formulation in terms of *dissipation distance*.

Within this section, the ideas will be first presented in form of five assumptions mainly supported by some physical observations. These assumptions will be then used for derivation of the reorientation dissipation distance.

Assumptions of a two-step transformation

During a forward MT a specific form of internal structure of martensite which is compatible with the structure of austenite must be formed nearby the phase interface (Otsuka and Ren, 2005). Requirements of crystallographic coherence between the parent phase and the product phase impose some conditions on the crystallographic structure of the formed martensite and application of an external load leads to further (usually complex) evolution of this structure. Extending this observation for any material element, we formulate the first assumption as follows:

(A1) *Austenite transforms to martensite always through formation of transformation favorable martensite (TFM) structure. This structure has zero macroscopic strain at the moment of creation and its possible reorientation depends on applied external stress.*

We once again recall a series of experiments on a NiTiCu alloy carried out in Frost et al. (2010), which were used for construction of the stress-temperature phase diagram in Fig. 4.2. There, transformation from austenite to a reoriented martensite was initiate both by cooling a specimen and subsequent loading and by loading it and subsequent cooling. It was observed that the strain achieved in both cases was the same. Based on this observation, we assume that there are two separated processes involved in the experiments. The first one is the phase transformation from austenite to a specific form of martensite which exhibits no macroscopic strain and which is called *transformation favourable martensite* (TFM). The second considered process is a subsequent structure evolution of martensite stimulated by an applied external load. Thus, one assumes that cooling of the (initially austenitic) SMA at constant applied load occurs by concurrent formation of TFM with zero macroscopic strain and evolution of the structure of entire martensite. The evolution is macroscopically demonstrated by the mean strain evolution.

The idea of TFM is now extended to the reverse transformation, i.e. we suppose that TFM is also always present during disappearance of martensite:

(A2) *A necessary condition for initialisation of a reverse transformation in any amount of martensite is formation of TFM within it.*

The formulation emphasizes that if the actual structure of martensite does not meet the requirement of TFM, then the structure of the disappearing martensite is *adjusted first*; only then the reverse transformation may proceed.

Now we can assign two additive contributions to dissipation during thermomechanical loading of SMAs. The first one is connected with phase transformation between austenite and TFM and we call it transformation part of dissipation. The second contribution is connected to structure evolution of martensite and it is called reorientation part of dissipation. d^{tr} is assumed to be given by formulas (4.16) and (4.17) and it is not further discussed in this section.

Together, we established contributions to the irreversible transformation energy mentioned by Liu and Favier, see Subsection 1.2, and we can attempt to reinterpret their experimental observations within our simple concept in the following way:

(a) To start the reverse transformation in a deformed specimen a TFM structure must be formed first. To initiate this process, a higher driving force for reorientation must be reached with respect to undeformed specimen, which is demonstrated by higher value of critical temperature for start of the reverse transformation. Moreover, an additional energy must be dissipated due to formation of more TFM. Thus, the total transformation heat is increased by the contribution of reorientation dissipation.

(b) Increasing amount of reoriented martensite transforming to TFM implies increase in reorientation dissipation. As a direct consequence, the total transformation heat increases with increasing deformation.

(c) After cooling, the TFM structure is formed and the response of the sample in subsequent cycles coincides with the response prior to the deformation.

To sum up, as proposed in Assumptions (A1) and (A2), we assume that it is possible to split the martensite formation or disappearance during MT into two processes, no matter if induced by temperature, stress or both of them.

Assumption of a linear dependence of dissipation on transformation strain difference

In this notion, a natural way for description of martensite at the macroscopic level is the mean transformation strain of martensite, $\boldsymbol{\varepsilon}^{\mathrm{tr}}$, and martensite volume fraction, ξ, as introduced in Section 4.1. We suppose that in a good approximation, the dissipation is proportional to the (norm of) difference between transformation strain states.

(A3) *If an amount of martensite is subject to reorientation, the corresponding dissipation distance is proportional to the norm of the difference between its initial and final transformation strain.*

Assumption of the inelastic strain of mixture

We make an assumption on the state of mixture of reoriented martensite and TFM when forward phase transformation is in progress:

(A4) *At the moment of formation of TFM at presence of some reoriented martensite, the emerging mixture preserves the inelastic strain of the present martensite.*

Hence, we suppose that the transformation strain is distributed homogenously when the mixture is formed.

Assumption of temperature dependence of dissipation

Let us now recall a simplified SMA stress-temperature phase diagram in Figure 1.1. As noted in Section 1.2, decreasing dependence of stress needed for initialisation of martensite reorientation (at constant temperature) on temperature is often observed. The phase boundaries (solid lines in the figure) are diverging, which indicates that the total dissipated energy in a completed transformation cycle is lower at higher temperatures.

Based on these observations, an assumption of temperature dependence of dissipation is expressed as follows:

(A5) *Dissipation accompanying reorientation processes is temperature-dependent.*

Reorientation part of the dissipation function

In order to derive the reorientation-induced dissipation, we now follow the assumptions formulated above. We suppose that the material evolves from an initial thermomechanical state, A, to a terminal state, B, and distinguish corresponding variables by subscripts.

When austenite to martensite transformation occurs (i.e. $\xi_A < \xi_B$), a mixture of present martensite and newly appearing TFM is formed. Due to Assumption

(A4), at the moment of formation, the mixture preserves the inelastic strain of the present martensite. The mean transformation strain of the mixture reads

$$\boldsymbol{\varepsilon}^{\mathrm{tr}}_{\mathrm{mix}} := \frac{\boldsymbol{\varepsilon}^{\mathrm{tr}}_A \xi_A}{\xi_B} \tag{4.41}$$

Depending on the external conditions, the whole mixture can change the inelastic strain immediately. The dissipation distance between the two states takes the following form:

$$\begin{aligned}\delta^{\mathrm{reo}}(\boldsymbol{\varepsilon}_A, \xi_A, \boldsymbol{\varepsilon}_B, \xi_B) &= \sigma^{\mathrm{reo}}(T_B)\xi_B \|\boldsymbol{\varepsilon}^{\mathrm{tr}}_B - \boldsymbol{\varepsilon}^{\mathrm{tr}}_{\mathrm{mix}}\| = \sigma^{\mathrm{reo}}(T_B)\xi_B \|\boldsymbol{\varepsilon}^{\mathrm{tr}}_B - \frac{\boldsymbol{\varepsilon}^{\mathrm{tr}}_A \xi_A}{\xi_B}\| \\ &= \sigma^{\mathrm{reo}}(T_B)\|\xi_B \boldsymbol{\varepsilon}^{\mathrm{tr}}_B - \xi_A \boldsymbol{\varepsilon}^{\mathrm{tr}}_A\|, \end{aligned} \tag{4.42}$$

where $\sigma^{\mathrm{reo}}(T)$ represents the dependence of stress needed for initialisation of martensite reorientation on temperature as proposed in Assumption (A5). An analogous consideration leads to extending the definition also for pure reorientation, i.e. $\xi_B = \xi_A$.

When martensite disappears (i.e. $\xi_A > \xi_B$), the disappearing and remaining martensite shall be treated separately. In line with Assumption (A2), disappearing martensite forms TFM, which is characterised by zero mean transformation strain. Thus, considering the temperature dependence as above, the dissipation distance reads

$$\begin{aligned}\delta^{\mathrm{reo}}_1(\boldsymbol{\varepsilon}_A, \xi_A, \boldsymbol{\varepsilon}_B, \xi_B) &= \sigma^{\mathrm{reo}}(T_B)\|(\xi_B - \xi_A)\boldsymbol{\varepsilon}^{\mathrm{tr}}_A - \mathbf{0}\| \\ &= \sigma^{\mathrm{reo}}(T_B)|\xi_B - \xi_A|\,\|\boldsymbol{\varepsilon}^{\mathrm{tr}}_A\|. \end{aligned} \tag{4.43}$$

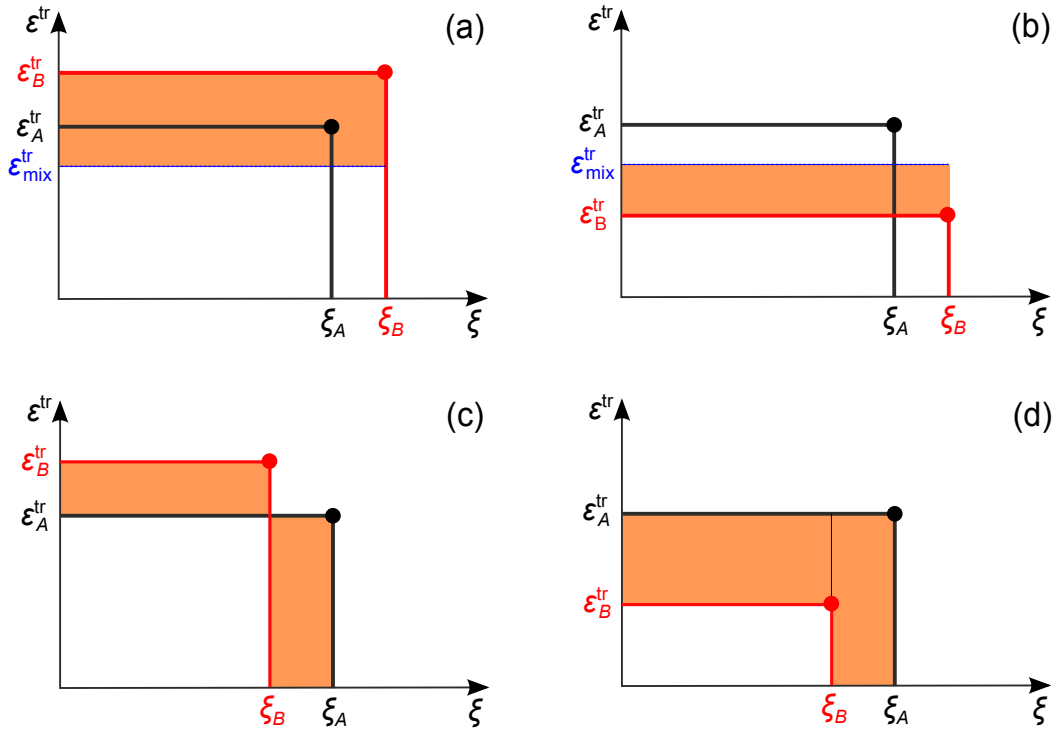

Figure 4.4: Dissipation schema when one-dimensional internal variable $\varepsilon^{\mathrm{tr}}$ is considered. a) $\xi_A \leq \xi_B$ and $\varepsilon^{\mathrm{tr}}_A \leq \varepsilon^{\mathrm{tr}}_B$, b) $\xi_A \leq \xi_B$ and $\varepsilon^{\mathrm{tr}}_A > \varepsilon^{\mathrm{tr}}_B$, c) $\xi_A > \xi_B$ and $\varepsilon^{\mathrm{tr}}_A \leq \varepsilon^{\mathrm{tr}}_B$, d) $\xi_A > \xi_B$ and $\varepsilon^{\mathrm{tr}}_A > \varepsilon^{\mathrm{tr}}_B$. Value of the reorientation part of the dissipation distance for $\sigma^{\mathrm{reo}} = 1$ is equal to the shaded areas in each picture.

Moreover, the remaining martensite can reorient, which adds the second term

$$\delta_2^{\mathrm{reo}}(\boldsymbol{\varepsilon}_A, \xi_A, \boldsymbol{\varepsilon}_B, \xi_B) = \sigma^{\mathrm{reo}}(T_B)\xi_B \|\boldsymbol{\varepsilon}_B^{\mathrm{tr}} - \boldsymbol{\varepsilon}_A^{\mathrm{tr}}\|. \tag{4.44}$$

The total dissipation is then given by the sum

$$\delta^{\mathrm{reo}}(\boldsymbol{\varepsilon}_A, \xi_A, \boldsymbol{\varepsilon}_B, \xi_B) = \sigma^{\mathrm{reo}}(T_B) \left[\|(\xi_B - \xi_A)\boldsymbol{\varepsilon}_A^{\mathrm{tr}}\| + \xi_B \|\boldsymbol{\varepsilon}_B^{\mathrm{tr}} - \boldsymbol{\varepsilon}_A^{\mathrm{tr}}\| \right]. \tag{4.45}$$

In a simple illustrative case in which transformation strain tensor is reduced to a scalar, one can sketch a simple two-dimensional "dissipation" schema, see Fig. 4.4. The reorientation part of the dissipation distance for $\sigma^{\mathrm{reo}} = 1$ is then represented by the areas shaded in the picture.

If we now suppose that σ^{reo} in the form (4.19) and employ the relation $\boldsymbol{\varepsilon}^{\mathrm{in}} = \xi\boldsymbol{\varepsilon}^{\mathrm{tr}}$, we obtain exactly the terms for the reorientation dissipation distance in (4.39). However, we note again that the treatment of this section is in no way intended as a *justification* of the dissipation function introduced in Section 4.3.

Chapter 5

Mathematical Analysis of the Constitutive Model

In this chapter, we will utilize the mathematical theory for rate-dependent processes developed and continuously extended by A. Mielke and coworkers in the last two decades (e.g. Mielke et al., 2009; Mielke and Theil, 2004; Mielke et al., 2002). The theory is based on the concept of so-called *energetic solutions*. Loosely speaking, such a solution is required to satisfy the first law of thermodynamic in an integral form for any time interval $[0, t], t \leq \mathcal{T}$ and the so-called *stability condition* in any time t, which may be understood as an independent constitutive assumption similar in its nature to well-known extremum principles of thermodynamics as the maximum dissipation principle or the minimum principle for dissipation potential formulated in Section 2.3. In (Mielke et al., 2002) the stability condition is derived from the so-called *postulate of realizability*, whose essence is the following: as soon as some dissipative process can occur from the point of view of thermodynamics, it will occur.

The framework of energetic solution has proved to be useful and general enough so that it has been already extensively used for analysis of models for phase transition both in single crystals (Mielke et al., 2009, 2002) and polycrystals (Auricchio et al., 2008) of shape memory alloys, but also for models of plasticity (Mielke, 2003), damage and fracture (Bouchitté et al., 2009) and other rate-independent systems (Mielke and Theil, 2004). Thus, the effort to include our model to this family is the first motivation for exploiting the framework in the following mathematical analysis.

Another reason is that within a general formulation the notion of dissipation distance is employed, which exactly matches with derivations in Section 4.5.

An important step of the analysis within the framework is investigation of properties of a time-incremental minimization problem. Since the numerical treatment introduced in Chapter 6 is based on such a kind of minimization procedure, a side benefit of the analysis will be a rigorous proof of existence of a numerical solution in each time step, although a slightly modified (regularized) form of Helmoholz free energy will be considered.

Last but not least, the framework is subject of further development, e.g. (Bartels et al., 2012), and such extensions may be advantageously utilized for possible future extensions of our model.

In this chapter, we first establish the basic mathematical assumptions on

imposed loading and material parameters considered in the system (4.32)–(4.38). Then we formulate a time-incremental minimization problem corresponding to the system and show it has a solution. This is useful both for the numerical treatment described in the next chapter and for the last section of this chapter, where the existence of an energetic solution of a regularized evolutionary system is proven.

5.1 Basic assumptions and data qualification

Let $\Omega \subset \mathbb{R}^3$ be the domain of the specimen at reference configuration, assumed to be connected and with Lipschitz boundary. The Lebesgue $\mathbb{R}^3$-measure of Ω is denoted $|\Omega|$. We focus on the evolution of the specimen in a time interval $[0, \mathcal{T}] \subset \mathbb{R}$. For brevity, we will usually omit the notation of spatial dependence, x, of variables and parameters in the following. Let us suppose that $\partial\Omega = \Gamma_{\mathrm{D}} \cup \Gamma_{\mathrm{N}} \cup \Gamma_0$, where Lebesgue $\mathbb{R}^2$-measure of Γ_0 is zero and it is positive for Γ_{D} denoting the part with Dirichlet boundary condition, $U(t)$, prescribed.

We will consider temperature as a prescribed loading in time, since we *do not include full thermomechanical coupling* in present formulation of the model. In line with this assumption, energy and dissipation functions are considered to be dependent on variables as follows:

$$f(t, \boldsymbol{\varepsilon}, \boldsymbol{\varepsilon}^{\mathrm{in}}, \xi, \eta), \quad d(t, \boldsymbol{\varepsilon}^{\mathrm{in}}, \xi, \dot{\boldsymbol{\varepsilon}}^{\mathrm{in}}, \dot{\xi}). \tag{5.1}$$

Let us note the time variable may also enter f through the (time-dependent) Dirichlet boundary condition.

Hereinafter, we call the internal variables *admissible* if it satisfy (in an appropriate sense specified later) all applicable internal constraints:

$$0 \leq \xi \leq 1, \quad 0 \leq \eta \leq 1 - \xi, \quad \langle \boldsymbol{\varepsilon}^{\mathrm{in}} \rangle \leq \xi. \tag{5.2}$$

Since we suppose that the function $\langle \cdot \rangle$ is convex, positively 1-homogenous and it holds

$$\langle \boldsymbol{\varepsilon}^{\mathrm{in}} \rangle = 0 \Rightarrow \boldsymbol{\varepsilon}^{\mathrm{in}} = 0, \tag{5.3}$$

it is possible to find positive constants C, C^* such that for all $\boldsymbol{\varepsilon}^{\mathrm{in}}$ it holds

$$C\|\boldsymbol{\varepsilon}^{\mathrm{in}}\| \leq \langle \boldsymbol{\varepsilon}^{\mathrm{in}} \rangle \leq C^*\|\boldsymbol{\varepsilon}^{\mathrm{in}}\|. \tag{5.4}$$

To simplify the notation, C will denote a generic constant whose value is changing from equation to equation. If an explicit dependence on a particular variable, v, is to be emphasised, we use the notation $C(v)$.

Now we will more specify the qualification of material parameters and loading and boundary conditions so that we will be able to smoothly follow the theory of energetic solutions. Let us emphasize that we do not attempt to formulate the least restricting requirements, but restrict ourselves to physically well-acceptable ones.

Boundary conditions and temperature loading

For the volume and surface forces we choose the following regularity:

$$F_{\text{vol}} \in \mathrm{C}^1([0,\mathcal{T}],\mathrm{L}^2(\Omega,\mathbb{R}^3)), \tag{5.5}$$
$$F_{\text{surf}} \in \mathrm{C}^1([0,\mathcal{T}],\mathrm{L}^2(\Gamma_{\mathrm{N}},\mathbb{R}^3)). \tag{5.6}$$

For definitions of respective function spaces see the nomenclature.

Let us assume there exists an extension of the Dirichlet boundary condition, $U(t)$, to all $\overline{\Omega}$, still denoted $U(t)$ so that

$$U \in \mathrm{C}^1([0,\mathcal{T}],\mathrm{W}^{1,2}(\Omega,\mathbb{R}^3)), \tag{5.7}$$

and its trace on Γ_{D} is equal to prescribed $U(t)$ for all $t \in [0,\mathcal{T}]$.

Also temperature is considered as a prescribed loading in the present formulation of the model. In this chapter it will be concerned *homogeneous* within the body at any time instance t – which is the case of all numerical simulations presented in the next chapter – i. e. we assume

$$T \in \mathrm{C}^1([0,\mathcal{T}],\mathbb{R}). \tag{5.8}$$

Parameters of energy function and dissipation function

The chosen formula for the shear modulus of a phase mixture

$$\frac{1}{G(\xi,\eta)} = (1-\xi-\eta)\frac{1}{G^A} + \eta\frac{1}{G^R} + \xi\frac{1}{G^M}, \tag{5.9}$$

implies that $G(\xi,\eta)$ is obviously positive for any admissible pair (ξ,η) if we naturally assume $G^i > 0,\ \forall\, i \in A,R,M$. It can be rewritten into the form

$$G(\xi,\eta) = \frac{G^A G^R G^M}{G^R G^M + \xi(G^A - G^M)G^R + \eta(G^A - G^R)G^M} \tag{5.10}$$

and we can conclude that the denominator thus must be positive. We also assume that K, G^A, G^R, G^M are chosen such that the corresponding fourth-order isotropic elasticity tensor of a mixture[1], $\mathbb{C}(\xi,\eta)$, is positive definite for any admissible pair (ξ,η).

Since austenite is the high temperature phase we may assume $\Delta s^{AR} > 0$, thus

$$R := \Delta s^{AR}\frac{R_{\mathrm{s}} - R_{\mathrm{f}}}{2} > 0. \tag{5.11}$$

due to the definition $R_{\mathrm{s}} > R_{\mathrm{f}}$. For the same reason $\Delta s^{AM} > 0$, and we will require

$$M_{\mathrm{f}} \le M_{\mathrm{s}} < T_0 < A_{\mathrm{s}} \le A_{\mathrm{f}}. \tag{5.12}$$

so that transformation part of the dissipation function is positive whenever $\dot{\xi} \neq 0$.

[1]Due to definitions of the bulk modulus, K, and the shear modulus, $G(\xi,\eta)$, of the phase mixture, we can construct a fourth-order isotropic elasticity tensor, $\mathbb{C}(\xi,\eta)$, for any ξ,η satisfying $0 \le \eta \le 1-\xi > 0$.

After possible rescaling of u_0^A, we may assume

$$u_0^A - s_0^A T(t) + c^A \left[(T(t) - T_0) - T(t) \ln \left(\frac{T(t)}{T_0} \right) \right] > 0 \quad \forall\, t \in [0, \mathcal{T}]. \tag{5.13}$$

We will also suppose that parameters $\sigma_0^{\mathrm{reo}} > 0$ and $\Sigma^{\mathrm{reo}} < 0$ of the linear function $\sigma^{\mathrm{reo}}(T)$ and the temperature range of the problem are such that there is a constant s^*:

$$\sigma^{\mathrm{reo}}(T(t)) \geq s^* > 0 \quad \forall\, t \in [0, \mathcal{T}]. \tag{5.14}$$

5.2 Existence of solutions of time-disretized problem

To obtain a time discretization of the model suitable for implementation into a finite element software, we introduce a partition of the time interval from time 0 to $\mathcal{T}$ in the form $0 = t_0 \leq t_1 \leq \ldots \leq t_N = \mathcal{T}$. Let us introduce a simplification of notation: for a time-dependent function $g(t)$ we denote $g_k := g(t_k)$.

If we directly proceed by semi-implicit discretization of the governing system (4.32)–(4.37) in time by replacing derivatives with differences, we obtain:

$$\begin{aligned}
-\mathrm{div}\,(\boldsymbol{\sigma}_k) &= F_{\mathrm{vol,k}} && \text{in } \Omega, && (5.15)\\
\boldsymbol{\sigma}_k\, n &= F_{\mathrm{surf,k}} && \text{on } \Gamma_{\mathrm{N}}, && (5.16)\\
u_k &= U_k && \text{on } \Gamma_{\mathrm{D}}, && (5.17)\\
\boldsymbol{X}_k &\in \partial_{\dot{\boldsymbol{\varepsilon}}^{\mathrm{in}}} d(t_k, \boldsymbol{\varepsilon}^{\mathrm{in}}_{k-1}, \xi_{k-1}, \Delta_k \boldsymbol{\varepsilon}^{\mathrm{in}}, \Delta_k \xi) && \text{in } \Omega, && (5.18)\\
\pi_k &\in \partial_{\dot{\boldsymbol{\varepsilon}}^{\mathrm{in}}} d(t_k, \boldsymbol{\varepsilon}^{\mathrm{in}}_{k-1}, \xi_{k-1}, \Delta_k \boldsymbol{\varepsilon}^{\mathrm{in}}, \Delta_k \xi) && \text{in } \Omega, && (5.19)\\
N_k &= 0 && \text{in } \Omega, && (5.20)
\end{aligned}$$

where we defined

$$\Delta_k \boldsymbol{\varepsilon}^{\mathrm{in}} := \frac{\boldsymbol{\varepsilon}^{\mathrm{in}}(t_k) - \boldsymbol{\varepsilon}^{\mathrm{in}}(t_{k-1})}{t_k - t_{k-1}}, \tag{5.21}$$

$$\Delta_k \xi := \frac{\xi(t_k) - \xi(t_{k-1})}{t_k - t_{k-1}}. \tag{5.22}$$

To motivate a more general formulation, let us introduce the dissipation functional as:

$$D(t, \boldsymbol{\varepsilon}^{\mathrm{in}}(t), \xi(t), \dot{\boldsymbol{\varepsilon}}^{\mathrm{in}}(t), \dot{\xi}(t)) := \int_\Omega d(t, \boldsymbol{\varepsilon}^{\mathrm{in}}(t), \xi(t), \dot{\boldsymbol{\varepsilon}}^{\mathrm{in}}(t), \dot{\xi}(t))\, \mathrm{d}V \tag{5.23}$$

and, motivated by variational formulation of elasticity, the functional of (Gibbs free) energy in the form:

$$\begin{aligned}
\widetilde{E}(t, u(t), \boldsymbol{\varepsilon}^{\mathrm{in}}(t), \xi(t), \eta(t)) := &\int_\Omega f(t, \boldsymbol{\varepsilon}(u(t)), \boldsymbol{\varepsilon}^{\mathrm{in}}(t), \xi(t), \eta(t))\, \mathrm{d}V \\
&- \int_\Omega F_{\mathrm{vol}}(t) u(t)\, \mathrm{d}V - \int_{\Gamma_{\mathrm{N}}} F_{\mathrm{surf}}(t) u(t)\, \mathrm{d}S.
\end{aligned} \tag{5.24}$$

A direct computation then shows (cf. Francfort and Mielke, 2006) that the system (5.15)–(5.20) together with initial conditions (4.38) is a *necessary* first order optimality condition for finding a minimum of the following sum

$$\begin{aligned}&\widetilde{E}(t_k, v, \boldsymbol{\varepsilon}^{\mathrm{in}}, \xi, \eta) + (t_k - t_{k-1})\, D\left(t_k, \boldsymbol{\varepsilon}^{\mathrm{in}}_{k-1}, \xi_{k-1}, \frac{\boldsymbol{\varepsilon}^{\mathrm{in}} - \boldsymbol{\varepsilon}^{\mathrm{in}}_{k-1}}{t_k - t_{k-1}}, \frac{\xi - \xi_{k-1}}{t_k - t_{k-1}}\right)\\ &= \widetilde{E}(t_k, v, \boldsymbol{\varepsilon}^{\mathrm{in}}, \xi, \eta) + D(t_k, \boldsymbol{\varepsilon}^{\mathrm{in}}_{k-1}, \xi_{k-1}, \boldsymbol{\varepsilon}^{\mathrm{in}} - \boldsymbol{\varepsilon}^{\mathrm{in}}_{k-1}, \xi - \xi_{k-1})\end{aligned} \tag{5.25}$$

when it is considered in the weak sense. We employed positive 1-homogeneity of the dissipation function in rate variables in (5.25). Moreover, due to the convexity of both functions (see below), the discrete system would be a necessary *and sufficient* condition for finding a *global minimum* of (5.25). Hence, in the numerical implementation of the model, instead of solving a system of inequalities and activation conditions – well-known from numerical procedures in classical plasticity – we shall solve a time-incremental minimization problem (TIP) defined below.

For convenience, let us introduce the following notation:

$$\begin{aligned}\langle l(t), u(t) + U(t)\rangle &:= \int_\Omega F_{\mathrm{vol}}(t)(u(t) + U(t))\,\mathrm{d}V\\ &\qquad + \int_{\Gamma_{\mathrm{N}}} F_{\mathrm{surf}}(t)(u(t) + U(t))\,\mathrm{d}S, &(5.26)\\ \langle m(t), \xi(t)\rangle &:= \int_\Omega \Delta s^{AM}(T(t) - T_0)\xi(t)\,\mathrm{d}V, &(5.27)\\ \langle q(t), \eta(t)\rangle &:= \int_\Omega \Delta s^{AR}(T(t) - R_{\mathrm{s}})\eta(t)\,\mathrm{d}V, &(5.28)\\ \langle w(t), 1\rangle &:= \int_\Omega u_0^A - s_0^A T(t) + c^A\left[(T(t) - T_0) - T(t)\ln\left(\frac{T(t)}{T_0}\right)\right]\mathrm{d}V, &(5.29)\end{aligned}$$

and let us notice that the time-dependence of $m(t), q(t), w(t)$ is because of *temperature-dependence* of these terms only. Introducing an additive decomposition $u(t) := v(t) - U(t)$, we also set

$$\begin{aligned}&E(\,t, u(t), \boldsymbol{\varepsilon}^{\mathrm{in}}, \xi(t), \eta((t)) := \widetilde{E}(t, u(t) + U(t), \boldsymbol{\varepsilon}^{\mathrm{in}}, \xi(t), \eta(t))\\ &\quad = \int_\Omega f(t, \boldsymbol{\varepsilon}(u + U(t)), \boldsymbol{\varepsilon}^{\mathrm{in}}(t), \xi(t), \eta(t))\,\mathrm{d}V - \langle l(t), u(t) + U(t)\rangle.\end{aligned} \tag{5.30}$$

Now we are ready to formulate the time-incremental minimization problem and its solution. They play a key role not only in the numerical implementation in Chapter 6, but also, as will be seen, in mathematical analysis of time-evolutionary problem.

Definition 5.2.1 (Time-discrete solution)**.** Let $u_0, \boldsymbol{\varepsilon}^{\mathrm{in}}_0, \xi_0, \eta_0$ be the initial conditions of the rate-independent evolution satisfying constraints (5.2). Let boundary conditions and temperature be prescribed in accordance with data qualifications in Section 5.1 at time points t_k, $k = 1, \dots, N$. Then we call the quadruplet $(u_k, \boldsymbol{\varepsilon}^{\mathrm{in}}_k, \xi_k, \eta_k) \in \mathrm{W}^{1,2}_0(\Omega; \mathbb{R}^3) \times \mathrm{L}^2(\Omega; \mathbb{R}^{3\times 3}_{\mathrm{sym},0}) \times \mathrm{L}^\infty(\Omega; \mathbb{R}) \times \mathrm{L}^\infty(\Omega; \mathbb{R})$ that satisfies the boundary conditions and constraints

$$0 \le \xi_k(x) \le 1, \quad 0 \le \eta_k(x) \le 1 - \xi_k(x) \ \text{ and } \ \langle \boldsymbol{\varepsilon}^{\mathrm{in}}_k(x)\rangle \le \xi_k(x) \ \text{ for a.a. } x \in \Omega \tag{5.31}$$

a time-discrete solution of the specimen evolution at time t_k if it solves the following *time-incremental minimization problem*

$$\begin{aligned}&\text{Minimize } E(t_k, u, \boldsymbol{\varepsilon}^{\text{in}}, \xi, \eta) + D(t_k, \xi_{k-1}, \boldsymbol{\varepsilon}^{\text{in}}_{k-1}, \xi - \xi_{k-1}, \boldsymbol{\varepsilon}^{\text{in}} - \boldsymbol{\varepsilon}^{\text{in}}_{k-1})\\ &\text{subject to}\\ &(u, \boldsymbol{\varepsilon}^{\text{in}}, \xi, \eta) \in \mathrm{W}^{1,2}_0(\Omega;\mathbb{R}^3) \times \mathrm{L}^2(\Omega;\mathbb{R}^{3\times 3}_{\text{sym},0}) \times \mathrm{L}^\infty(\Omega;\mathbb{R}) \times \mathrm{L}^\infty(\Omega;\mathbb{R}).\end{aligned} \tag{TIP}$$

In the above definition, the explicit form of the (discretized) energy functional is

$$\begin{aligned}E(t_k, u, \boldsymbol{\varepsilon}^{\text{in}}, \xi, \eta) = \int_\Omega & f^{\text{el}}(t_k, u + U(t_k), \boldsymbol{\varepsilon}^{\text{in}}, \xi, \eta)\\ &+ \frac{R\eta^2}{1-\xi} + w(t_k) + m(t_k)\xi + q(t_k)\eta - l(t_k)(u + U(t_k))\,\mathrm{d}V\end{aligned} \tag{5.32}$$

and (discretized) dissipation functional is

$$D(t_k, \boldsymbol{\varepsilon}^{\text{in}}_{k-1}, \xi_{k-1}, \xi - \xi_{k-1}, \boldsymbol{\varepsilon}^{\text{in}} - \boldsymbol{\varepsilon}^{\text{in}}_{k-1}) = \int_\Omega d(t_k, \boldsymbol{\varepsilon}^{\text{in}}_{k-1}, \xi_{k-1}, \xi - \xi_{k-1}, \boldsymbol{\varepsilon}^{\text{in}} - \boldsymbol{\varepsilon}^{\text{in}}_{k-1})\,\mathrm{d}V \tag{5.33}$$

where the discretized version of dissipation potential is obtained as:

$$\begin{aligned}&d(t_k, \varepsilon^{\text{in}}_{k-1}, \xi_{k-1}, \xi - \xi_{k-1}, \boldsymbol{\varepsilon}^{\text{in}} - \boldsymbol{\varepsilon}^{\text{in}}_{k-1})\\ &\quad= \begin{cases} \Delta s^{AM}[T_0 - M_{\text{s}} + \xi_{k-1}(M_{\text{s}} - M_{\text{f}})] \cdot |\xi - \xi_{k-1}| & \\ \quad + \sigma^{\text{reo}}(T(t_k))\|\boldsymbol{\varepsilon}^{\text{in}} - \boldsymbol{\varepsilon}^{\text{in}}_{k-1}\| & \text{if } \xi \geq \xi_{k-1}\\ \Delta s^{AM}[A_{\text{f}} - T_0 + \xi_{k-1}(A_{\text{s}} - A_{\text{f}})] \cdot |\xi - \xi_{k-1}| & \\ \quad + \sigma^{\text{reo}}(T(t_k))\|\frac{\xi - \xi_{k-1}}{\xi_{k-1}}\boldsymbol{\varepsilon}^{\text{in}}_{k-1}\| & \text{if } \xi < \xi_{k-1}\\ \quad + \sigma^{\text{reo}}(T(t_k))\|\boldsymbol{\varepsilon}^{\text{in}} - \boldsymbol{\varepsilon}^{\text{in}}_{k-1} - \frac{\xi - \xi_{k-1}}{\xi_{k-1}}\boldsymbol{\varepsilon}^{\text{in}}_{k-1}\| & \end{cases}\end{aligned} \tag{5.34}$$

Note that $\xi < \xi_{k-1}$ implies $\xi_{k-1} > 0$ and all the terms in (5.34) are well-defined.

Proposition 5.2.2 (Existence of a discrete solution)**.** *Let* $\xi_{k-1} \in \mathrm{L}^\infty(\Omega;\mathbb{R})$, $\boldsymbol{\varepsilon}^{\text{in}}_{k-1} \in \mathrm{L}^2(\Omega;\mathbb{R}^{3\times 3}_{\text{sym},0})$. *Let material parameters, boundary conditions and temperature loading be given in accordance with data qualifications in Section 5.1. Then there exists a solution of the time-incremental problem* (TIP).

Proof. We will utilize the direct method of calculus of variations (cf. e.g. Dacorogna, 2008). Denoting the functional to be minimized as $J : \mathcal{B} \to \{\mathbb{R} \cup \infty\}$, where $\mathcal{B}$ is a functional space we work on, we want to find a minimizer, i.e. $\chi_{\min} \in \mathcal{B}$ such that $J(\chi_{\min}) \leq J(\chi)$ for all $\chi \in \mathcal{B}$. If the functional is bounded from below, there must be a minimizing sequence, $\chi_n \in \mathcal{B}$, so that $\lim_{n\to\infty} J(\chi_n) = \inf_{\chi\in\mathcal{B}} J(\chi)$. If $\mathcal{B}$ is a closed bounded subset of a reflexive Banach space and the minimizing sequence is bounded, we can choose a subsequence, χ_{n_k}, with a weak limit, $\chi_0 \in \mathcal{B}$, i.e. $\chi_{n_k} \rightharpoonup \chi_0$. Finally, if J is weak lower semi-continuous, it holds that $\chi_{n_k} \rightharpoonup \chi_0 \;\Rightarrow \liminf_{k\to\infty} J(\chi_{n_k}) \geq J(\chi_0)$. Of course, $J(\chi_0) \geq \inf_{\chi\in\mathcal{B}} J(\chi)$. Thus,

$$\inf_{\chi\in\mathcal{B}} J(\chi) = \lim_{n\to\infty} J(\chi_n) = \lim_{k\to\infty} J(\chi_{n_k}) \geq J(\chi_0) \geq \inf_{\chi\in\mathcal{B}} J(\chi), \tag{5.35}$$

and we may conclude that χ_0 is a minimizer.

To follow this approach, we need to satisfy four conditions mentioned above. First, due to choice of reflexive functional spaces in which the solution is searched, and since constraints (5.31) delimit closed convex sets in them, we work in a closed subset of a reflexive Banach space. Note that since closed convex subsets are also weakly closed (i.e. closed for a weak convergence), the minimizer found by the above proceeding will also satisfy the constraints (5.31).

Second, we will show that if the energy functional in (TIP) is bounded for any admissible sequence, then the sequence itself must be bounded. This specially means that any minimizing sequence is bounded. Actually, we will show the contrapositive statement, which may be formulated as follows: if we take a sequence of admissible quadruplets $(u, \boldsymbol{\varepsilon}^{\mathrm{in}}, \eta, \xi)$ converging in the norm to ∞ ($t_k, \boldsymbol{\varepsilon}^{\mathrm{in}}_{k-1}, \xi_{k-1}, \eta_{k-1}$ are fixed), then, necessary, $E + D \to \infty$.

Property (5.4) of the function $\langle\cdot\rangle$ particularly assures that there exists a constant, $\rho > 0$, such that

$$\langle \boldsymbol{\varepsilon}^{\mathrm{in}}(x)\rangle \leq 1 \Rightarrow \|\boldsymbol{\varepsilon}^{\mathrm{in}}(x)\| \leq \rho \quad \text{for a.a. } x \in \Omega. \tag{5.36}$$

And, owing to constraints imposed on ξ, η, norms of all internal variables are bounded. Hence D is bounded from above, and it is enough to show that if $\|u_n\|_{\mathrm{W}^{1,2}(\Omega)} \to \infty, n \in \mathbb{R}$ then $E \to \infty$.

The specific form of the elastic energy (4.10) may be represented by a quadratic form $\langle \mathbb{C}(\xi,\eta)(\boldsymbol{\varepsilon} - \boldsymbol{\varepsilon}^{\mathrm{in}}), (\boldsymbol{\varepsilon} - \boldsymbol{\varepsilon}^{\mathrm{in}})\rangle$ with a positive definite fourth order elasticity tensor $\mathbb{C}(\xi,\eta)$. Thus, there is a positive constant[2] independent on ξ, η such that $\langle \mathbb{C}(\xi,\eta)(\boldsymbol{\varepsilon} - \boldsymbol{\varepsilon}^{\mathrm{in}}), (\boldsymbol{\varepsilon} - \boldsymbol{\varepsilon}^{\mathrm{in}})\rangle \geq C\langle \boldsymbol{\varepsilon} - \boldsymbol{\varepsilon}^{\mathrm{in}}, \boldsymbol{\varepsilon} - \boldsymbol{\varepsilon}^{\mathrm{in}}\rangle$. Then

$$\begin{aligned}
&\int_\Omega f^{\mathrm{el}}(t_k, u, \boldsymbol{\varepsilon}^{\mathrm{in}}, \xi, \eta)\,\mathrm{d}V \\
&\qquad \geq C\|\boldsymbol{\varepsilon}(u + U_k) - \boldsymbol{\varepsilon}^{\mathrm{in}}\|^2_{\mathrm{L}^2(\Omega)} \\
&\qquad \geq C(\|\boldsymbol{\varepsilon}(u) + \boldsymbol{\varepsilon}(U_k)\|^2_{\mathrm{L}^2(\Omega)} - 2\|\boldsymbol{\varepsilon}(u) + \boldsymbol{\varepsilon}(U_k)\|_{\mathrm{L}^2(\Omega)} \underbrace{\|\boldsymbol{\varepsilon}^{\mathrm{in}}\|_{\mathrm{L}^2(\Omega)}}_{\leq \rho} + \underbrace{\|\boldsymbol{\varepsilon}^{\mathrm{in}}\|^2_{\mathrm{L}^2(\Omega)}}_{>0}) \\
&\qquad \geq C\Big(\|\boldsymbol{\varepsilon}(u)\|^2_{\mathrm{L}^2(\Omega)} + 2\|\boldsymbol{\varepsilon}(u)\|_{\mathrm{L}^2(\Omega)}\|\boldsymbol{\varepsilon}(U_k)\|_{\mathrm{L}^2(\Omega)} + \|\boldsymbol{\varepsilon}(U_k)\|^2_{\mathrm{L}^2(\Omega)} \\
&\qquad\quad - 2\rho\|\boldsymbol{\varepsilon}(u)\|_{\mathrm{L}^2(\Omega)} - 2\rho\|\boldsymbol{\varepsilon}(U_k)\|_{\mathrm{L}^2(\Omega)}\Big) \\
&\qquad \geq C\Big(\|u\|^2_{\mathrm{W}^{1,2}(\Omega)} - 2[\rho - \|\boldsymbol{\varepsilon}(U_k)\|_{\mathrm{L}^2(\Omega)}]\|u\|_{\mathrm{W}^{1,2}(\Omega)} - 1\Big)
\end{aligned} \tag{5.37}$$

for any $(u, \boldsymbol{\varepsilon}^{\mathrm{in}}, \eta, \xi)$. We utilized a variation of the first Korn's inequality in the last step.

Making profit of boundedness of internal variables, there is (maybe a negative) constant so that integral of all but the last term in (5.32) may be bounded from below. Then, due to data qualification (5.5)–(5.7) and Hölder inequality, we get

$$\begin{aligned}
&\int_\Omega F_{\mathrm{vol},k} \cdot (u + U_k)\,\mathrm{d}V + \int_{\Gamma_{\mathrm{N}}} F_{\mathrm{surf},k} \cdot (u + U_k)\,\mathrm{d}S \\
&\qquad \leq \|F_{\mathrm{vol},k}\|_{\mathrm{L}^2(\Omega)}\|u\|_{\mathrm{L}^2(\Omega)} + \|F_{\mathrm{surf},k}\|_{\mathrm{L}^2(\Gamma_N)}\|u\|_{\mathrm{L}^2(\Gamma_N)} + \|F_{\mathrm{vol},k}\|_{\mathrm{L}^2(\Omega)}\|U_k\|_{\mathrm{L}^2(\Omega)} \\
&\qquad\quad + \|F_{\mathrm{surf},k}\|_{\mathrm{L}^2(\Gamma_N)}\|U_k\|_{\mathrm{L}^2(\Gamma_N)} \\
&\qquad \leq \|l_k\|_{\mathrm{L}^2(\Omega)}\|u\|_{\mathrm{L}^2(\Omega)} + C \\
&\qquad \leq \|l_k\|_{\mathrm{L}^2(\Omega)}\|u\|_{\mathrm{W}^{1,2}(\Omega)} + C
\end{aligned} \tag{5.38}$$

[2]Let us note that in our case the constant may be chosen as $2\min\{G(\xi,\eta) : \forall\, \xi, \eta : 0 \leq \eta \leq 1 - \xi \geq 0\}$.

Finally,

$$E(t_k, u, \varepsilon^{\text{in}}, \xi, \eta) \geq C(\|u\|^2_{\mathrm{W}^{1,2}(\Omega)} - 2\tilde{\rho}\|u\|_{\mathrm{W}^{1,2}(\Omega)}) - \|l_k\|_{\mathrm{L}^2(\Omega)}\|u\|_{\mathrm{W}^{1,2}(\Omega)} - C$$
$$\geq \|u\|^2_{\mathrm{W}^{1,2}(\Omega)} \left(\underbrace{C}_{>0} - \frac{2\tilde{\rho}}{\|u\|_{\mathrm{W}^{1,2}(\Omega)}} - \frac{\|l_k\|_{\mathrm{L}^2}(\Omega)}{\|u\|_{\mathrm{W}^{1,2}(\Omega)}} \right) - C, \quad (5.39)$$

where the last constant depends on w_k, m_k, q_k. It is easy to see the term on right hand-side of (5.39) converges to ∞ if $\|u_n\|_{\mathrm{W}^{1,2}(\Omega)} \to \infty, n \in \mathbb{R}$.

Third, from (5.39) (and recalling that D is constructed to be always non-negative, i.e. bounded from below by 0) it can be also seen that $E + D$ is bounded from below at t_k for any quadruplet $(u, \boldsymbol{\varepsilon}^{\text{in}}, \eta, \xi)$ satisfying constraints (5.31) under aforementioned data qualifications.

Finally, due to the particular form of our functional $E + D$, it is enough to verify that the discretized integrands f and d in (5.32) and (5.33), respectively, are convex functions with respect to minimized variables for any admissible fixed $t_k, \boldsymbol{\varepsilon}^{\text{in}}_{k-1}, \xi_{k-1}, \eta_{k-1}$. Then, we obtain sequential weak lower semicontinuity of the functional $E + D$ due to its convexity (Dacorogna, 2008).

Concerning E, $w(t_k)$ is a constant and the last three terms in (5.32) are linear, thus the first two terms really matter. It is easy to show the convexity of a function $h(y, z) = Cy^2/z$ for $C > 0$, $y \in \mathbb{R}$ and $0 \leq z \in \mathbb{R}$ (the image of the function is considered in $\mathbb{R} \cup \infty$). This result can be directly used for the second term in (5.32). As far as elastic energy is concerned, the first term in (4.10) makes no trouble; for the shear energy term we employ convexity of $h(y, z)$ making use of the explicit form in (5.10).[3]

With regard to d, it is enough to use the mid-point convexity criterium (recall d is continuous for fixed $\boldsymbol{\varepsilon}^{\text{in}}_{k-1}, \xi_{k-1}$), which takes the particular form:

$$d(t_k, \boldsymbol{\varepsilon}^{\text{in}}_{k-1}, \xi_{k-1}, \frac{\boldsymbol{\varepsilon}^{\text{in}}_A + \boldsymbol{\varepsilon}^{\text{in}}_B}{2} - \boldsymbol{\varepsilon}^{\text{in}}_{k-1}, \frac{\xi_A + \xi_B}{2} - \xi_{k-1})$$
$$\leq \frac{1}{2} d(t_k, \boldsymbol{\varepsilon}^{\text{in}}_{k-1}, \xi_{k-1}, \boldsymbol{\varepsilon}^{\text{in}}_A - \boldsymbol{\varepsilon}^{\text{in}}_{k-1}, \xi_A - \xi_{k-1})$$
$$+ \frac{1}{2} d(t_k, \boldsymbol{\varepsilon}^{\text{in}}_{k-1}, \xi_{k-1}, \boldsymbol{\varepsilon}^{\text{in}}_B - \boldsymbol{\varepsilon}^{\text{in}}_{k-1}, \xi_B - \xi_{k-1}). \quad (5.40)$$

This relation may be proven by computation of four cases implied by the particular forms of dissipation function in (5.34). Actually, they are consequences of triangle inequalities for (Euclidean) norms.

□

By the above time discretization we obtained a conceptual numerical alghorithm through (TIP). The full numerical treatment will be described in detail in Chapter 6.

5.3 Energetic formulation

We are going to follow a general proceeding of the work by Francfort and Mielke (2006) and show that there is an energetic solution based on an energy $\mathcal{E}$ and a

[3] Let us recall that convexity is not affected by an affine mapping.

dissipation distance $\mathcal{D}$. However, to be able to smoothly follow the theory, we will introduce a regularization term in the form of a gradient of the dissipative variables into the Helmohltz free energy. This term may be avoided in the theory only in some special cases (see Mielke and Theil, 2004, for details). However, the term may be introduced multiplied by an arbitrary small parameter (constant).

In their paper, Francfort and Mielke (2006) utilize a dissipation distance as the primary entity responsible for dissipation processes. Thus, we can take advantage of derivations in Section 4.4 and employ the derived dissipation distances in the analysis. By this way, we will obtain existence of solution for the evolutionary problem where regularized energy and dissipation distances are considered. Additionally, since there is a direct relation between the dissipation distances and dissipation function, see (4.40), we will be able to establish existence of energetic solutions when dissipation function is considered instead.

There are two reasons, why we present the whole theory here and do not only rely on referencing to the aforementioned paper. First, our form of the dissipation distance is more general than the form considered there: in addition to being asymmetric and state-dependent (which is considered in (Francfort and Mielke, 2006)), it also *depends on time through the external loading by temperature*. Therefore, we have to slightly modify the form of the total dissipated energy functional and show some estimates on (both integrated and total) dissipation distance explicitly. Second, we also introduced another non-dissipative variable (η) into the energy function and we want to assure ourselves that procedures of the proof are not affected by that extension.

We recall the simplified notation of dissipative internal variables:

$$\alpha := (\boldsymbol{\varepsilon}^{\mathrm{in}}, \xi).$$

Let us define a regularized energy function:

$$\psi(t, v(t), \alpha(t), \eta(t)) := f(t, \varepsilon(v(t)), \alpha(t), \eta(t)) + \nu \|\nabla \alpha(t)\|^2, \tag{5.41}$$

where $\nu > 0$ is a (small) positive regularization constant, and a regularized energy functional:

$$\begin{aligned} &\mathcal{E}(t, u(t), \alpha(t), \eta(t)) := E(t, u(t), \alpha(t), \eta(t)) + \int_\Omega \nu \|\nabla \alpha(t)\|^2 \,\mathrm{d}V \\ &= \int_\Omega f(t, \boldsymbol{\varepsilon}(u + U(t)), \alpha(t), \eta(t)) + \nu \|\nabla \alpha(t)\|^2 \,\mathrm{d}V - \langle l(t), u(t) + U(t) \rangle. \end{aligned} \tag{5.42}$$

We also introduce the integrated dissipation distance (recall (4.39)):

$$\begin{aligned} \mathcal{D}(t, \alpha, \tilde{\alpha}) &:= \mathcal{D}^{\mathrm{tr}}(t, \alpha, \tilde{\alpha}) + \mathcal{D}^{\mathrm{reo}}(t, \alpha, \tilde{\alpha}) \\ &:= \int_\Omega \delta^{\mathrm{tr}}(t, \alpha, \tilde{\alpha}) \,\mathrm{d}V + \int_\Omega \delta^{\mathrm{reo}}(t, \alpha, \tilde{\alpha}) \,\mathrm{d}V \end{aligned} \tag{5.43}$$

Owing to the time-dependence of the dissipation distance through function $\sigma^{\mathrm{reo}}(T(t))$, we introduce the (total) dissipation for all $t \in [0, \mathcal{T}]$ as:

$$\mathrm{Diss}_{\mathcal{D}}(\alpha, [0, t]) := \mathrm{Diss}^{\mathrm{tr}}(\alpha, [0, t]) + \mathrm{Diss}^{\mathrm{reo}}(\alpha, [0, t]). \tag{5.44}$$

Hereinafter, the abbreviation "a.p.p." will denote "all possible partitions". For all $t \in [0, \mathcal{T}]$ we define

$$\mathrm{Diss}^{\mathrm{tr}}(\alpha, [0,t]) := \sup_{N\in\mathbb{N}}\{\sum_{i=1}^{N}\mathcal{D}^{\mathrm{tr}}(\alpha(t_{i-1}),\, \alpha(t_i)) \ : \\ \text{a.p.p. } 0 = t_0 \le t_1 \le \ldots \le t_N = t\}. \tag{5.45}$$

where explicit time-dependence of $\mathrm{Diss}^{\mathrm{tr}}$ was omitted since its form actually depends on time only through internal variables (it is even independent on $\boldsymbol{\varepsilon}^{\mathrm{tr}}$), and

$$\mathrm{Diss}^{\mathrm{reo}}(\alpha, [0,t]) := \int_0^t \sigma^{\mathrm{reo}}(T(s))\,\mathrm{d}\mu_\alpha(s). \tag{5.46}$$

Here we denoted by μ_α the measure defined on $[0, \mathcal{T}]$ by prescribing its values on every closed set $S = [s, z] \subset [0, \mathcal{T}]$, as

$$\mu_\alpha(S) := \sup_{N\in\mathbb{N}}\left\{\sum_{i=1}^{N}\overline{\mathcal{D}}^{\mathrm{reo}}(\alpha(t_{i-1}), \alpha(t_i)) \ : \ \text{a.p.p. } s = t_0 \le t_1 \le \ldots \le t_N = z\right\}. \tag{5.47}$$

$\overline{\mathcal{D}}^{\mathrm{reo}}(t_i, \alpha(t_{i-1}), \alpha(t_i))$ is defined as $\mathcal{D}^{\mathrm{reo}}(t_i, \alpha(t_{i-1}), \alpha(t_i))$ for $\sigma^{\mathrm{reo}}(T) \equiv 1$, i.e. we suppressed the explicit time-dependence through $\sigma^{\mathrm{reo}}(T(t))$ – the dependence is recovered in (5.46). Hence, due to its definition, $\overline{\mathcal{D}}^{\mathrm{reo}}$ is also dependent on time only through internal variables.

Finally, let us remind the following definition of total variation:

$$\mathrm{Var}_{\mathrm{L}^1}(\alpha, [0,t]) := \sup_{N\in\mathbb{N}}\{\sum_{i=1}^{N}\|\alpha(t_{i-1}) - \alpha(t_i)\|_{\mathrm{L}^1(\Omega)} \ : \\ \text{a.p.p. } 0 = t_0 \le t_1 \le \ldots \le t_N = t\}. \tag{5.48}$$

Let us note that again all possible partitions of the respective time interval are considered in definitions (5.47) and (5.48).

Based on the aforementioned framework (Francfort and Mielke, 2006) and with respect to our case we define:

Definition 5.3.1 (Energetic solution)**.** Let $\mathcal{E}, \mathcal{D}$ be given by definitions (5.42) and (5.43) with data qualifications in Section 5.1 and let

$$\mathcal{U} := \mathrm{W}^{1,2}_0(\Omega, \mathbb{R}^3), \tag{5.49}$$

$$\mathcal{V} := \{\boldsymbol{\varepsilon}^{\mathrm{in}} \in \mathrm{W}^{1,2}(\Omega, \mathbb{R}^{3\times3}_{\mathrm{sym},0}) \ : \ \langle\boldsymbol{\varepsilon}^{\mathrm{in}}(x)\rangle \le \xi(x) \text{ for a.a. } x \in \Omega\} \\ \times \{\xi \in \mathrm{W}^{1,2}(\Omega, \mathbb{R}) \ : \ 0 \le \xi(x) \le 1 \text{ for a.a. } x \in \Omega\} \tag{5.50}$$

$$\mathcal{Z} := \{\eta \in \mathrm{L}^\infty(\Omega, \mathbb{R})) \ : \ 0 \le \eta(x) \le 1 \text{ for a.a. } x \in \Omega\}. \tag{5.51}$$

If $\partial_t\mathcal{E}(t, u(t), \alpha(t), \eta(t)) \in \mathrm{L}^1((0, \mathcal{T}), \mathbb{R})$, then the triplet $(u(t), \alpha(t), \eta(t)) : [0, \mathcal{T}] \to \mathcal{U} \times \mathcal{V} \times \mathcal{Z}$ such that $\eta(x) \le 1 - \xi(x)$ for a.a. $x \in \Omega$ satisfying for all $t \in [0, \mathcal{T}]$

- **Stability condition:**

$$\mathcal{E}(t, u(t), \alpha(t), \eta(t)) \le \mathcal{E}(t, \tilde{u}, \tilde{\alpha}, \tilde{\eta}) + \mathcal{D}(t, \alpha(t), \tilde{\alpha}) \quad \forall\,(\tilde{u}, \tilde{\alpha}, \tilde{\eta}) \in \mathcal{U} \times \mathcal{V} \times \mathcal{Z} \tag{5.52}$$

- **Energy balance:**

$$\mathcal{E}(t, u(t), \alpha(t), \eta(t)) + \mathrm{Diss}_{\mathcal{D}}(\alpha, [0,t]) \\ = \mathcal{E}(0, u(0), \alpha(0), \eta(0)) + \int_0^t \partial_t \mathcal{E}(s, u(s), \alpha(s), \eta(s)) \,\mathrm{d}s. \tag{5.53}$$

is called an energetic solution of the rate-independent problem associated with $\mathcal{E}$ and $\mathcal{D}$.

The final aim of this chapter is to prove the following theorem:

Theorem 5.3.2 (Existence of an energetic solution)**.** *Let $\mathcal{E}, \mathcal{D}$ be defined by (5.42) and (5.43), let data qualifications in Section 5.1 hold true and let initial conditions $(u_0, \alpha_0, \eta_0) \in \mathcal{U} \times \mathcal{V} \times \mathcal{Z}$ satisfy $\eta_0(x) \leq 1 - \xi_0(x)$ for a.a. $x \in \Omega$ and the stability condition (5.52). Then there exists an energetic solution of the rate-independent problem associated with $\mathcal{E}$ and $\mathcal{D}$.*

Outline of the proof of Theorem 5.3.2. To prove the theorem, we will follow the rather standard approach of Francfort and Mielke (2006) consisting of 6 steps, which will be described in following subsections:

Subsection 5.3.1 First, we choose a partition $0 = t_0 \leq t_1 \leq \ldots \leq t_N = \mathcal{T}$ of the time interval $[0, \mathcal{T}]$. We formulate a time incremental minimization problem and show, in a very similar fashion to the proof of Proposition 5.2.2, that it has a solution for any time step of a chosen discretization. Moreover, such a discrete solution satisfies the stability condition and a modification of the energy balance.

Subsection 5.3.2 Having a sequence of solutions corresponding to a sequence of time points t_i, $0 \leq i \leq N$, we may construct interpolating functions on $[0, \mathcal{T}]$ which are piece-wise constant and equal to the last time-steps solution between the time points. We will obtain some useful estimates on such interpolants.

Subsection 5.3.3 With respect to the estimates, we will select some special subsequences of the interpolants. Their limits form a triplet of key importance: it will be proven to be the desired energetic solution.

Subsection 5.3.4 To confirm that the triplet is an energetic solution, we will utilize the stability of discrete solutions to show that the obtained limits satisfy the stability condition.

Subsection 5.3.5 Finally, we will show the upper and the lower energy inequality to prove that the triplet satisfies also the energy balance.

Subsection 5.3.6 We will show some further properties of the entities related to the solution and discuss further generalizations of the result.

To avoid a sequence of technical manipulations and lengthy terms in what follows, we will suppose that $U(t) = C \equiv 0$ on Γ_{D} in Sections 5.3.1–5.3.5, i.e. we will employ *time-independent* Dirichlet condition. In Subsection 5.3.6, we discuss the consequences for the proof if time-dependent Dirichlet condition is considered. □

Prior to the first step of the proof, we formulate two simple, albeit useful lemmas:

Lemma 5.3.3 (Coercivity of integrated dissipation distance)**.** *For any $\alpha_A, \alpha_B \in \mathrm{L}^1(\Omega)$ there is a constant $c^* > 0$ independent on $t \in [0, \mathcal{T}]$ such that:*

$$\mathcal{D}(t, \alpha_A, \alpha_B) \geq c^* \|\alpha_A - \alpha_B\|_{\mathrm{L}^1(\Omega)}. \tag{5.54}$$

Proof. Employing data qualification (5.12), we observe that for any two states $\alpha_A = (\boldsymbol{\varepsilon}_A^{\mathrm{in}}, \xi_A)$ and $\alpha_B = (\boldsymbol{\varepsilon}_B^{\mathrm{in}}, \xi_B)$ the following inequalities hold true:

$$|\xi_B - \xi_A| \cdot [T_0 - M_{\mathrm{s}} + \xi_A(M_{\mathrm{s}} - M_{\mathrm{f}})] \geq |\xi_B - \xi_A|(T_0 - M_{\mathrm{s}}), \tag{5.55}$$

$$|\xi_B - \xi_A| \cdot [A_{\mathrm{s}} - T_0 + (1 - \xi_A)(A_{\mathrm{f}} - A_{\mathrm{s}})] \geq |\xi_B - \xi_A|(A_{\mathrm{s}} - T_0), \tag{5.56}$$

and

$$\|\frac{\xi_B - \xi_A}{\xi_A}\boldsymbol{\varepsilon}_A^{\mathrm{in}}\| + \|\boldsymbol{\varepsilon}_B^{\mathrm{in}} - \boldsymbol{\varepsilon}_A^{\mathrm{in}} - \frac{\xi_B - \xi_A}{\xi_A}\boldsymbol{\varepsilon}_A^{\mathrm{in}}\| \geq \|\boldsymbol{\varepsilon}_B^{\mathrm{in}} - \boldsymbol{\varepsilon}_A^{\mathrm{in}}\|. \tag{5.57}$$

Then, recalling (5.12) and (5.14), it is enough to define

$$c^* := \min\{\Delta s^{AM}(T_0 - M_{\mathrm{s}}), \Delta s^{AM}(A_{\mathrm{s}} - T_0), s^*\} > 0, \tag{5.58}$$

note that it is time-independent. □

Lemma 5.3.4 (Dissipation triangle inequality)**.** *The integrated dissipation distance defined in (5.43) satisfies the triangle inequality in the form:*

$$\mathcal{D}(t, \alpha_A, \alpha_C) \leq \mathcal{D}(t, \alpha_A, \alpha_B) + \mathcal{D}(t, \alpha_B, \alpha_C) \tag{5.59}$$

for any three states α_A, α_B and α_C from $\mathrm{L}^1(\Omega)$.

Brief sketch of the proof. Due to definition (5.43) and positivity of dissipation distance, one may investigate the inequality for the dissipation distance at an arbitrary point $x \in \Omega$. Because of the different definition of forward and reverse cases and 3 different states A, B, C considered, there are 6 different possible situations (e.g. $\xi_A \leq \xi_B \leq \xi_C$, $\xi_A \leq \xi_C \leq \xi_B$, ...) to be examined. By lengthy but straightforward calculations based mostly on triangle inequality for Euclidean norms, it is possible to show that the triangle inequality even holds for the transformation and reorientation parts of dissipation distance separately. □

5.3.1 Reformulation of time-incremental problem and properties of its solutions

The initial step of the proof is the formulation of a discrete problem and investigation of its solution. Hence, we define:

Definition 5.3.5 (Regularized time-incremental problem)**.** Let u_0, α_0, η_0 be the initial conditions of the rate-independent evolution satisfying constraints (5.2). Let boundary conditions and temperature be prescribed in accordance with data qualifications in Section 5.1 at time points t_k, $k = 1, \ldots, N$. We solve the following problem at t_k:

Minimize $\mathcal{E}(t_k, u, \alpha, \eta) + \mathcal{D}(t_k, \alpha_{k-1}, \alpha - \alpha_{k-1})$
subject to $(u, \alpha, \eta) \in \mathcal{U} \times \mathcal{V} \times \mathcal{Z}$ and $0 \leq \eta(x) \leq 1 - \xi(x)$ for a.a. $x \in \Omega$. (RTIP)

Similarly to proceeding in Section 5.2 we formulate a proposition of existence of a solution:

Proposition 5.3.6 (Existence of a discrete solution of (RTIP))**.** *Let $\alpha_{k-1} \in \mathcal{V}$. Let material parameters, boundary conditions and temperature loading be given in accordance with data qualification in Section 5.1. Then there exists a solution of the time-incremental minimization problem* (RTIP) *at the time t_k.*

Proof. We could exactly follow the direct method used in the proof of Proposition 5.2.2. Since we minimize on a closed convex subset of a reflexive Banach space, we need to assure that the functional in (RTIP) is bounded from below (i.e. there is a infimizing sequence), coercive (in the sence that any infimizing sequence is bounded) and weak lower semicontinuous. Then, taking an infimizing sequence, the coercivity allows us the to find a subsequence which has a weak limit and the lower semicontinuity assures that the limit is indeed a minimizer.

An important fact is that the dissipation distances introduced in Section 4.5 exactly match the discretization of the dissipation function used in the minimization problem (TIP) and Proposition 5.2.2 (cf. (5.34) and (4.39)). Thus, the only difference between minimized functionals in (TIP) and (RTIP) is the regularization term $\|\nabla\alpha\|^2$ added to f. However, it actually does not restrict utilization of the key ingredients used in proof of Proposition 5.2.2 if α is now considered in $\mathrm{W}^{1,2}(\Omega,\mathbb{R}^{3\times3}_{\mathrm{sym},0}) \times \mathrm{W}^{1,2}(\Omega;\mathbb{R})$. Indeed, due to its quadratic form, the convexity is preserved. Coercivity now demands to be $\mathcal{E}+\mathcal{D} \to \infty$ whenever $\|u_n\|_{\mathrm{L}^2(\Omega)} \to \infty$ or $\|\nabla\alpha\|_{\mathrm{L}^2(\Omega)} \to \infty$ (recall that $\|\alpha\|_{\mathrm{L}^2(\Omega)}$ is bounded). This is immediately seen if we add the term $\|\nabla\alpha\|^2_{\mathrm{L}^2(\Omega)}$ to both sides of (5.39). And we also obtain the following bound on the energy:

$$\exists\, C(t_k):\ \mathcal{E}(t_k,u_k,\alpha_k,\eta_k) \geq -C(t_k) \quad \text{for a time-discrete solution } (u_k,\alpha_k,\eta_k), \tag{5.60}$$

which, together with positivity of $\mathcal{D}$, implies that the functional $\mathcal{E}+\mathcal{D}$ in (RTIP) is bounded from below.

Moreover, owing to chosen form of the energy and dissipation functionals, the time-discrete solution at t_k depends only on α_{k-1} (and not on u_{k-1},η_{k-1}). Since the constraints on α_{k-1} are time-independent, we may – with regard to (5.39) – conclude that for *any* time-discrete solution of (RTIP), the energy functional $\mathcal{E}$ is t-independently bounded from below, i.e. the constant in (5.60) may be found time- and discretization-independent. □

Moreover, the discrete solution satisfies a discrete version of the stability condition and a modified energy balance:

Theorem 5.3.7 (Discrete version of stability condition and energy balance)**.** *Let the initial condition $(u_0,\alpha_0,\eta_0) \in \mathcal{U}\times\mathcal{V}\times\mathcal{Z}$ satisfies the discrete stability condition defined below. Then every solution $(u_k,\alpha_k,\eta_k) \in \mathcal{U}\times\mathcal{V}\times\mathcal{Z}$, $k\in\{1,\dots,N\}$ of* (RTIP) *satisfies the discrete stability condition and energy inequlatities in the form:*

- ***Stability condition:***

$$\mathcal{E}(t_k,u_k,\alpha_k,\eta_k) \leq \mathcal{E}(t_k,\tilde{u},\tilde{\alpha},\tilde{\eta}) + \mathcal{D}(t_k,\alpha_k,\tilde{\alpha}) \quad \forall\,(\tilde{u},\tilde{\alpha},\tilde{\eta}) \in \mathcal{U}\times\mathcal{V}\times\mathcal{Z} \tag{5.61}$$

- ***Energy inequalities:***

$$\int_{t_{k-1}}^{t_k} \partial\mathcal{E}_t(s,u_k(s),\alpha_k(s),\eta_k(s))\,\mathrm{d}s$$
$$\leq \mathcal{E}(t_k,u_k,\alpha_k,\eta_k)+\mathcal{D}(t_k,\alpha_{k-1},\alpha_k)-\mathcal{E}(t_{k-1},u_{k-1},\alpha_{k-1},\eta_{k-1})$$
$$\leq \int_{t_{k-1}}^{t_k} \partial_t\mathcal{E}(s,u_{k-1}(s),\alpha_{k-1}(s),\eta_{k-1}(s))\,\mathrm{d}s \tag{5.62}$$

Proof. Let us (within this proof) denote $e_k := \mathcal{E}(t_k,u_k,\alpha_k,\eta_k)$ and $b_k := \mathcal{D}(t_k,\alpha_{k-1},\alpha_k)$.

The any solution of (RTIP) is a minimizer, for any $k\in\{1,\dots,N\}$ and for any $(\tilde u,\tilde\alpha,\tilde\eta)\in\mathcal{U}\times\mathcal{V}\times\mathcal{Z}$ we have:

$$e_k+b_k\leq \mathcal{E}(t_k,\tilde u,\tilde\alpha,\tilde\eta)+\mathcal{D}(t_k,\alpha_{k-1},\tilde\alpha). \tag{5.63}$$

Using the triangle inequality $\mathcal{D}(t_k,\alpha_{k-1},\tilde\alpha)\leq b_k+\mathcal{D}(t_k,\alpha_k,\tilde\alpha)$ (see Lemma 5.3.4) at the right-hand side of (5.63), we obtain

$$\begin{aligned} e_k+b_k &\leq \mathcal{E}(t_k,\tilde u,\tilde\alpha,\tilde\eta)+b_k+\mathcal{D}(t_k,\alpha_k,\tilde\alpha)\\ e_k &\leq \mathcal{E}(t_k,\tilde u,\tilde\alpha,\tilde\eta)+\mathcal{D}(t_k,\alpha_k,\tilde\alpha). \end{aligned} \tag{5.64}$$

But this is actually the stability condition (5.52) for a solution (u_k,α_k,η_k) of (RTIP), which had to be proven.

Testing (5.63) with the triplet $(\tilde u,\tilde\alpha,\tilde\eta) := (u_{k-1},\alpha_{k-1},\eta_{k-1})$ gives:

$$e_k+b_k\leq \mathcal{E}(t_k,u_{k-1},\alpha_{k-1}\eta_{k-1})+\underbrace{\mathcal{D}(t_k,\alpha_{k-1},\alpha_{k-1})}_{=0}$$
$$=\underbrace{\mathcal{E}(t_k,u_{k-1},\alpha_{k-1},\eta_{k-1})-\mathcal{E}(t_{k-1},u_{k-1},\alpha_{k-1},\eta_{k-1})}_{=\int_{t_{k-1}}^{t_k}\partial_t\mathcal{E}(s,u_{k-1},\alpha_{k-1},\eta_{k-1})\,\mathrm{d}s}+\mathcal{E}(t_{k-1},u_{k-1},\alpha_{k-1},\eta_{k-1})$$

i.e.

$$e_k+b_k-e_{k-1}\leq\int_{t_{k-1}}^{t_k}\partial_t\mathcal{E}(s,u_{k-1},\alpha_{k-1},\eta_{k-1})\,\mathrm{d}s. \tag{5.65}$$

which is the upper estimate of energy balance. Due to data qualifications (5.5)–(5.8), the derivative $\partial_t\mathcal{E}$ is well-defined:

$$\begin{aligned}&\partial_t\mathcal{E}(t,u_{k-1},\alpha_{k-1},\eta_{k-1})\\ &=\langle\dot l(t),u_{k-1}\rangle+\langle m'(T)\dot T(t),\xi_{k-1}\rangle+\langle q'(T)\dot T(t),\eta_{k-1}\rangle+\langle w'(T)\dot T(t),1\rangle,\end{aligned} \tag{5.66}$$

where the prime, $'$, denotes derivation with respect to temperature, T.

The lower estimate is obtained in the same manner by testing the solution at t_{k-1} with $(\tilde u,\tilde\alpha,\tilde\eta) := (u_k,\alpha_k,\eta_k)$. □

Now, summation of (5.65) for $k=1,\dots,l$ for any $l\in\{1,...,N\}$ gives the following inequality:

$$\mathcal{E}(t_l,u_l,\alpha_l,\eta_l)-\mathcal{E}(0,u_0,\alpha_0,\eta_0)+\sum_{k=1}^{l}\mathcal{D}(t_k,\alpha_{k-1},\alpha_k)$$
$$\leq\sum_{k=1}^{l}\int_{t_{k-1}}^{t_k}\partial_t\mathcal{E}(s,u_{k-1},\alpha_{k-1},\eta_{k-1})\,\mathrm{d}s \tag{5.67}$$

5.3.2 Construction of interpolants; a priori estimates

Based on solutions of (RTIP) established in the previous subsection, we are going to introduce *piece-wise constant* interpolation functions at $[0,\mathcal{T}]$ and show some estimates on them.[4]

Let us define the piece-wise constant interpolants

$$u^N(t) : [0,\mathcal{T}] \to \mathrm{W}^{1,2}_0(\Omega,\mathbb{R}^3), \qquad \eta^N(t) : [0,\mathcal{T}] \to \mathrm{L}^\infty(\Omega,\mathbb{R}),$$

$$\alpha^N(t) : [0,\mathcal{T}] \to \mathrm{W}^{1,2}(\Omega,\mathbb{R}^{3\times 3}_{\mathrm{sym},0}) \times \mathrm{W}^{1,2}(\Omega,\mathbb{R})$$

as follows:

$$u^N(t) := u_k \quad \text{if } t \in [t_k,t_{k+1}) \text{ and } u^N(\mathcal{T}) := u_N \tag{5.68}$$

$$\alpha^N(t) := \alpha_k \quad \text{if } t \in [t_k,t_{k+1}) \text{ and } \alpha^N(\mathcal{T}) := \alpha_N \tag{5.69}$$

$$\eta^N(t) := \eta_k \quad \text{if } t \in [t_k,t_{k+1}) \text{ and } \eta^N(\mathcal{T}) := \eta_N \tag{5.70}$$

For further proceedings, we need to prove the following lemma:

Lemma 5.3.8. *Let u^N,α^N,η^N be defined as above. Then*

$$\|u^N\|_{\mathrm{L}^\infty([0,\mathcal{T}],\mathrm{W}^{1,2}(\Omega))} \le C, \qquad \|\eta^N\|_{\mathrm{L}^\infty([0,\mathcal{T}],\mathrm{L}^\infty(\Omega))} \le C,$$

$$\|\alpha^N\|_{\mathrm{L}^\infty([0,\mathcal{T}],\mathrm{W}^{1,2}(\Omega))} \le C, \qquad \mathrm{Var}_{\mathrm{L}^1(\Omega)}(\alpha^N,[0,\mathcal{T}]) \le C.$$

Proof. First, rewriting (5.67) one obtains:

$$\underbrace{\mathcal{E}(t_l,u^N(t_l),\alpha^N(t_l),\eta^N(t_l)) + \sum_{i=1}^{l} \mathcal{D}(t_i,\alpha^N(t_{i-1}),\alpha^N(t_i))}_{(LHS)}$$

$$\le \underbrace{\mathcal{E}(0,u^N(0),\alpha^N(0),\eta^N(0)) + \int_0^{t_l} |\partial_t\mathcal{E}(s,u^N(s),\alpha^N(s),\alpha^N(s))|\,\mathrm{d}s}_{(RHS)} \tag{5.71}$$

Let us denote

$$\mathcal{E}_0 := \mathcal{E}(0,u^N(0),\alpha^N(0),\eta^N(0)),$$

$$u^N_l := u^N(t_l), \quad \alpha^N_l := \alpha^N(t_l), \quad \eta^N_l := \eta^N(t_l)$$

and

$$\theta^N := \partial_t\mathcal{E}(t,u^N(t),\alpha^N(t),\eta^N(t)).$$

[4] The interpolation functions are actually *simple functions*. We say that function $g : [0,\mathcal{T}] \to V$, V is a Banach space, is simple, if it takes only finite number of values $v_i \in V$ and $A_i := u^{-1}(v_i)$ is Lebesgue measurable.

Due to data qualification (5.5)–(5.8) and since components ξ_k, η_k of any solution of (TIP) are bounded, $\forall\, t \in [0, \mathcal{T}]$:

$$\begin{aligned}
|\theta^N(t)| &\leq |\langle \dot{l}(t), u^N(t)\rangle| + |\langle m'(T)\dot{T}(t), \xi^N(t)\rangle| + |\langle q'(T)\dot{T}(t), \eta^N(t)\rangle| \\
&\quad + |\langle w'(T)\dot{T}(t), 1\rangle| \\
&\leq \int_\Omega |\dot{F}_{\mathrm{vol}}(t)u^N(t)|\,\mathrm{d}V + \int_{\Gamma_\mathrm{N}} |\dot{F}_{\mathrm{surf}}(t)u^N(t)|\,\mathrm{d}S + \|m'(T)\dot{T}(t)\|_{\mathrm{L}^2(\Omega)} \\
&\quad \times \|\xi^N(t)\|_{\mathrm{L}^2(\Omega)} + \|q'(T)\dot{T}(t)\|_{\mathrm{L}^1(\Omega)}\|\eta^N(t)\|_{\mathrm{L}^\infty(\Omega)} + |\Omega|\,|w'(T)\dot{T}(t)| \\
&\leq \|\dot{F}_{\mathrm{vol}}\|_{\mathrm{L}^2(\Omega)}\|u^N(t)\|_{\mathrm{L}^2(\Omega)} + \|\dot{F}_{\mathrm{surf}}\|_{\mathrm{L}^2(\Gamma_\mathrm{N})}\|u^N(t)\|_{\mathrm{L}^2(\Gamma_\mathrm{N})} \\
&\quad + \ C\|\dot{T}(t)\|_{\mathrm{L}^2(\Omega)}(\|\xi^N(t)\|_{\mathrm{L}^2(\Omega)} + \|\eta^N(t)\|_{\mathrm{L}^2(\Omega)} + 1) \qquad (5.72) \\
&\leq \frac{1}{2}\left(\|\dot{F}_{\mathrm{vol}}\|^2_{\mathrm{L}^2(\Omega)} + \|u^N(t)\|^2_{\mathrm{L}^2(\Omega)}\right) + \frac{1}{2}\left(\|\dot{F}_{\mathrm{surf}}\|^2_{\mathrm{L}^2(\Gamma_\mathrm{N})} + \|u^N(t)\|^2_{\mathrm{L}^2(\Gamma_\mathrm{N})}\right) \\
&\leq C(1 + \frac{1}{2}\|u^N(t)\|^2_{\mathrm{W}^{1,2}(\Omega)}) \qquad (5.73) \\
&\leq C(1 + \|\boldsymbol{\varepsilon}(u^N(t))\|^2_{\mathrm{L}^2(\Omega)}) \qquad (5.74)
\end{aligned}$$

Hölder's inequality was used to get inequality (5.72), Young's inequality to get the penultimate inequality (5.73) and a modification of Korn's first inequality to get the last one. Note that the constant may be chosen time-independent due to the data qualifications (5.5) and (5.6). Therefore, the right-hand side of (5.71) may be estimated

$$(RHS) \leq \mathcal{E}_0 + \int_0^{t_l} C(1 + \|\boldsymbol{\varepsilon}(u^N(s))\|^2_{\mathrm{W}^{1,2}(\Omega)})\,\mathrm{d}s. \qquad (5.75)$$

Now let us turn attention to the left-hand side of Eq. (5.71). Since the integrated dissipation distance is always non-negative, we may estimate

$$\sum_{i=1}^{l} \mathcal{D}(t_i, \alpha^N(t_{i-1}), \alpha^N(t_i)) \geq 0.$$

We need the following estimate of energy:

$$\begin{aligned}
\int_\Omega \psi(u_l^N, \alpha_l^N, \eta_l^N)\,\mathrm{d}V &= \int_\Omega f^{\mathrm{el}}(u_l^N, \boldsymbol{\varepsilon}_l^{\mathrm{in},N}, \xi_l^N, \eta_l^N)\,\mathrm{d}V \\
&\quad + \int_\Omega \underbrace{R\frac{(\eta_l^N)^2}{1-\xi_l^N}}_{\geq 0} + \nu\,\|\nabla\alpha_l^N\|^2\,\mathrm{d}V + \langle m_l^N, \xi_l^N\rangle + \langle q_l^N, \eta_l^N\rangle + \langle w_l^N, 1\rangle,
\end{aligned}$$

and finding $T_{\min} := \min_{t\in[0,\mathcal{T}]} T(t)$ (due to data qualification (5.8)) we can estimate

$$\langle m^N(t), \xi^N(t)\rangle \geq -C, \quad \langle q^N(t), \eta^N(t)\rangle \geq -C \quad \text{and} \quad \langle w^N(t), 1\rangle \geq -C \qquad (5.76)$$

Thus,

$$\int_\Omega \psi(u_l^N, \alpha_l^N, \eta_l^N)\,\mathrm{d}V \geq \int_\Omega f^{\mathrm{el}}(u_l^N, \alpha_l^N, \eta_l^N)\,\mathrm{d}V + \nu\|\nabla\alpha_l^N\|^2_{\mathrm{L}^2(\Omega)} - C \qquad (5.77)$$

We recall the extended Young's inequality for $0 \leq a, b \in \mathbb{R}$ with $\gamma > 0$

$$ab \leq \frac{\gamma a^2}{2} + \frac{b^2}{2\gamma} \qquad (5.78)$$

and utilize it in coercivity inequality of the elastic contribution to energy derived in (5.37) so that:

$$\begin{aligned}\int_\Omega f^{\mathrm{el}}(t,u_l^N,\alpha_l^N,\eta_l^N)\,\mathrm{d}V&\\ &\geq C\left(\|\boldsymbol{\varepsilon}(u)\|^2_{\mathrm{L}^2(\Omega)}-2\rho\|\boldsymbol{\varepsilon}(u)\|_{\mathrm{L}^2(\Omega)}+\rho^2\right)\\ &\geq C\left(\|\boldsymbol{\varepsilon}(u_l)\|^2_{\mathrm{L}^2(\Omega)}-2\frac{\gamma_1\|\boldsymbol{\varepsilon}(u_l)\|^2_{\mathrm{L}^2(\Omega)}}{2}-2\frac{\rho^2}{2\gamma_1}+\rho^2\right)\end{aligned}\tag{5.79}$$

Also, after applying Hölder inequality,

$$\begin{aligned}\langle l_l^N,u_l^N\rangle &\leq \|F_{\mathrm{vol},l}\|_{\mathrm{L}^2(\Omega)}\|u_l^N\|_{\mathrm{L}^2(\Omega)}+\|F_{\mathrm{surf},l}\|_{\mathrm{L}^2(\Gamma)}\|u_l^N\|_{\mathrm{L}^2(\Gamma)}\\ &\leq \|u_l^N\|_{\mathrm{L}^2(\Omega)}\left(\|F_{\mathrm{vol},l}\|_{\mathrm{L}^2(\Omega)}+C\|F_{\mathrm{surf},l}\|_{\mathrm{L}^2(\Gamma)}\right)\\ &\leq \frac{\gamma_2\|u_l^N\|^2_{\mathrm{L}^2(\Omega)}}{2}+\frac{\|F_{\mathrm{vol},l}\|^2_{\mathrm{L}^2(\Omega)}+C\|F_{\mathrm{surf},l}\|^2_{\mathrm{L}^2(\Gamma)}}{2\gamma_2}\\ &\leq C^*\frac{\gamma_2}{2}\|\boldsymbol{\varepsilon}(u_l^N)\|^2_{\mathrm{L}^2(\Omega)}+\frac{1}{2\gamma_2}\left(\|F_{\mathrm{vol},l}\|^2_{\mathrm{L}^2(\Omega)}+C\|F_{\mathrm{surf},l}\|^2_{\mathrm{L}^2(\Gamma)}\right)\end{aligned}\tag{5.80}$$

Now, we may choose suitable values of the positive constants γ_1,γ_2 so that the left-hand side of (5.71) may be finally estimated:

$$\begin{aligned}(LHS)\ &\geq\ \mathcal{E}(t_l,u_l^N,\alpha_l^N,\eta_l^N)=\int_\Omega\psi(u_l^N,\alpha_l^N,\eta_l^N)\,\mathrm{d}x-\langle l_l^N,u_l^N\rangle\\ &\geq\ C\left(\|\boldsymbol{\varepsilon}(u_l^N)\|^2_{\mathrm{L}^2(\Omega)}-1\right)+\nu\|\nabla\alpha_l^N\|^2_{\mathrm{L}^2(\Omega)}.\end{aligned}\tag{5.81}$$

Both upper and lower estimates give together:

$$\begin{aligned}\|\boldsymbol{\varepsilon}(u^N(t_l))\|^2_{\mathrm{L}^2(\Omega)}+\nu\|\nabla\alpha^N(t_l)\|^2_{\mathrm{L}^2(\Omega)}&\leq C+\sum_{k=1}^{l}C\int_{t_{k-1}}^{t_k}\|\boldsymbol{\varepsilon}(u^N(s))\|^2_{\mathrm{L}^2(\Omega)}\,\mathrm{d}s\\ &=C+\sum_{k=1}^{l}C(t_k-t_{k-1})\|\boldsymbol{\varepsilon}(u^N(t_{k-1}))\|^2_{\mathrm{L}^2(\Omega)}.\end{aligned}\tag{5.82}$$

Applying a discrete form of Gronwall's lemma[5] (with gradient term on the left-hand side omitted) one obtains the following estimates:

$$\sup_{t\in[0,\mathcal{T}]}\|\boldsymbol{\varepsilon}(u^N(t))\|^2_{\mathrm{L}^2(\Omega)}\leq C\tag{5.83}$$

Korn's inequality then implies:

$$\sup_{t\in[0,\mathcal{T}]}\|u^N(t)\|^2_{\mathrm{W}^{1,2}(\Omega)}\leq C\tag{5.84}$$

i.e.

$$u^N\in L^\infty([0,\mathcal{T}],\mathrm{W}^{1,2}(\Omega)).\tag{5.85}$$

[5] Let y_k and g_k be nonnegative sequences, K a nonnegative constant. If $y_l\leq K+\sum_{0\leq k<l}g_k y_k$ for $l\geq 0$, then $y_l\leq K\exp\left(\sum_{0\leq k<l}g_k\right)$ for $l\geq 0$.

Investigation of (5.82) in the view of (5.83) provides further result:

$$\sup_{t\in[0,\mathcal{T}]} \|\nabla\alpha^N(t)\|^2_{\mathrm{L}^2(\Omega)} \leq C, \tag{5.86}$$

Due to bounds on internal variables, it is apparent that

$$\sup_{t\in[0,\mathcal{T}]} \|\alpha^N(t)\|^2_{\mathrm{L}^\infty(\Omega)} \leq C \quad \text{and} \quad \sup_{t\in[0,\mathcal{T}]} \|\eta^N(t)\|^2_{\mathrm{L}^\infty(\Omega)} \leq C \tag{5.87}$$

Employing Poincaré inequality we see[6]

$$\alpha^N \in L^\infty([0,\mathcal{T}],\mathrm{W}^{1,2}(\Omega)), \tag{5.88}$$

and clearly

$$\eta^N \in L^\infty([0,\mathcal{T}],\mathrm{L}^\infty(\Omega)). \tag{5.89}$$

Reinspecting (5.74) in view of (5.83), we discover that $|\theta^N(t)| \leq C$ (independently of time), which leads to

$$\partial_t\mathcal{E}(t,u^N(t),\alpha^N(t),\eta^N(t)) \in L^\infty([0,\mathcal{T}],\mathbb{R}). \tag{5.90}$$

The bound together with coercivity of integrated dissipation distance (5.54), gives:

$$\begin{aligned}\mathrm{Var}_{\mathrm{L}^1(\Omega)}(\alpha^N,[0,\mathcal{T}]) &= \sum_{k=1}^N \|\alpha_k^N-\alpha_{k-1}^N\|_{\mathrm{L}^1(\Omega)} \leq \sum_{k=1}^N \frac{1}{c^*}\mathcal{D}(t_k,\alpha_{k-1}^N,\alpha_k^N)\\ &\leq \frac{1}{c^*}\left(e_0-e_N+\int_0^{\mathcal{T}}|\theta^N(s)|\,\mathrm{d}s\right)\\ &\leq \frac{1}{c^*}\left(e_0-e_N+C\cdot\mathcal{T}\right),\end{aligned} \tag{5.91}$$

which is again a constant due to bounds (5.60) and (5.74). Thus, finally

$$\mathrm{Var}_{\mathrm{L}^1(\Omega)}(\alpha^N,[0,\mathcal{T}]) = \|\alpha^N\|_{\mathrm{BV}([0,\mathcal{T}],\mathrm{L}^1(\Omega))} \leq C, \tag{5.92}$$

where the constant is discretization-independent. □

5.3.3 Selection of subsequences

Now, we proceed by selecting specific subsequences of the constructed interpolants. Let choose a sequence of partitions $\Pi^N = \{0 \leq t_0^N \leq \cdots \leq t_N^N = \mathcal{T}\}$ so that $\Pi^N \subset \Pi^{N+1}, N \in \mathbb{N}$ whose fineness $\Delta_N := \max\{t_j^N - t_{j-1}^N|\ j=1,\ldots,N\}$ tends to 0 and obtain the associated interpolants (u^N,α^N,η^N).

By application of a suitable version of Helly's selection theorem (see Theorem 1.126 and Remark 1.127 in Barbu and Precupanu, 2012) and property (5.88) of α^N, one can find a subsequence α^{N_k} and a limit function $\alpha \in L^\infty([0,\mathcal{T}],\mathrm{W}^{1,2}(\Omega))\cap \mathrm{BV}([0,\mathcal{T}],\mathrm{L}^1(\Omega))$ so that

$$\forall\, t\in[0,\mathcal{T}]\ :\ \alpha^{N_k}(t) \rightharpoonup \alpha(t) \text{ in } \mathrm{W}^{1,2}(\Omega) \tag{5.93}$$

[6] We have even $\alpha^N \in L^\infty([0,\mathcal{T}],\mathrm{W}^{1,2}(\Omega))\cap L^\infty([0,\mathcal{T}],\mathrm{L}^\infty(\Omega))$.

Due to compact embedding of $\mathrm{W}^{1,2}(\Omega)$ into $\mathrm{L}^1(\Omega)$ it is also true that

$$\forall\, t \in [0,\mathcal{T}] \;:\; \alpha^{N_k}(t) \to \alpha(t) \text{ in } \mathrm{L}^1(\Omega). \tag{5.94}$$

Reminding (5.90) and choosing a further subsequence if necessary, we may assume

$$\theta^{N_k} \overset{*}{\rightharpoonup} \theta^* \text{ in } \mathrm{L}^\infty((0,\mathcal{T}),\mathbb{R}). \tag{5.95}$$

Defining $\theta(t) := \limsup_{k\to\infty} \theta^{N_k}(t)$ and applying Fatou's lemma[7] (also recall (5.90)) we know that

$$\theta(t) \in \mathrm{L}^1((0,\mathcal{T}),\mathbb{R}) \tag{5.96}$$

and

$$\theta_*(t) \le \theta(t) \quad \text{for almost all } t \in [0,\mathcal{T}]. \tag{5.97}$$

In accordance with (5.85) and (5.89), for fixed $t \in [0,\mathcal{T}]$ we can choose a time-dependent subsequence $(N_l^t)_{l\in\mathbb{N}}$ of $(N_k)_{k\in\mathbb{N}}$ such that

$$\theta^{N_l^t}(t) \to \theta(t) \quad \text{for } l\to\infty \text{ in } \mathbb{R}, \tag{5.98}$$

$$u^{N_l^t}(t) \rightharpoonup u(t) \quad \text{for } l\to\infty \text{ in } \mathrm{W}_0^{1,2}(\Omega), \tag{5.99}$$

$$\eta^{N_l^t}(t) \overset{*}{\rightharpoonup} \eta(t) \quad \text{for } l\to\infty \text{ in } \mathrm{L}^\infty(\Omega). \tag{5.100}$$

To sum up, we have chosen some cluster points of subsequences of piece-wise constant sequences provided by (RTIP). It remains to show that (u,α,η) chosen in that way is an energetic solution, i.e. it satisfies the stability condition and energy balance.

5.3.4 Stability of the limit functions

We need to establish that the limit of the sequence of triplets $(u^{N_l^t}(t), \alpha^{N_l^t}(t), \eta^{N_l^t}(t))$ satisfies the stability condition. We will show a slightly more general result.

First, we recall that due to convexity of ψ in the internal variables (see the proof of Proposition 5.3.6), the energy function $\mathcal{E}$ is weakly lower semi-continuous. Moreover, $\mathcal{E}(t,\cdot,\cdot,\cdot)$ is continuous in the time variable since all respective time-dependent terms, $\langle l(t),u\rangle$, $\langle m(t),\xi\rangle$, $\langle q(t),\eta\rangle$, $\langle w(t),1\rangle$, are continuous linear functionals for fixed $(u,\alpha,\eta) \in \mathcal{U}\times\mathcal{V}\times\mathcal{Z}$ due to data qualification (5.5)–(5.8).

Thus, for any $t_j \to t$, $u_j \rightharpoonup u$ in $\mathcal{U}$, $\alpha_j \rightharpoonup \alpha$ in $\mathcal{U}$ and $\eta_j \overset{*}{\rightharpoonup} \eta$ in $\mathcal{Z}$ with each (u_j,α_j,η_j) being a stable triplet at t_j (i.e. satisfying inequality (5.61)) and for any $(\tilde u,\tilde\alpha,\tilde\eta) \in \mathcal{U}\times\mathcal{V}\times\mathcal{Z}$, we have

$$\begin{aligned} \mathcal{E}(t,u,\alpha,\eta) &\le \liminf_{j\to\infty} \mathcal{E}(t_j,u_j,\alpha_j,\eta_j) \\ &\le \liminf_{j\to\infty} \mathcal{E}(t_j,\tilde u,\tilde\alpha,\tilde\eta) + \mathcal{D}(t_j,\alpha_j,\tilde\alpha) = \mathcal{E}(t,\tilde u,\tilde\alpha,\tilde\eta) + \mathcal{D}(t,\alpha,\tilde\alpha), \end{aligned} \tag{5.101}$$

where we used in turn weak lower semi-continuity of $\mathcal{E}$, stability of (u_j,α_j,η_j) at t_j, time-continuity of $\mathcal{E}$ and passed to the limit

$$\lim_{j\to\infty} \mathcal{D}(t_j,\alpha_j,\tilde\alpha) = \mathcal{D}(t,\alpha,\tilde\alpha). \tag{5.102}$$

[7] Let $\{f_n\}_{n\in\mathbb{N}}$ be a sequence of real-valued measurable function defined on Ω. If there is an integrable function g on Ω such that $f_n \le g$ for all $f_n, n \in \mathbb{N}$, then $\limsup_{n\to\infty} \int_\Omega f_n \,\mathrm{d}V \le \int_\Omega \limsup_{n\to\infty} f_n \,\mathrm{d}V$.

If the last step is proved, we may take $\tau_l^t \nearrow t$ for $l \to \infty$ defined as $\tau_l^t := \max\{\hat{t} \in \Pi^{N_l^t} : \hat{t} \leq t\}$ and a sequence $(u^{N_l^t}(t),\ \alpha^{N_l^t}(t),\ \eta^{N_l^t}(t))$ and follow the previous proceeding: since t is fixed, we know that

$$(u^{N_l^t}(t), \alpha^{N_l^t}(t), \eta^{N_l^t}(t)) \rightharpoonup (u(t), \alpha(t), \eta(t)) \ \text{ in } \mathcal{U} \times \mathcal{V} \times \mathcal{Z} \tag{5.103}$$

and the triplet $(u^{N_l^t}(t), \alpha^{N_l^t}(t), \eta^{N_l^t}(t))$ satisfies the condition of stability for τ_l^t due to discrete stability. Thus, we will be able to conclude that the limit (u, α, η) satisfies the stability condition, after we prove the following lemma:

Lemma 5.3.9. *Let $t_j \to t$, $\alpha_j \rightharpoonup \alpha \in \mathcal{V}$ and $\tilde{\alpha} \in \mathcal{V}$. Then*

$$\lim_{j\to\infty} \mathcal{D}(t_j, \alpha_j, \tilde{\alpha}) = \mathcal{D}(t, \alpha, \tilde{\alpha}).$$

Proof. First, let us consider the reorientation part. We observe:

$$\begin{aligned}
0 &\leq |\mathcal{D}^{\mathrm{reo}}(t, \alpha, \tilde{\alpha}) - \mathcal{D}^{\mathrm{reo}}(t_j, \alpha_j, \tilde{\alpha})| \\
&= |\sigma^{\mathrm{reo}}(T(t))\overline{\mathcal{D}}^{\mathrm{reo}}(\alpha, \tilde{\alpha}) - \sigma^{\mathrm{reo}}(T(t_j))\overline{\mathcal{D}}^{\mathrm{reo}}(\alpha_j, \tilde{\alpha})| \\
&\leq \sigma^{\mathrm{reo}}(T(t)) \left|\overline{\mathcal{D}}^{\mathrm{reo}}(\alpha, \tilde{\alpha}) - \overline{\mathcal{D}}^{\mathrm{reo}}(\alpha_j, \tilde{\alpha})\right| \\
&\qquad + |\sigma^{\mathrm{reo}}(T(t)) - \sigma^{\mathrm{reo}}(T(t_j))| \cdot \left|\overline{\mathcal{D}}^{\mathrm{reo}}(\alpha_j, \tilde{\alpha})\right| \\
&\leq \sigma^{\mathrm{reo}}(T(t)) \int_\Omega \left|\overline{\delta}^{\mathrm{reo}}(\alpha, \tilde{\alpha}) - \overline{\delta}^{\mathrm{reo}}(\alpha_j, \tilde{\alpha})\right| \,\mathrm{d}V \\
&\qquad + |\sigma^{\mathrm{reo}}(T(t)) - \sigma^{\mathrm{reo}}(T(t_j))| \int_\Omega \left|\overline{\delta}^{\mathrm{reo}}(\alpha_j, \tilde{\alpha})\right| \,\mathrm{d}V,
\end{aligned} \tag{5.104}$$

since $\sigma^{\mathrm{reo}}(T)$ is space-independent and positive, and it remains to show that the right hand-side converges to zero for $j \to \infty$.

For the first integral on the right-hand side of (5.104), we will utilize continuity of the *Nemytskiĭ mapping* of the function $\overline{\delta}^{\mathrm{reo}}_{\tilde{\alpha}}(x, \alpha) := \overline{\delta}^{\mathrm{reo}}(\alpha, \tilde{\alpha})$ with $\tilde{\alpha}$ fixed.[8] First, we need to verify that $\overline{\delta}^{\mathrm{reo}}_{\tilde{\alpha}}$ is a so-called *Carathéodory mapping*. It requires $\overline{\delta}^{\mathrm{reo}}_{\tilde{\alpha}}(x, \cdot)$ to be continuous for almost all $x \in \Omega$ – this is a consequence of the definition of the reorientation part of the dissipation distance, particulary its continuity in $\alpha = \tilde{\alpha}$ – and, further, $\overline{\delta}^{\mathrm{reo}}_{\tilde{\alpha}}(\cdot, \alpha)$ must be measurable for all $\alpha \in \mathbb{R}^{3\times3}_{\mathrm{sym},0} \times \mathbb{R}$, which is clear. Now, if there is a constant, C, and function $\lambda(x) \in \mathrm{L}^1(\Omega)$ so that

$$|\overline{\delta}^{\mathrm{reo}}_{\tilde{\alpha}}(x, \alpha)| \leq C\|\alpha\|^2 + \lambda(x), \tag{5.105}$$

then the Nemytskii mapping $\mathcal{N}_\delta : \Omega \to \mathbb{R}$ defined by $[\mathcal{N}_\delta(\alpha)](x) := \delta^{\mathrm{reo}}_{\tilde{\alpha}}(x, \alpha)$ is bounded continuous mapping from $\mathrm{L}^2(\Omega, \mathbb{R}^{3\times3}_{\mathrm{sym},0}) \times \mathrm{L}^2(\Omega, \mathbb{R})$ to $\mathrm{L}^1(\Omega, \mathbb{R})$, which implies:

$$\begin{aligned}
&\|\alpha_j - \alpha\|_{\mathrm{L}^2(\Omega)} \to 0 \\
&\Rightarrow \quad \|\overline{\delta}^{\mathrm{reo}}_{\tilde{\alpha}}(x, \alpha) - \overline{\delta}^{\mathrm{reo}}_{\tilde{\alpha}}(x, \alpha_j)\|_{\mathrm{L}^1(\Omega)} = \int_\Omega \left|\overline{\delta}^{\mathrm{reo}}_{\tilde{\alpha}}(x, \alpha) - \overline{\delta}^{\mathrm{reo}}_{\tilde{\alpha}}(x, \alpha_j)\right| \,\mathrm{d}V \to 0
\end{aligned} \tag{5.106}$$

But, due to compact embedding of $\mathrm{W}^{1,2}(\Omega)$ into $\mathrm{L}^2(\Omega)$, we know that $\alpha_j \to \alpha$ in $\mathrm{L}^2(\Omega)$ and are be able to conclude that the first term on the right-hand side of

[8] Let us note that we temporarily include the space-dependence of dissipation distance in this paragraph so that application of Nemytskiĭ mapping is more clear.

(5.104) converges to zero if condition (5.105) is verified. We investigate (5.105) for the reverse phase transformation:[9]

$$
\begin{aligned}
|\tilde{\xi}| < |\xi| : \ |\overline{\delta}^{\mathrm{reo}}_{\tilde{\alpha}}(x,\alpha)| &= \left\| \frac{\tilde{\xi}-\xi}{\xi} \boldsymbol{\varepsilon}^{\mathrm{in}} \right\| + \left\| \tilde{\boldsymbol{\varepsilon}}^{\mathrm{in}} - \boldsymbol{\varepsilon}^{\mathrm{in}} - \frac{\tilde{\xi}-\xi}{\xi} \boldsymbol{\varepsilon}^{\mathrm{in}} \right\| \\
&\leq \left| \frac{\tilde{\xi}}{\xi} \right| \cdot \|\boldsymbol{\varepsilon}^{\mathrm{in}}\| + \|\boldsymbol{\varepsilon}^{\mathrm{in}}\| + \|\tilde{\boldsymbol{\varepsilon}}^{\mathrm{in}}\| + \|\boldsymbol{\varepsilon}^{\mathrm{in}}\| + \left| \frac{\tilde{\xi}}{\xi} \right| \cdot \|\boldsymbol{\varepsilon}^{\mathrm{in}}\| + \|\boldsymbol{\varepsilon}^{\mathrm{in}}\| \\
&\leq 5\|\boldsymbol{\varepsilon}^{\mathrm{in}}\| + \|\tilde{\boldsymbol{\varepsilon}}^{\mathrm{in}}\| \leq 5\|\alpha\| + \|\tilde{\alpha}\|, \qquad (5.107)
\end{aligned}
$$

where we omitted the explicit dependence of internal variables on (now fixed) x. Since $\tilde{\alpha} \in \mathrm{L}^1(\Omega)$, we may to rescale (5.107) by taking $C := 5$ and $\lambda(x) := \|\tilde{\alpha}(x)\| + 1$ to satisfy the condition (5.105). Making profit of the inequality (5.59), we can use the same estimate for the forward transformation, i.e. $|\tilde{\xi}| \geq |\xi|$.

Eventually, $\sigma^{\mathrm{reo}}(T(t))$ is a continuous function of time due to data qualification (5.14) and the sequence α_j is bounded in $\mathrm{L}^1(\Omega)$. Hence, applying the triangle inequality on the difference in the last term on the right-hand side of (5.104) assures the term converges to zero.

As far as the transformation part of integrated dissipation distance, $\mathcal{D}^{\mathrm{tr}}(\alpha,\tilde{\alpha})$, is concerned, we need to show

$$
\begin{aligned}
&\alpha_j \rightharpoonup \alpha \text{ in } \mathrm{W}^{1,2}(\Omega) \\
&\Rightarrow \quad \|\delta^{\mathrm{tr}}_{\tilde{\alpha}}(x,\alpha) - \delta^{\mathrm{tr}}_{\tilde{\alpha}}(x,\alpha_j)\|_{\mathrm{L}^1(\Omega)} = \int_\Omega \left| \delta^{\mathrm{tr}}_{\tilde{\alpha}}(x,\alpha) - \delta^{\mathrm{tr}}_{\tilde{\alpha}}(x,\alpha_j) \right| \mathrm{d}V \to 0, \qquad (5.108)
\end{aligned}
$$

where $\overline{\delta}^{\mathrm{tr}}_{\tilde{\alpha}}(x,\alpha) := \overline{\delta}^{\mathrm{tr}}(\alpha,\tilde{\alpha})$. But this is achieved by the same approach as above. Recalling the compact embedding of $\mathrm{W}^{1,2}(\Omega)$ into $\mathrm{L}^2(\Omega)$ the implication (5.105) will be a direct consequence of continuity of the Nemytskiĭ mapping chosen as $[\mathcal{N}_\delta(\alpha)](x) := \delta^{\mathrm{tr}}_{\tilde{\alpha}}(x,\alpha)$ if the Carathéodory conditions and an analogy of (5.105) are satisfied. But now

$$
\begin{aligned}
|\tilde{\xi}| < |\xi| : \ |\delta^{\mathrm{tr}}_{\tilde{\alpha}}(x,\alpha)| &= |\xi - \tilde{\xi}| \cdot [A_{\mathrm{s}} - T_0 + (1-\xi)(A_{\mathrm{f}} - A_{\mathrm{s}})] \\
&\leq |\xi| [A_{\mathrm{f}} - T_0] \leq |\xi| \max\{A_{\mathrm{f}} - T_0, T_0 - M_{\mathrm{f}}\} \qquad (5.109)
\end{aligned}
$$

and the last estimate be verified also for $|\tilde{\xi}| \geq |\xi|$. The Carathéodory conditions are again satisfied, which completes the proof. □

We finally show several useful consequences of the so-far elaboration. We show that

$$
\mathcal{E}(t,u,\alpha,\eta) = \lim_{l\to\infty} \mathcal{E}(t, u^{N_l^t}(t), \alpha^{N_l^t}(t), \eta^{N_l^t}(t)). \qquad (5.110)
$$

The lower estimate

$$
\mathcal{E}(t,u(t),\alpha(t),\eta(t)) \leq \liminf_{l\to\infty} \mathcal{E}(t, u^{N_l^t}(t), \alpha^{N_l^t}(t), \eta^{N_l^t}(t)) \qquad (5.111)
$$

[9] Now we will formally extend validity of $\overline{\delta}^{\mathrm{reo}}_{\tilde{\alpha}}$ and $\delta^{\mathrm{tr}}_{\tilde{\alpha}}$ so that both are defined for any $\alpha \in \mathbb{R}^{3\times 3}_{\mathrm{sym},0} \times \mathbb{R}$. We just extend the definition (5.34) simply by replacing the conditions $\tilde{\xi} \geq \xi$ and $\tilde{\xi} < \xi$ by $|\tilde{\xi}| \geq |\xi|$ and $|\tilde{\xi}| < |\xi|$, respectively. Note also that continuity in α is not violated.

is a consequence of lower semi-continuity of the (convex) function $\mathcal{E}(t,\cdot,\cdot,\cdot)$. The upper estimate results from

$$\begin{aligned}\mathcal{E}(t,u(t),\alpha(t),\eta(t)) &= \lim_{l\to\infty}\mathcal{E}(t,u(t),\alpha(t),\eta(t)) + \underbrace{\mathcal{D}(t,\alpha^{N_l^t}(t),\alpha(t))}_{\to 0}\\ &\geq \limsup_{l\to\infty}\mathcal{E}(t,u^{N_l^t}(t),\alpha^{N_l^t}(t),\eta^{N_l^t}(t)),\end{aligned}\tag{5.112}$$

where we employed weak continuity of $\mathcal{D}$ for fixed t and the stability condition – proved in the previous subsection – tested by the triplet $(u(t),\alpha(t),\eta(t))$.

Next, one may also observe that

$$\lim_{l\to\infty}\partial_t\mathcal{E}(t,u^{N_l^t}(t),\alpha^{N_l^t}(t),\eta^{N_l^t}(t)) = \partial_t\mathcal{E}(t,u(t),\alpha(t),\eta(t)).\tag{5.113}$$

Indeed, recalling data qualification (5.5)–(5.8) and the fact that weak convergence in (5.103) and compact embedding of $\mathrm{W}^{1,2}(\Omega)$ into $\mathrm{L}^2(\Omega)$ imply even strong convergence in $\mathrm{L}^2(\Omega)$, we have

$$\langle \dot{l}(t), u^{N_l^t}(t)\rangle \to \langle \dot{l}(t), u(t)\rangle \qquad \text{for (index) } l\to\infty \text{ in } \mathbb{R},\tag{5.114}$$

$$\langle m'(T)\dot{T}(t), \xi^{N_l^t}(t)\rangle \to \langle m'(T)\dot{T}(t), \xi(t)\rangle \qquad \text{for } l\to\infty \text{ in } \mathbb{R},\tag{5.115}$$

$$\langle q'(T)\dot{T}(t), \eta^{N_l^t}(t)\rangle \to \langle q'(T)\dot{T}(t), \eta(t)\rangle \qquad \text{for } l\to\infty \text{ in } \mathbb{R},\tag{5.116}$$

which together with (5.66) results in the claim.

5.3.5 Energy estimates and proof of energy balance

The last step of the proof of Theorem 5.3.2 is to confirm that (u,α,η) satisfies the energy balance (5.53). We will proceed by proving two energy inequalities, upper and lower, which together provide the required balance. Prior to it, some consideration on the dissipation term are made.

A special attention must be paid for treating the dissipation term, since we can follow the standard approach for time-independent transformation part and not for time-dependent reorientation one. Let us prove a useful lemma first:

Lemma 5.3.10. *Let $g(t):[0,\mathcal{T}]\to\mathbb{R}$ be a continuous function with a positive image, i.e. $g(t)>0$ for any $t\in[0,\mathcal{T}]$. Let μ_1,μ_2 be two measures defined on $[0,\mathcal{T}]$ such that for any $[s,z]\subset[0,\mathcal{T}]$ we have*

$$\mu_1([s,z]) \leq \mu_2([s,z]).\tag{5.117}$$

Then

$$\int_0^{\mathcal{T}} g(t)\,\mathrm{d}\mu_1(t) \leq \int_0^{\mathcal{T}} g(t)\,\mathrm{d}\mu_2(t).\tag{5.118}$$

Proof. We will construct a sequence of interpolation functions of $g(t)$, every member being a sum of simple functions. For $n\in\mathbb{N}$ we set an equidistant partition $0=\tau_0\leq\tau_1\leq\ldots\leq\tau_n=\mathcal{T}$ such that $\tau_i=\tau_0+ih$ for $i\in\{0,\ldots,n\}$ with $h:=\mathcal{T}/n$; i.e. $[0,\mathcal{T}]=\bigcup_{i=1}^{n-1}[\tau_{i-1},\tau_i)\cup[\tau_{n-1},\tau_n]=:\bigcup_{i=1}^n A_i$. Then we define a sequence of functions $g_n(t):[0,\mathcal{T}]\to\mathbb{R}$ as $g_n(t):=\sum_{i=1}^n g_n(\tau_{i-1})\mathbf{1}_{A_i}(t)$, where $\mathbf{1}_X$ is the characteristic function of a set X, i.e. $\mathbf{1}_X(x)=1$ if $x\in X$ and $\mathbf{1}_X(x)=0$

elsewhere. Due to such a construction and with respect to continuity of g, we see that $\lim_{n\to\infty} g_n(t) = g(t)$ for all $t \in [0, \mathcal{T}]$ point-wise.

Further, to be able to measure also other than closed subsets of $[0, \mathcal{T}]$, we introduce an extension of measures μ_1, μ_2, so-called *outer measures* $\tilde{\mu}_1, \tilde{\mu}_2$. Let X be any subinterval of $[0, \mathcal{T}]$ and $\mathcal{C}_X$ be a set of all countable collections of closed subintervals $[0, \mathcal{T}]$ whose union covers X. Then we define

$$\tilde{\mu}_j(X) := \inf \left\{ \sum_{B \in \mathcal{C}_X} \mu_j(B) \right\}, \quad j \in \{1, 2\}. \tag{5.119}$$

and note that new measures equal to the original ones on closed subsets.

The relation (5.117) then implies:

$$\tilde{\mu}_1(A_i) = \inf \left\{ \sum_{B \in \mathcal{C}_{A_i}} \mu_1(B) \right\} \leq \inf \left\{ \sum_{B \in \mathcal{C}_{A_i}} \mu_2(B) \right\} = \tilde{\mu}_2(A_i), \quad \forall\, i \in \{1, \dots, n\}. \tag{5.120}$$

Since g_n are simple functions and $g(t) > 0$ for any $t \in [0, \mathcal{T}]$:

$$\int_0^{\mathcal{T}} g_n(t)\, \mathrm{d}\tilde{\mu}_1(t) = \sum_{i=1}^{n} g_n(\tau_{i-1}) \tilde{\mu}_1(A_i) \leq \sum_{i=1}^{n} g_n(\tau_{i-1}) \tilde{\mu}_2(A_i) = \int_0^{\mathcal{T}} g_n(t)\, \mathrm{d}\tilde{\mu}_2(t). \tag{5.121}$$

We may take limit $n \to \infty$ and apply the Lebesgue's dominated convergence theorem[10] on both the first and the last terms since the subsequence g_n is converging point-wise to g and it is bounded from above by a constant function $\max_{t\in[0,\mathcal{T}]} g(t)$ on $[0, \mathcal{T}]$. Hence,

$$\int_0^{\mathcal{T}} g(t)\, \mathrm{d}\tilde{\mu}_1(t) \leq \int_0^{\mathcal{T}} g(t)\, \mathrm{d}\tilde{\mu}_2(t). \tag{5.122}$$

As measures $\tilde{\mu}_j$ and μ_j, $j \in \{1, 2\}$ are equal on closed subintervals of $[0, \mathcal{T}]$, we obtain the claim. □

Transformation part of dissipation

It is not difficult to see that for any *interpolant* $\alpha^N(t)$ defined in (5.69) it holds true:

$$\sum_{i=1}^{N} \mathcal{D}^{\mathrm{tr}}(\alpha^N(t_{i-1}), \alpha^N(t_i)) = \mathrm{Diss}^{\mathrm{tr}}(\alpha^N, [0, t]). \tag{5.123}$$

We denote $\mathrm{Diss}^{\mathrm{tr}}(\alpha^N, [0, t]) =: \beta^N(t) \in \mathbb{R}$. Due to positivity of dissipation distance, we know that $\beta^N(t) \leq \beta^{N+1}(t)$ and $\{\beta^N(t)\}_{k\in\mathbb{N}}$ is a non-decreasing sequence of real numbers. Hence,

$$\lim_{k\to\infty} \mathrm{Diss}^{\mathrm{tr}}(\alpha^{N_k}, [0, t]) =: \beta(t) \in \mathbb{R} \cup \{\infty\}. \tag{5.124}$$

Lower semi-continuity of $\mathrm{Diss}^{\mathrm{tr}}$ then gives

$$\mathrm{Diss}^{\mathrm{tr}}(\alpha, [0, t]) \leq \beta(t). \tag{5.125}$$

[10] Let f_n, $n \in \mathbb{N}$ be a sequence of real-valued measurable functions on a measure space (S, Σ, μ), $f_n \to f$ point-wise and there is some integrable function h such that $|f_n(x)| \leq h(x)$ for all $n \in \mathbb{N}$ and a.a. $x \in S$. Then f is integrable and $\lim_{n\to\infty} \int_S f_n\, \mathrm{d}\mu = \int_S f\, \mathrm{d}\mu$.

On the other hand, with respect to suprema in definitions of contributions to the total dissipation (5.45) and (5.46), it holds true:

$$\sum_{i=1}^{N} \mathcal{D}^{\mathrm{tr}}(\alpha(t_{i-1}), \alpha(t_i)) \leq \mathrm{Diss}^{\mathrm{tr}}(\alpha(t), [0,t]). \tag{5.126}$$

Reorientation part of dissipation

Treating the reorientation part of dissipation requires more subtle approach. Recall we have defined the sequence $\alpha^{N_k}(t) \to \alpha(t)$ in $\mathrm{L}^1(\Omega)$ for any $t \in [0, \mathcal{T}]$ in Subsection 5.3.3. Now let us take any interval $[s,z] \subset [0,\mathcal{T}]$ and define an partition $s = \tau_0 \leq \tau_1 \leq \ldots \leq \tau_K = z$ with $\Delta_K := \max\{\tau_i - \tau_{i-1} \,:\, i = 1, \ldots, K\}$. An important observation is that

$$\lim_{k\to\infty} \overline{\mathcal{D}}^{\mathrm{reo}}(\alpha^{N_k}(\tau_{i-1}), \alpha^{N_k}(\tau_i)) = \overline{\mathcal{D}}^{\mathrm{reo}}(\alpha(\tau_{i-1}), \alpha(\tau_i)). \tag{5.127}$$

This result is a consequence of the strong convergence in (5.94) and of applying the Nemytskiĭ mapping technique introduced in the proof of Lemma 5.3.9 to $\overline{\delta}^{\mathrm{reo}}(x, \alpha_j, \alpha_m) := \overline{\delta}^{\mathrm{reo}}(\alpha^{N_k}(\tau_{i-1}), \alpha^{N_k}(\tau_i))$ where $\alpha_j \to \alpha(\tau_{i-1})$ and $\alpha_m \to \alpha(\tau_i)$ in $\mathrm{L}^1(\Omega)$. The main difference with respect to that proof is that no internal variable is fixed, now. Thus, when investigating the Carathéodory condition on continuity, we need to employ the condition $\langle \boldsymbol{\varepsilon}_n^{\mathrm{in}} \rangle \leq \xi_n$ for any sequence $\alpha_n \in \mathcal{V}$, $n \in \mathbb{N}$ – particularly $\boldsymbol{\varepsilon}_n^{\mathrm{in}} \to 0$ whenever $\xi_n \to 0$ – to obtain continuity for $\xi_j \to 0 \wedge \xi_m \to 0$. The inequality (5.105) may be shown in the same manner as in that proof (when now taking $C := 5$ and $\lambda(x) := 6$).

Hence, after summation of (5.127) for $i = 1, \ldots, K$ and with respect to definition (5.47), we may write

$$\begin{aligned}
\sum_{i=1}^{K} \overline{\mathcal{D}}^{\mathrm{reo}}(\alpha(\tau_{i-1}), \alpha(\tau_i)) &= \liminf_{k\to\infty} \sum_{i=1}^{K} \overline{\mathcal{D}}^{\mathrm{reo}}(\alpha^{N_k}(\tau_{i-1}), \alpha^{N_k}(\tau_i)) \\
&\leq \liminf_{k\to\infty} \sup\{\sum_{i=1}^{K} \overline{\mathcal{D}}^{\mathrm{reo}}(\alpha^{N_k}(\tau_{i-1}), \alpha^{N_k}(\tau_i)) \,: \\
&\qquad \text{a.p.p.} \;\; s = \tau_0 \leq \tau_1 \leq \ldots \leq \tau_K = z\} = \liminf_{k\to\infty} \mu_{\alpha^{N_k}}([s,z]).
\end{aligned} \tag{5.128}$$

The measure $\mu_{\alpha^{N_k}}$ is derived from α^{N_k} by (5.47). The last term on the right-hand side of (5.128) is independent on partition of $[s,z]$. Taking suprema of both sides we may conclude:

$$\begin{aligned}
\mu_\alpha([s,z]) &= \sup_{K\to\infty} \left\{ \sum_{i=1}^{K} \overline{\mathcal{D}}^{\mathrm{reo}}(\alpha(\tau_{i-1}), \alpha(\tau_i)) \,:\; \text{a.p.p.} \;\; s = \tau_0 \leq \tau_1 \leq \ldots \leq \tau_K = z \right\} \\
&\leq \liminf_{k\to\infty} \mu_{\alpha^{N_k}}([s,z]).
\end{aligned} \tag{5.129}$$

Hence, we proved lower semicontinuity of the measure μ for any subinterval $[s,z] \subset [0,\mathcal{T}]$.

Making profit of Lemma 5.3.10 applied to (5.129) we obtain

$$\int_s^z \sigma^{\mathrm{reo}}(T(t))\, \mathrm{d}\mu_\alpha(t) \leq \liminf_{k\to\infty} \int_s^z \sigma^{\mathrm{reo}}(T(t))\, \mathrm{d}\mu_{\alpha^{N_k}}(t). \tag{5.130}$$

Concerning the right-hand side of (5.130), we introduce an auxiliary time interpolation function $\sigma^{\mathrm{reo}}_{N_k}(T(t)) : [0,\mathcal{T}] \to \mathbb{R}(\Omega)$ of the function $\sigma^{\mathrm{reo}}(T(t))$ motivated by definitions in Subsection 5.3.2 as follows:

$$\sigma^{\mathrm{reo}}_{N_k}(T(t)) := \sigma^{\mathrm{reo}}(T(t)) \quad \text{if } t \in [t_k, t_{k+1}) \text{ and } \sigma^{\mathrm{reo}}_{N_k}(T((\mathcal{T})) := \sigma^{\mathrm{reo}}(T(\mathcal{T})) \tag{5.131}$$

Then,

$$\begin{aligned}\liminf_{k\to\infty} \int_s^z \sigma^{\mathrm{reo}}(T(t))\,\mathrm{d}\mu_{\alpha^{N_k}} &\\ = \liminf_{k\to\infty} \int_s^z [\sigma^{\mathrm{reo}}(T(t)) - \sigma^{\mathrm{reo}}_{N_k}(T(t))] + \sigma^{\mathrm{reo}}_{N_k}(T(t))\,\mathrm{d}\mu_{\alpha^{N_k}} &\\ = \liminf_{k\to\infty} \int_s^z \sigma^{\mathrm{reo}}_{N_k}(T(t))\,\mathrm{d}\mu_{\alpha^{N_k}}. &\end{aligned} \tag{5.132}$$

To see the second equality we observe

$$\begin{aligned}0 \le \lim_{k\to\infty} \int_s^z |\sigma^{\mathrm{reo}}(T(t)) - \sigma^{\mathrm{reo}}_{N_k}(T(t))|\,\mathrm{d}\mu_{\alpha^{N_k}} &\\ \le \lim_{k\to\infty} \max_{t\in[0,\mathcal{T}]} |\sigma^{\mathrm{reo}}(T(t)) - \sigma^{\mathrm{reo}}_{N_k}(T(t))| \int_s^z \mathrm{d}\mu_{\alpha^{N_k}}, &\end{aligned} \tag{5.133}$$

since $\sigma^{\mathrm{reo}}(T(t))$ and $\sigma^{\mathrm{reo}}_{N_k}(T(t))$ are homogenous in space. Owing to results of Lemma 5.3.8, $\exists\, C :\ \|\alpha^{N_k}\|_{\mathrm{BV}([0,\mathcal{T}],\mathrm{L}^1(\Omega))} \le C$ for all the interpolants α^{N_k}. Hence, we may obtain a bound on the last integral in (5.133) since the measure μ_{N_k} is derived form α^{N_k} according to (5.47). Recalling construction of interpolants we eventually see that the second equality in (5.132) is valid[11]

The term on the right-hand side of (5.130) is then equal to the last term on the right-hand side of (5.132) and, recalling definition (5.46), we finally arrive at

$$\mathrm{Diss}^{\mathrm{reo}}(\alpha,[s,z]) = \int_s^z \sigma^{\mathrm{reo}}(T(t))\,\mathrm{d}\mu_\alpha(t) \le \liminf_{k\to\infty} \int_s^z \sigma^{\mathrm{reo}}_{N_k}(t)\,\mathrm{d}\mu_{\alpha^{N_k}} \tag{5.134}$$

for any time interval $[s,z] \subset [0,\mathcal{T}]$.

Now we are ready to prove two energy inequalities.

Upper energy inequality

The upper energy inequality is based on the discrete upper estimate (5.71). Due to the construction of interpolants, it holds true

$$(u^{N_k}(t), \alpha^{N_k}(t), \eta^{N_k}(t)) = (u^{N_k}(t^{N_k}_m), \alpha^{N_k}(t^{N_k}_m), \eta^{N_k}(t^{N_k}_m))$$

for any time t such that $0 \le t - t^{N_k}_m \le \Delta^{N_k}_m := |t^{N_k}_m - t^{N_k}_{m-1}|$, $m \in \{1,\dots,N_k\}$. Naturally, $\Delta^{N_k}_m \to 0$ for $k \to \infty$ (recall Subsection 5.3.3). Continuity of $\partial_t\mathcal{E}$ in time on the compact set $[0,\mathcal{T}]$ (due to data qualification (5.5)–(5.8)) implies Lipschitz continuity of $\mathcal{E}$, hence

$$\begin{aligned}&\exists\, C > 0 :\\ &|\mathcal{E}(t, u^{N_k}(t), \alpha^{N_k}(t), \eta^{N_k}(t)) - \mathcal{E}(t^{N_k}_m, u^{N_k}(t^{N_k}_m), \alpha^{N_k}(t^{N_k}_m), \eta^{N_k}(t^{N_k}_m))| \le C\Delta^{N_k}_m.\end{aligned} \tag{5.135}$$

[11] Let $\{a_i\}_{i\in\mathbb{N}}, \{b_i\}_{i\in\mathbb{N}}$ are sequences of real numbers. Then if $\lim_{i\to\infty} a_i = 0$, then $\liminf_{i\to\infty}(a_i + b_i) = \liminf_{i\to\infty} b_i$.

And, as $\partial_t \mathcal{E}$ is bounded,

$$\left| \int_0^t \theta^{N_k}(s)\,\mathrm{d}s - \int_0^{t_m^{N_k}} \theta^{N_k}(s)\,\mathrm{d}s \right| \leq C\Delta_m^{N_k}. \tag{5.136}$$

Then, utilizing in turn (5.135), (5.71) and (5.136) we obtain

$$\begin{aligned}
&\mathcal{E}(t, u^{N_k}(t), \alpha^{N_k}(t), \eta^{N_k}(t)) + \sum_{i=1}^{m} \mathcal{D}(t_{i-1}^{N_k}, \alpha^{N_k}(t_{i-1}^{N_k}), \alpha^{N_k}(t_i^{N_k})) \\
&\quad \leq \mathcal{E}(t_m^{N_k}, u^{N_k}(t_m^{N_k}), \alpha^{N_k}(t_m^{N_k}), \eta^{N_k}(t_m^{N_k})) + C\Delta_m^{N_k} \\
&\qquad\qquad + \sum_{i=1}^{m} \mathcal{D}(t_{i-1}^{N_k}, \alpha^{N_k}(t_{i-1}^{N_k}), \alpha^{N_k}(t_i^{N_k})) \\
&\quad \leq \mathcal{E}(0, u(0), \alpha(0), \eta(0)) + C\Delta_m^{N_k} + \int_0^{t_m^{N_k}} \theta^{N_k}(s)\,\mathrm{d}s \\
&\quad \leq \mathcal{E}_0 + C\Delta_m^{N_k} + \int_0^t \theta^{N_k}(s)\,\mathrm{d}s.
\end{aligned} \tag{5.137}$$

Due to definition of interpolating functions, we can add the term $\mathcal{D}(t_m^{N_k}, \alpha^{N_k}(t_m^{N_k}), \alpha^{N_k}(t)) = 0$ to the left-hand side of (5.137) with no influence on the inequality. Denoting $t_M^{N_k} := t$ and $\mathbb{M} := \{1, \dots, m\} \cup M$, we employ (5.134) to find out

$$\begin{aligned}
&\liminf_{k\to\infty} \sum_{i\in\mathbb{M}} \mathcal{D}^{\mathrm{reo}}(t_{i-1}^{N_k}, \alpha^{N_k}(t_{i-1}^{N_k}), \alpha^{N_k}(t_i^{N_k})) \\
&= \liminf_{k\to\infty} \sum_{i\in\mathbb{M}} \sigma_{N_k}^{\mathrm{reo}}(t_{i-1}) \overline{\mathcal{D}}^{\mathrm{reo}}(\alpha^{N_k}(t_{i-1}^{N_k}), \alpha^{N_k}(t_i^{N_k})) = \liminf_{k\to\infty} \int_0^t \sigma_{N_k}^{\mathrm{reo}}(t)\,\mathrm{d}\mu_{\alpha^{N_k}} \\
&\geq \mathrm{Diss}^{\mathrm{reo}}(\alpha, [0,t])
\end{aligned} \tag{5.138}$$

Thanks to the limit in (5.110), (5.124) and (5.138), we may proceed by applying limes inferior for $k \to \infty$ on the left-hand side of (5.137); thanks to the weak convergence in (5.95) we may also proceed with the same limit ($k \to \infty \Rightarrow \Delta_m^{N_k} \to 0$) on the right-hand side of (5.137) with the result

$$\mathcal{E}(t, u(t), \alpha(t), \eta(t)) + \beta(t) + \mathrm{Diss}^{\mathrm{reo}}(\alpha, [0,t]) \leq \mathcal{E}(0, u(0), \alpha(0), \eta(0)) + \int_0^t \theta^*(s)\,\mathrm{d}s \tag{5.139}$$

Reminding the result of Fatou's lemma in (5.97) and utilizing (5.125), we finally arrive at the upper energy estimate

$$\mathcal{E}(t, u(t), \alpha(t), \eta(t)) + \mathrm{Diss}_{\mathcal{D}}(\alpha, [0,t]) \leq \mathcal{E}_0 + \int_0^t \partial_t \mathcal{E}(s, u(s), \alpha(s), \eta(s))\,\mathrm{d}s. \tag{5.140}$$

Lower energy inequality

The lower energy estimate is a direct consequence of the stability of the limit triplet found in Subsection 5.3.4. Let $0 \leq \tau_1 \leq \ldots \leq \tau_K = t$, $t \in (0, \mathcal{T}]$ be a partition of $[0,t]$ with $\Delta_K := \max\{\tau_j - \tau_{j-1} \ : \ j = 1, \dots, K\}$.

Let us define a piece-wise constant interpolant $\sigma_K^{\mathrm{reo}}(T(t)) : [0,\mathcal{T}] \to \mathrm{P}^0(\Omega,\mathbb{R})$ as follows:

$$\sigma_K^{\mathrm{reo}}(T(t)) := \sigma^{\mathrm{reo}}(T(\tau_j)) \quad \text{if } t \in [\tau_j,\tau_{j+1}) \text{ and } \sigma_K^{\mathrm{reo}}(T(\mathcal{T})) := \sigma^{\mathrm{reo}}(T(\mathcal{T})). \tag{5.141}$$

Due to presumed continuity of σ^{reo} on the (closed) interval $[0,\mathcal{T}]$ (recall (5.8)) providing an upper bound on σ^{reo}, we may employ Lebesgue's dominated convergence theorem again to see that for a sequence of partitions with $K \to \infty \Rightarrow \Delta_K \to 0$ it holds true:

$$\lim_{K\to\infty} \int_0^{\mathcal{T}} \sigma_K^{\mathrm{reo}}(T(t))\,\mathrm{d}\mu_\alpha(t) = \int_0^{\mathcal{T}} \sigma^{\mathrm{reo}}(T(t))\,\mathrm{d}\mu_\alpha(t). \tag{5.142}$$

Moreover, exploiting the definition of the interpolant σ_K^{reo} and positivity of σ^{reo} in (5.14), we obtain the following inequality:

$$\begin{aligned}
\int_0^{\mathcal{T}} \sigma_K^{\mathrm{reo}}(T(t))\,\mathrm{d}\mu_\alpha(t) &= \sum_{j=1}^{K} \int_{\tau_{j-1}}^{\tau_j} \sigma_K^{\mathrm{reo}}(T(\tau_{j-1}))\,\mathrm{d}\mu_\alpha(t) \\
&= \sum_{j=1}^{K} \sigma_K^{\mathrm{reo}}(T(\tau_{j-1})) \int_{\tau_{j-1}}^{\tau_j} \mathrm{d}\mu_\alpha(t) \\
&\geq \sum_{j=1}^{K} \sigma_K^{\mathrm{reo}}(T(\tau_{j-1})) \int_{\tau_{j-1}}^{\tau_j} \mathrm{d}\mu_\alpha^*(t) \\
&= \sum_{j=1}^{K} \sigma_K^{\mathrm{reo}}(T(\tau_{j-1}))\overline{\mathcal{D}}^{\mathrm{reo}}(\alpha(\tau_{j-1}),\alpha(\tau_j)) = \mathcal{D}^{\mathrm{reo}}(\tau_{j-1},\alpha(\tau_{j-1}),\alpha(\tau_j)),
\end{aligned} \tag{5.143}$$

where the measure μ_α^* is defined for every closed set $S := [s,z] \subset [0,\mathcal{T}]$ simply as

$$\mu_\alpha^*(S) := \overline{\mathcal{D}}^{\mathrm{reo}}(\alpha(s),\alpha(z)), \tag{5.144}$$

and the inequality in (5.143) can be seen by comparison with the definition (5.47).

Now, testing the stability of the triplet $(u(\tau_{j-1}),\alpha(\tau_{j-1}),\eta(\tau_{j-1}))$ by $(\tilde{u},\tilde{\alpha},\tilde{\eta}) = (u(\tau_j),\alpha(\tau_j),\eta(\tau_j))$ gives

$$\begin{aligned}
&\mathcal{E}(\tau_{j-1},u(\tau_{j-1}),\alpha(\tau_{j-1}),\eta(\tau_{j-1})) \\
&\qquad \leq \mathcal{E}(\tau_{j-1},u(\tau_j),\alpha(\tau_j),\eta(\tau_j)) + \mathcal{D}(\tau_{j-1},\alpha(\tau_{j-1}),\alpha(\tau_j)) \\
&\qquad = \mathcal{E}(\tau_j,u(\tau_j),\alpha(\tau_j),\eta(\tau_j)) - \int_{\tau_{j-1}}^{\tau_j} \partial_t\mathcal{E}(s,u(\tau_j),\alpha(\tau_j),\eta(\tau_j))\,\mathrm{d}s \\
&\qquad\quad + \mathcal{D}(\tau_{j-1},\alpha(\tau_{j-1}),\alpha(\tau_j))
\end{aligned} \tag{5.145}$$

After summation over $j = 1,\dots,K$ and applying (5.126) and (5.143) to elaborate

the first estimate in the following, we find:

$$\begin{aligned}
&\mathcal{E}(t,u(t),\alpha(t),\eta(t)) + \mathrm{Diss}^{\mathrm{tr}}(\alpha,[0,t]) + \int_0^{\mathcal{T}} \sigma_K^{\mathrm{reo}}(T(t))\,\mathrm{d}\mu_\alpha - \mathcal{E}(0,u(0),\alpha(0),\eta(0)) \\
&\quad \geq \mathcal{E}(t,u(t),\alpha(t),\eta(t)) + \sum_{j=1}^{K} \mathcal{D}^{\mathrm{tr}}(\alpha(\tau_{j-1}),\alpha(\tau_j)) \\
&\qquad\quad + \sum_{j=1}^{K} \mathcal{D}^{\mathrm{reo}}(\tau_{j-1},\alpha(\tau_{j-1}),\alpha(\tau_j)) - \mathcal{E}(0,u(0),\alpha(0),\eta(0)) \\
&\quad \geq \sum_{j=1}^{K} \int_{\tau_{j-1}}^{\tau_j} \partial_t\mathcal{E}(s,u(\tau_j),\alpha(\tau_j),\eta(\tau_j))\,\mathrm{d}s \\
&\quad = \sum_{j=1}^{K} \partial_t\mathcal{E}(\tau_j,u(\tau_j),\alpha(\tau_j),\eta(\tau_j))|\tau_j-\tau_{j-1}| - \sum_{j=1}^{K} \varrho_j|\tau_j-\tau_{j-1}|, \qquad (5.146)
\end{aligned}$$

where we define

$$\varrho_j := \frac{1}{|\tau_j-\tau_{j-1}|}\int_{\tau_{j-1}}^{\tau_j} [\partial_t\mathcal{E}(s,u(\tau_j),\alpha(\tau_j),\eta(\tau_j)) - \partial_t\mathcal{E}(\tau_j,u(\tau_j),\alpha(\tau_j),\eta(\tau_j))]\,\mathrm{d}s. \qquad (5.147)$$

The hoped-for lower energy estimate will be obtained after choosing a particular sequence of time-partition and applying the limit $K\to\infty$ in (5.146).

First, we utilize time-continuity of $\partial_t\mathcal{E}(\cdot,u,\alpha,\eta)$ imposed by data qualification, which – due to Heine-Cantor theorem – implies uniform continuity on the compact interval $[0,\mathcal{T}]$, i.e.

$$\begin{aligned}
&\exists\,\omega:[0,\mathcal{T}]\to[0,\infty)\wedge\ \omega \text{ is non-decreasing } \wedge\,\omega(\tau)\to 0 \text{ for } \tau\searrow 0: \\
&\forall t_1,t_2\in[0,\mathcal{T}]: |\partial_t\mathcal{E}(t_1,u,\alpha,\eta) - \partial\mathcal{E}(t_2,u,\alpha,\eta)| \leq \omega(|t_1-t_2|). \qquad (5.148)
\end{aligned}$$

where function ω is so-called *modulus of continuity*. Therefore,

$$|\varrho_j| \leq \frac{1}{|\tau_j-\tau_{j-1}|}\int_{\tau_{j-1}}^{\tau_j} \omega(|s-\tau_j|)\,\mathrm{d}s \leq \omega(\Delta_K) \qquad (5.149)$$

and the last sum on the right-hand side of (5.146) may be then estimated from above by $\omega(\Delta_K)\mathcal{T}\to 0$ when the partition is refined, i.e. $\Delta_K\to\ \infty$.

For the first term of the right-hand side of (5.146), we will use the following useful theorem (see Lemma 4.12 in Dal Maso et al., 2005):

Theorem 5.3.11. *Let X be a Banach space and $F\in \mathrm{L}^1((0,t),X)$. Then there exists a sequence of partitions $\Pi: 0=s_0^n\leq s_1^n\leq\ldots\leq s_{k(n)}^n=t$, $S_n := \max_{1\leq i\leq k(n)}|s_i^n-s_{i-1}^n|$, $\lim_{n\to\infty}S_n=0$, such that*

$$\lim_{n\to\infty}\sum_{i=1}^{k(n)}\left\| F(s_i^n)|s_i^n-s_{i-1}^n| - \int_{s_{i-1}^n}^{s_i^n} F(s)\,\mathrm{d}s\right\|_X = 0. \qquad (5.150)$$

By direct application to the studied case ($F(s):=\theta(s)\in\mathrm{L}^1((0,\mathcal{T}),\mathbb{R})$ due to (5.90) and $X:=\mathbb{R}$), we may define a sequence of time-partitions $0\leq\tau_1\leq\ldots\leq$

$\tau_K = t$, $t \in (0, \mathcal{T}]$ with $K \to \infty \Rightarrow \Delta_K \to 0$ so that:

$$\lim_{K\to\infty} \sum_{j=1}^{K} \left| \partial_t \mathcal{E}(\tau_j, u(\tau_j), \alpha(\tau_j), \eta(\tau_j))|\tau_j - \tau_{j-1}| - \int_{\tau_{j-1}}^{\tau_j} \partial_t \mathcal{E}(t, u(t), \alpha(t), \eta(t)) \right| = 0, \tag{5.151}$$

and, thus, with increasing refinement ($K \to \infty$), the first term on the right hand-side of (5.146) represents an approximation of the Lebesgue integral via Riemann sums. Recalling (5.142) and proceeding by the same limit ($K \to \infty$) on the left-hand side of (5.146), we finally obtain the lower energy estimate in the form:

$$\mathcal{E}(t, u(t), \alpha(t), \eta(t)) + \mathrm{Diss}_{\mathcal{D}}(\alpha, [0, t]) - \mathcal{E}_0 \geq \int_0^t \partial_t \mathcal{E}(s, u(s), \alpha(s), \eta(s)) \, \mathrm{d}s. \tag{5.152}$$

To conclude the subsection, the last result together with the upper energy inequality (5.140) implies that $(u, \alpha, \eta) : [0, \mathcal{T}] \to \mathcal{U} \times \mathcal{V} \times \mathcal{Z}$ is an energetic solution.

5.3.6 Further properties and concluding remarks

By reordering and comparing the lower energy estimate (5.152), lower semi-continuity of dissipation (5.125), upper energy estimate (5.139) and consequence of Fatou's lemma (5.97), one sees

$$\begin{aligned}
\mathcal{E}(0, u(0), \alpha(0), \eta(0)) + \int_0^t \theta(s) \, \mathrm{d}s &\leq \mathcal{E}(t, u(t), \alpha(t), \eta(t)) + \mathrm{Diss}_{\mathcal{D}}(\alpha, [0, t]) \\
&\leq \mathcal{E}(t, u(t), \alpha(t), \eta(t)) + \beta(t) + \mathrm{Diss}^{\mathrm{reo}}(\alpha, [0, t]) \\
&\leq \mathcal{E}(0, u(0), \alpha(0), \eta(0)) + \int_0^t \theta^*(s) \, \mathrm{d}s \\
&\leq \mathcal{E}(0, u(0), \alpha(0), \eta(0)) + \int_0^t \theta(s) \, \mathrm{d}s
\end{aligned} \tag{5.153}$$

Hence, all inequalities are in fact equalities and we may refine (5.125) as

$$\mathrm{Diss}^{\mathrm{tr}}_{\mathcal{D}}(\alpha, [0, t]) = \lim_{k\to\infty} \mathrm{Diss}^{\mathrm{tr}}_{\mathcal{D}}(\alpha^{N_k}, [0, t]), \tag{5.154}$$

and (5.97) as

$$\theta^*(t) = \theta(t) \quad \text{for almost all } t \in [0, \mathcal{T}]. \tag{5.155}$$

Employing Lemma 3.5[12] in (Francfort and Mielke, 2006) to the latter result even implies

$$\theta^{N_k} \to \theta \text{ in } \mathrm{L}^1((0, \mathcal{T}), \mathbb{R}). \tag{5.156}$$

Hence, after choosing a further subsequence denoted $n_l := N_{k_l}$, we have the following convergences for $l \to \infty$:

- for all $t \in [0, \mathcal{T}]$: $\alpha^{n_l}(t) \rightharpoonup \alpha(t)$ in $\mathrm{W}^{1,2}(\Omega)$,

[12] Let $\{f_k\}, k \in \mathbb{N}$ be a bounded sequence in $\mathrm{L}^\infty((0, \mathcal{T}), \mathbb{R})$ with $f_k \overset{*}{\rightharpoonup} f^*$ and $f^{\sup}(t) = \limsup_{k\to\infty} f_k(t)$. If $f^*(t) = f^{\sup}(t)$ for a.e. $t \in (0, \mathcal{T})$, then $\|f_k - f^*\|_{\mathrm{L}^1((0,\mathcal{T}),\mathbb{R})} \to 0$.

- for all $t \in [0, \mathcal{T}]$: $\mathcal{E}(t, u^{n_l}(t), \alpha^{n_l}(t), \eta^{n_l}(t)) \to \mathcal{E}(t, u(t), \alpha(t), \eta(t))$ in $\mathbb{R}$,
- for all $t \in [0, \mathcal{T}]$: $\mathrm{Diss}_{\mathcal{D}}(\alpha^{n_l}, [0, t]) \to \mathrm{Diss}_{\mathcal{D}}(\alpha, [0, t])$ in $\mathbb{R}$,
- for a.a. $t \in [0, \mathcal{T}]$: $\theta^{n_l} \to \theta$ in $\mathbb{R}$.

We recall that we have also found out that

$$u \in \mathrm{B}([0,T], \mathrm{W}^{1,2}(\Omega, \mathbb{R}^3)), \tag{5.157}$$
$$\boldsymbol{\varepsilon}^{\mathrm{in}} \in \mathrm{L}^\infty([0,T], \mathrm{W}^{1,2}(\Omega, \mathbb{R}^{3\times 3}_{\mathrm{sym},0})) \cap \mathrm{BV}([0,T], \mathrm{L}^1(\Omega, \mathbb{R}^{3\times 3}_{\mathrm{sym},0}))), \tag{5.158}$$
$$\xi \in \mathrm{L}^\infty([0,T], \mathrm{W}^{1,2}(\Omega, \mathbb{R})) \cap \mathrm{BV}([0,T], \mathrm{L}^1(\Omega, \mathbb{R})), \tag{5.159}$$
$$\eta \in \mathrm{L}^\infty([0,T], \mathrm{L}^\infty(\Omega, \mathbb{R})). \tag{5.160}$$

Let us add several final remarks:

(a) Now we return to a note made in the outline of the whole proof concerning the time-dependent Dirichlet boundary condition. We suppose there exists an extension of the Dirichlet boundary condition to all $\overline{\Omega}$ such that $U(t) \in \mathrm{C}^1([0, \mathcal{T}], \mathrm{W}^{1,2}(\Omega, \mathbb{R}^3))$. The function will appear in the elastic part of free energy, ψ, and in the loading term, $\langle l(t), u(t) \rangle$, (cf. Section 5.2) and, consequently, in the term $\partial_t \mathcal{E}$. Due to prescribed regularity, we may then proceed be repeating the arguments used in the proof. Of course, even less restrictive functional spaces may be considered in the data qualification while the results is still being valid, see e.g. (Francfort and Mielke, 2006) for details.

(b) Due to the results by Mielke and Rossi (2007), we know that if an energetic solution is enough smooth in time, then it also solves the weak form of the subdifferential formulation of our problem.

(c) The function u is guaranteed to be bounded, albeit not necessarily measurable on $[0, \mathcal{T}]$ due to (5.157). As discussed in (Mielke and Rossi, 2007), if the the functional $\mathcal{E}$ is uniformly convex and the integrated dissipation $\mathcal{D}$ satisfies a particular growth condition, then (under some other conditions) we may expect Lipschitz continuity of variables in time and uniqueness of the solution. Then, our analysis assures convergence of the derived numerical schema.

Chapter 6

Numerical Implementation of the Constitutive Model

In this chapter we present the numerical treatment of the model. We specify the form of the material function $\langle\cdot\rangle$, which has been established in Section 4.1, introduce the approach used for numerical solution of the time-incremental minimization problem and show how the model is then implemented into Abaqus finite element package. Finally, several numerical simulations are presented to demonstrate capabilities of the constitutive model.[1]

6.1 Specification of the transformation strain domain

To capture the transformation strain anisotropy and the tension-compression asymmetry, we specify the function $\langle\cdot\rangle$ as:

$$\langle\boldsymbol{\varepsilon}^{\mathbf{tr}}\rangle = \frac{I_2(\mathbb{D}\boldsymbol{\varepsilon}^{\mathrm{tr}})}{k}\frac{\cos\left(\frac{1}{3}\arccos(1-a(I_3(\mathbb{D}\boldsymbol{\varepsilon}^{\mathrm{tr}})+1))\right)}{\cos\left(\frac{1}{3}\arccos(1-2a)\right)}, \tag{6.1}$$

where

$$I_2(\boldsymbol{x}) = \sqrt{\frac{2}{3}x_{ij}x_{ij}} \tag{6.2}$$

corresponds to von Mises equivalent strain and

$$I_3(\boldsymbol{x}) = 4\frac{\det(\boldsymbol{x})}{(I_2(\boldsymbol{x}))^3}. \tag{6.3}$$

k is a material parameter representing the maximum transformation strain in tension and the material parameter a characterizes the tension-compression asymmetry. The parameter a ranges between 0 (no tension-compression asymmetry) and 1 (transformation strain in compression is a half of the strain in tension).

The linear mapping $\mathbb{D} : \mathbb{R}^6 \to \mathbb{R}^6$ (Voigt notation) is motivated by the work of Taillard et al. (2008):

$$\mathbb{D} = \frac{1}{\nu}\begin{bmatrix} \mathbb{P} & \mathbb{O} \\ \mathbb{O} & \mathbb{S} \end{bmatrix}, \tag{6.4}$$

[1] Let us note that in the numerical treatment, thus throughout this section, we use $\xi, \boldsymbol{\varepsilon}^{\mathrm{tr}}$ as the primary variables making profit of the relation $\boldsymbol{\varepsilon}^{\mathrm{in}} = \xi\boldsymbol{\varepsilon}^{\mathrm{tr}}$.

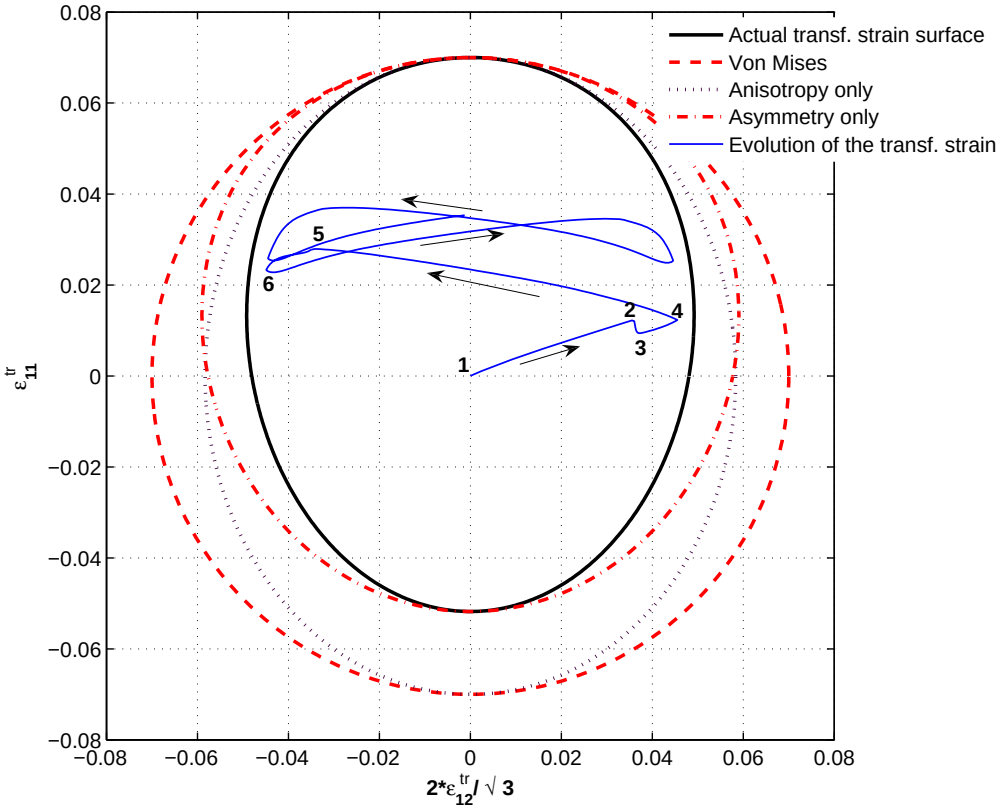

Figure 6.1: The shape of proposed transformation strain domain determined using the parameters in Table 6.1 in the plane of strain components $\varepsilon_{11}^{\mathrm{tr}}$-$\varepsilon_{12}^{\mathrm{tr}}$ compared with von Mises domain ($a = 0, \mathbb{D} = \mathbb{I}$), tension-compression asymmetry domain ($a = 0.8, \mathbb{D} = \mathbb{I}$) and anisotropy domain ($a = 0, \mathbb{D}$ according to Table 6.1). The central curve represents the evolution of transformation strain components in a combined tension-torsion test at $-30\,^{\circ}\mathrm{C}$ described in Subsection 6.4.4. (cf. also Fig. 6.8a) and b).)

where the components of the matrix $\mathbb{P} \in \mathbb{R}^{3\times3}$ take the following form:

$$P_{11} := \frac{2A}{3}\cos^2\varphi + \frac{2B}{3}\sin^2\varphi + \frac{1}{3}, \tag{6.5}$$

$$P_{22} = P_{33} := \left(\frac{A}{6} + \frac{B}{2}\right)\cos^2\varphi + \left(\frac{A}{2} + \frac{B}{6}\right)\sin^2\varphi + \frac{1}{3}, \tag{6.6}$$

$$P_{23} = P_{32} := \left(\frac{A}{6} - \frac{B}{2}\right)\cos^2\varphi + \left(\frac{B}{6} - \frac{A}{2}\right)\sin^2\varphi + \frac{1}{3}, \tag{6.7}$$

$$P_{12} = P_{21} = P_{13} = P_{31} := -\frac{A}{3}\cos^2\varphi - \frac{B}{3}\sin^2\varphi + \frac{1}{3}, \tag{6.8}$$

matrix $\mathbb{S} \in \mathbb{R}^{3\times3}$ has the diagonal form:

$$\mathbb{S} = \begin{bmatrix} \sqrt{L} & 0 & 0 \\ 0 & \sqrt{M} & 0 \\ 0 & 0 & \sqrt{N} \end{bmatrix}, \tag{6.9}$$

$$\nu = \sqrt{\frac{1}{2}[(P_{11} - P_{12})^2 + (P_{11} - P_{13})^2 + (P_{12} - P_{13})^2]}, \tag{6.10}$$

and $\mathbb{O} \in \mathbb{R}^{3\times3}$ denotes a zero (null) matrix. A, B, φ, L, M, N are material-dependent parameters such that $\mathbb{D}$ is invertible. Let us note that similar techniques for anisotropy and asymmetry handling were utilized e.g. in works of Lexcellent et al. (2006) or Taillard et al. (2008). The convexity of the function proposed in (6.1) is assured due to results in (Bigoni and Piccolroaz, 2004) and the fact that the convexity is not affected by a linear mapping. Positive 1-homogeneity can be shown by direct computation.

The shape of proposed transformation strain domain determined by the parameters in Table 6.1 compared with three other simpler cases – the von Mises domain ($a = 0, \mathbb{D} = \mathbb{I}$), the tension-compression asymmetry domain ($a = 0.8, \mathbb{D} = \mathbb{I}$) and the anisotropy domain ($a = 0, \mathbb{D}$ according to Table 6.1) – is shown in Fig. 6.1.

6.2 Numerical solution of the constrained minimization problem

In Section 5.2, we obtained the time-incremental boundary value problem (TIP) as the time-discrete version of the evolutionary problem originally expressed by governing system (4.32)–(4.38).

For effective solution of the boundary value minimization problem (TIP), we will split it into two subproblems.[2] The first one corresponds to minimization with respect to strain, and may be advantageously solved numerically by employing the finite element software. The second one corresponds to (TIP) with fixed strain, i.e. minimization only with respect to internal variables, and represents the constitutive relations implicitly included in the (TIP). Both problems must be solved consecutively and the resulting solution is equivalent to the solution of (TIP) for infinitesimally refined time discretization. In this work, the former problem is solved by Abaqus finite element package, see the next section. This program also provides a spatial discretization of the simulated body.

After spatial discretization, the latter subproblem leads to solving a reduced time-incremental minimization problem in a material point in the form:

$$\begin{aligned} &\text{Minimize } f(T_k, \boldsymbol{\varepsilon}_k, \boldsymbol{\varepsilon}^{\mathrm{tr}}, \xi, \eta) + d(T_k, \xi_{k-1}, \boldsymbol{\varepsilon}^{\mathrm{tr}}_{k-1}, \xi - \xi_{k-1}, \boldsymbol{\varepsilon}^{\mathrm{tr}} - \boldsymbol{\varepsilon}^{\mathrm{tr}}_{k-1}) + r(\boldsymbol{\varepsilon}^{\mathrm{tr}}, \xi, \eta) \\ &\text{subject to } (\boldsymbol{\varepsilon}^{\mathrm{tr}}, \xi, \eta). \end{aligned} \tag{6.11}$$

where the regularization energy, $r(\boldsymbol{\varepsilon}^{\mathrm{tr}}, \xi, \eta)$, is introduced in the model as an approximation of the indicator function $\mathcal{I}(\boldsymbol{\varepsilon}^{\mathrm{tr}}, \xi, \eta)$ to assure that constraints (4.3), (4.5) and (4.6) are fulfilled.

In the present work, the minimization problem (6.11) is solved by Nelder-Mead method introduced by Nelder and Mead (1965). It is a derivative-free optimization algorithm suitable for non-smooth functions as in our case. Let us note that we could consider also a derivative-based optimization method (e.g.

[2] Such an approach is sometimes termed combined minimization principle (e.g. Hackl and Fischer, 2008)

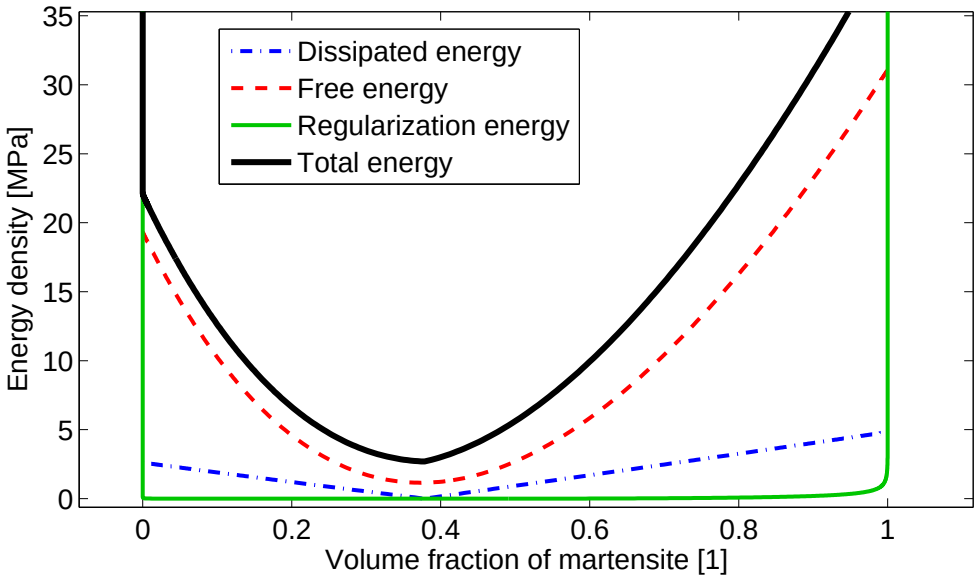

Figure 6.2: An example of the dependence of energy contributions on volume fraction of martensite for a particular choice of other parameters ($\xi_{k-1} = 0.38$).

gradient descent method) for which we had to carefully treat the points of non-smoothness. To do so, one could, for example, utilize an approach similar to the elastic predictor-transformation corrector return mapping methods often used in SMA modeling (Qidwai and Lagoudas, 2000*a*). In our case, we would have to perform calculations for one of four distinct cases ($\dot{\xi} = 0, \|\dot{\varepsilon}^{\mathrm{tr}}\| = 0$ or $\dot{\xi} \neq 0, \|\dot{\varepsilon}^{\mathrm{tr}}\| = 0$ or $\dot{\xi} = 0, \|\dot{\varepsilon}^{\mathrm{tr}}\| \neq 0$ or $\dot{\xi} \neq 0, \|\dot{\varepsilon}^{\mathrm{tr}}\| \neq 0$). Such a decision-making complicates the numerical implementation, therefore, using a derivative-based algorithm, although faster in general, needs not to be more efficient.

The regularization energy is defined by the maximum number reachable in computer precision (corresponding to $+\infty$) whenever any of constraints (4.3), (4.5) and (4.6) is violated. Otherwise, r takes the form $r(\boldsymbol{\varepsilon}^{\mathrm{tr}}, \xi, \eta) = r^{\mathrm{sm}}(\xi, \eta) + r^{\mathrm{hard}}(\boldsymbol{\varepsilon}^{\mathrm{tr}}, \xi)$, where:

$$r^{\mathrm{sm}}(\xi, \eta) = c^{\mathrm{reg}}[\operatorname{arctanh}^2(2\xi - 1) + \operatorname{arctanh}^2\left(\frac{2\eta}{1-\xi} - 1\right)(1 - \xi)], \tag{6.12}$$

c^{reg} is a small positive constant so that r^{sm} smoothly approximates the indicator function. In addition to approximating the indicator function, the term r^{hard} also captures the hardening-like response of martensite which can be important in some SMA systems, e.g. in those with a higher precipitate content:

$$r^{\mathrm{hard}}(\boldsymbol{\varepsilon}^{\mathrm{tr}}, \xi) = kE^{\mathrm{int}}\xi\frac{\langle\boldsymbol{\varepsilon}^{\mathrm{tr}}\rangle^2}{1 - \langle\boldsymbol{\varepsilon}^{\mathrm{tr}}\rangle^4}, \tag{6.13}$$

where E^{int} denotes a positive constant, which can be obtained from experiments. The form of this term was motivated by the work of Chemisky et al. (2011), see Section 3.2. The convexity of r was checked numerically. It should be emphasized that for the admissible values of internal variables the regularization energy is significantly lower than the free energy except for the close neighborhood of constraints (4.3), (4.5), (4.6). An example of comparison of the regularization energy term with the other energetic contributions is shown in Fig. 6.2.

6.3 Implementation of the constitutive model into the finite element package Abaqus

For development and optimal design of a general SMA structure a numerical implementation of the model into industrial software is needed. The finite element software Abaqus provides the tool called User MATerial subroutine (UMAT) enabling a user to implement constitutive models which are not included in the standard database.

The proposed model was implemented to Abaqus as a numerical subroutine UMAT written in C++ programming language. In each computational increment, the previous values of internal variables, $(\boldsymbol{\varepsilon}^{\mathrm{tr}}_{k-1}, \xi_{k-1}, \eta_{k-1})$, and the values of desired strain, $\boldsymbol{\varepsilon}_k$, and temperature, T_k, are obtained from Abaqus. The corresponding values, $\xi_k, \boldsymbol{\varepsilon}^{\mathrm{tr}}_k, \eta_k$, are determined by solving (6.11) by the Nelder-Mead minimization algorithm and, subsequently, the stress, is determined as (cf. 4.27)

$$\boldsymbol{\sigma}_k = K\mathrm{tr}(\boldsymbol{\varepsilon}_k)\boldsymbol{I} + 2G(\xi_k, \eta_k)(\mathrm{dev}(\boldsymbol{\varepsilon}_k) - \xi_k\boldsymbol{\varepsilon}^{\mathrm{tr}}_k). \tag{6.14}$$

Based on the differences between the previous and current value of internal variables, the active processes are determined: a process is active if the corresponding internal variable evolves, i.e. the difference is greater than some chosen tolerance δ.

After solving the minimization problem, tangent operators required for implementation in UMAT are to be determined additionally. Since we consider (uniformly distributed) temperature as a prescribed parameter in the present formulation of the model, only the mechanical tangent operator, L, is needed. The following analytical form can be derived:

$$L = \frac{\mathrm{d}\boldsymbol{\sigma}}{\mathrm{d}\boldsymbol{\varepsilon}} = \frac{\partial^2 e^T}{\partial \boldsymbol{\varepsilon}^2} - \frac{\partial \boldsymbol{\sigma}}{\partial \boldsymbol{v}}\left[\frac{\partial^2 e^T}{\partial \boldsymbol{v}^2}\right]^{-1}\left[\frac{\partial \boldsymbol{\sigma}}{\partial \boldsymbol{v}}\right]^{\top} \tag{6.15}$$

where $e := f + d + r$ is the sum appearing in the minimization problem and $^{\top}$ denotes matrix transposition. $\boldsymbol{v}$ represents the vector of all *actually evolving* internal variables. Numerical derivatives (central differences) were employed in expression (6.15) in the numerical implementation.

To account for possibility of large rigid-body rotations, the Hughes–Winget algorithm is employed in Abaqus (ABAQUS, 2010). Abaqus provides a matrix, R_k, representing an increment of a rigid body rotation of the local basis system, so that vector- or tensor-valued variables can be rotated appropriately to the reference configuration in UMAT (cf. Hartl and Lagoudas, 2009). The total rotation matrix at current step, Q_k, is given by multiplication of rotational increments from all previous steps, i.e.

$$Q_k = R_k \cdot R_{k-1} \cdot \cdots \cdot R_1 = R_k \cdot Q_{k-1}, \tag{6.16}$$

and Q_k is to be stored at the end of the increment. At the end of the UMAT, stress and the mechanical tangent operator must be rotated back to the local configuration before passing them to Abaqus. The schema of our final UMAT subroutine is depicted in Fig. 6.3.

The updated internal variables, stress and the mechanical tangent operator are sent to the main Abaqus routine in order to determine for each element the

Launch of UMAT subroutine

1. Input data $(T_k, \varepsilon_k, \varepsilon^{\mathrm{tr}}_{k-1}, \xi_{k-1}, \eta_{k-1}, R_k, Q_{k-1})$ loaded from Abaqus
2. Update of the rotation matrix Q_k and rotation of ε_k
3. Solving of the Minimization problem given by (6.11)
   by Nelder-Mead minimization method
   $\Rightarrow (\varepsilon^{\mathrm{tr}}_k, \xi_k, \eta_k)$
4. Computation of stress utilizing (6.14)
   $\Rightarrow \sigma_k$
5. Evolving variables determination:
   `if` $\|\varepsilon^{\mathrm{tr}}_k - \varepsilon^{\mathrm{tr}}_{k-1}\| > \delta_{\mathrm{tr}}$ `then` $\varepsilon^{\mathrm{tr}} \in v$ `else` $\varepsilon^{\mathrm{tr}} \notin v$
   `if` $|\xi_k - \xi_{k-1}| > \delta_\xi$ `then` $\xi \in v$ `else` $\xi \notin v$
   `if` $|\eta_k - \eta_{k-1}| > \delta_\eta$ `then` $\eta \in v$ `else` $\eta \notin v$
6. Tangent modulus computation utilizing (6.15)
   $\Rightarrow \mathrm{L}_k$
7. Rotation of stress and tangent modulus
8. Values $(\varepsilon^{\mathrm{tr}}_k, \xi_k, \eta_k, \sigma_k, \mathrm{L}_k, Q_k)$ transmitted to Abaqus

End of UMAT subroutine

Figure 6.3: A schema of numerical implementation of the model to UMAT subroutine of finite element software Abaqus. Subscript denotes the number of the time step.

value of the residual vector, composed of the internal and external nodal forces, and its Jacobian. The residual vector of the whole structure and its Jacobian are then calculated and the corresponding displacement solution is computed by the quasi-Newton iterative scheme (see ABAQUS, 2010, for details).

6.4 Numerical simulations

Having derived the model we shall present several numerical simulations to demonstrate its capabilities. The simulations were performed at LEM3 (Metz, France) computation centre with the commercially available nonlinear finite element code Abaqus utilizing parallel processing with eight processors.

6.4.1 Specification of material properties

The list of all model parameters with their respective values used in simulations is given in Table 6.1. An advantage of the model is that the influence of most of the parameters on the modelled behavior may be well estimated from their physical meaning. In our experience, Δs^{AM}, Δs^{AR}, elastic moduli have to be searched in a narrow value range. The transforation strain depends on the processing of the specimen (e.g. thin extruded wires, rolled sheets). The most complicated issue is to identify parameters of the dissipation function. First complication stems from simultaneous occurrence of transformation and reorientation both leading to dissipation. Second, when R-phase transformation is included in the model,

Parameter	Value	Unit	Comment
Elastic constants:			
E^A	71	[GPa]	Elastic properties of the wire in tension and
E^M	41	[GPa]	torsion were considered as independent (not
E^R	41	[GPa]	related through the bulk modulus) because of
G^A	25	[GPa]	the strong texture in the wire. The constants
G^M	22.3	[GPa]	were evaluated from experimental stress-strain
G^R	14.3	[GPa]	curves but correspond well also to the values obtained by ultrasound measurements (Šittner et al., 2006).
Parameters of transformation strain surface:			
k	0.07	[1]	Maximum transformation strain in tension.
a	0.8	[1]	Parameter for tension-compression asymmetry.
$[A; B; \varphi; \ldots$	[1;1;0;…		Parameters of Hill's hyper ellipsoid, $\mathbb{D}$, the
$L; M; N]$	1;1.44;1.44]	[1]	coordinate system was defined such that the wire axis is aligned with the x-axis.
Parameters of dissipation function:			
T_0	-20	[°C]	Equilibrium temperature of A and M. It influences the rate of dissipated energy in forward and reverse transformation.
M_s	-22	[°C]	M_s, M_f, A_s and A_f temperatures have the usual
M_f	-24	[°C]	meaning of transformation temperatures only if
A_s	-17	[°C]	transformation does not proceed through the
A_f	-13	[°C]	R-phase. Otherwise we should consider them only as parameters of the dissipation function (see σ-T phase diagrams in Section 6.4.3).
σ_0^reo	160	[MPa]	Reorientation stress at T_0.
Σ^reo	-0.9	[MPa/°C]	Change of reorientation stress with temperature describing also the change of hysteresis width with temperature.
Parameters of chemical and regularization energies:			
Δs^{AM}	0.364	[MPa/°C]	Difference between specific entropy of M and A; the value was computed using critical transformation slope.
Δs^{AR}	0.121	[MPa/°C]	Difference between specific entropy of R and A; the value was taken as a 1/3 of Δs^{AM}.
R_s	39	[°C]	Initial A to R transformation temperature.
R_f	1	[°C]	Final A to R transformation temperature.
c^reg	0.01	[MPa]	Parameter of the regulariz. energy term (6.12).
E^int	30	[MPa]	Parameter of the regulariz. energy term (6.13).

Table 6.1: Material parameters entering the model and their values used in simulations. A, R and M denote austenite, R-phase and martensite, respectively.

parameters M_s, M_f, A_s and A_f do not correspond to the transformation temperatures (obtainable, e.g., by a DSC measurement) anymore due to a considerable change of entropy associated with the austenite-R-phase transformation (see also stress-temperature phase diagrams generated with identical parameters with and without R-phase in Subection 6.4.3).

6.4.2 Sensitivity to the increment size

Figure 6.4 illustrates that there is no sensitivity to the increment size for a reasonable range of this numerical parameter. A simple superelastic response with pronounced tension-compression asymmetry was simulated. The transition from

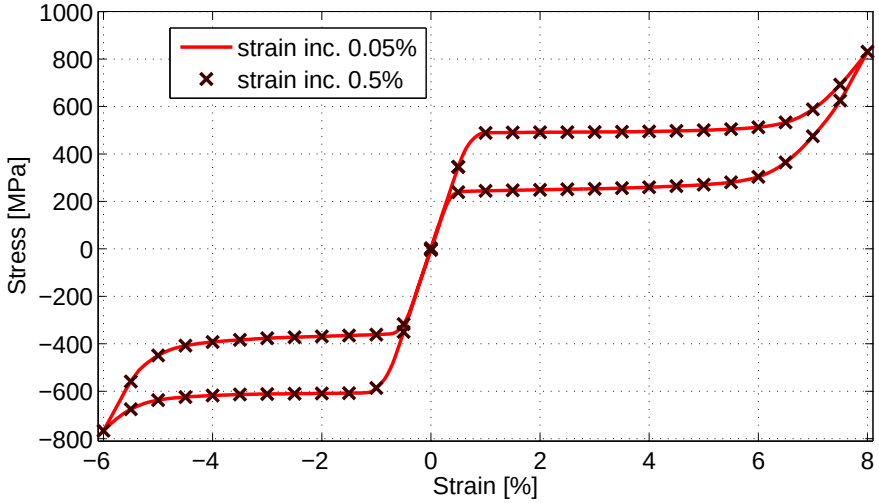

Figure 6.4: An illustration of increment size independence of the model.

elasticity to phase transformation and from phase transformation to saturation are well described during forward and reverse transformation.

6.4.3 Simulated stress-temperature phase diagrams

In order to explore the general thermomechanical behavior of SMA element predicted by the model we will use one-dimensional stress-temperature phase diagrams *generated* by the model with R-phase suppressed (Fig. 6.5) and with R-phase present (Fig. 6.6). To obtain the diagram without R-phase transformation, the transformation temperatures for transformation between austenite and R-phase (R_s, R_f) were set below the respective temperatures for transformation from austenite to martensite. In both figures the lines denote points where corre-

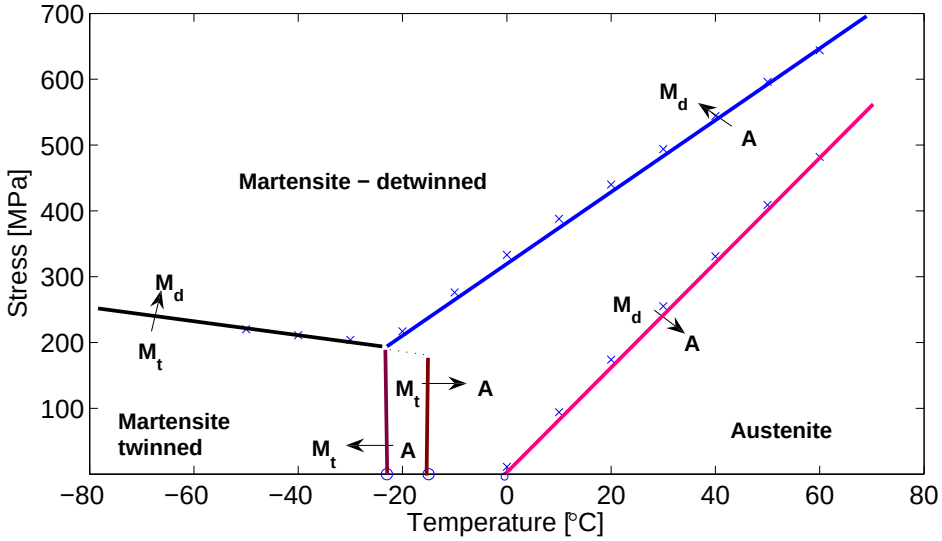

Figure 6.5: Stress-temperature phase diagram without R-phase generated by the model. See text for details.

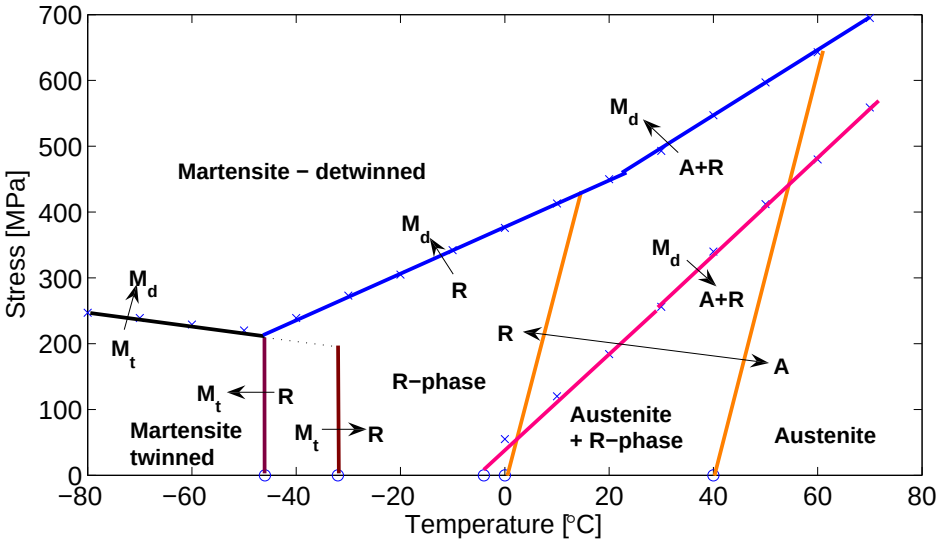

Figure 6.6: Stress-temperature phase diagram with R-phase generated by the model. See text for details.

sponding transformation process starts. Note that in this subsection, martensite is called "twinned" if the transformation strain is zero ($\boldsymbol{\varepsilon}^{\mathrm{tr}} \to \mathbf{0}$) and "detwinned" if the inelastic strain reaches the maximum value ($\langle \boldsymbol{\varepsilon}^{\mathrm{tr}} \rangle \to 1$).

When no R-phase is present (Fig. 6.5) straight lines for the transformation between austenite and detwinned martensite (A→$\mathrm{M_d}$ and $\mathrm{M_d}$ →A) are expected. These lines are not parallel because of the temperature dependence of the parameter $\sigma^{\mathrm{reo}}(T)$, which corresponds to decreasing hysteresis with increasing temperature. For the temperature induced phase transformation between austenite and twinned martensite (A→$\mathrm{M_t}$ and $\mathrm{M_t}$ →A) under low stress ($< \sigma_0^{\mathrm{reo}}$), the transformation temperatures are stress-independent since the formed martensite has a zero net transformation strain.

At low temperatures the linear temperature dependence of reorientation stress, $\sigma^{\mathrm{reo}}(T)$, is observed in the $\mathrm{M_t}$ →$\mathrm{M_d}$ transition. The model leads to the existence of a unique triple point of possible coexistence of austenite and both twinned and detwinned martensite. Let us note that, two limiting transformation temperatures for initiation of the martensite-to-austenite transformation at zero stress are distinguishable in the figure (corresponding to $\mathrm{M_d}$ →A and $\mathrm{M_t}$ →A). Since the transformation of detwinned martensite, having non-zero transformation strain, dissipates more energy than of the twinned one the transformation starts at a higher temperature. Then, if the material transforms to austenite from an intermediate state between fully detwinned and fully twinned martensite, the transformation temperature will lie between these two limiting values, as observed in martensite stabilization experiments by Liu and Favier (2000).

The phase diagram including R-phase can be compared in Fig. 6.6. A wide region of phase transformation from austenite to R-phase and vice versa occurs and it is bordered by two lines in the figure (A↔R). Generally, due to R-phase presence, the temperatures at which martensite starts to appear or disappear are shifted towards lower values with respect to the phase diagram without R-phase (if the same stress is considered). In particular, the phase boundary R→$\mathrm{M_d}$ exhibits

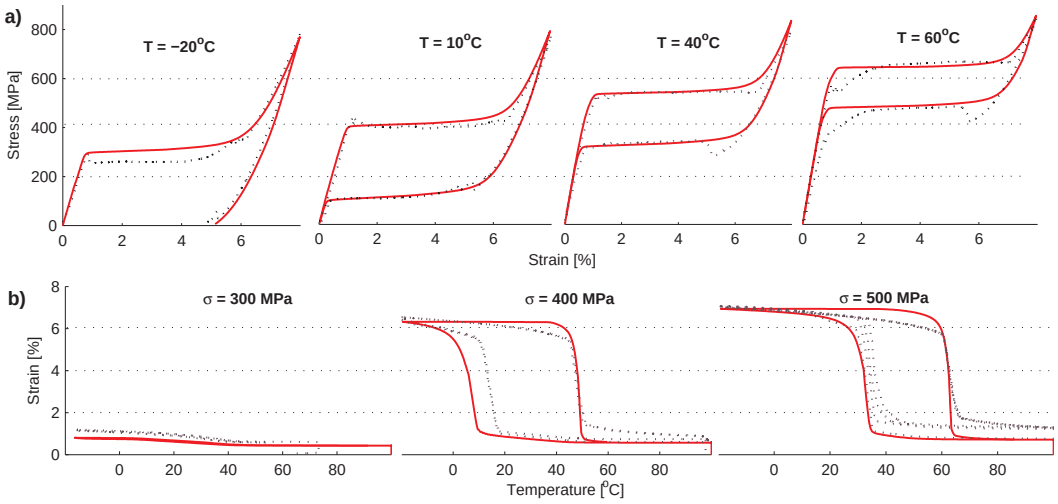

Figure 6.7: Comparison of experiments (dashed line) and simulations (full line). Tensile tests at various temperatures a), Thermal cycling tests at various applied stresses b).

different slope than the phase boundary A→M_d. This is in a good agreement with experiments (cf. Šittner et al., 2006).

6.4.4 Proportional and nonproportional loading tests

To further examine predictive capabilities of the presented model the following simulations of thermomechanical loading of a NiTi wire specimen were performed and compared with experimental data:

i. Tensile tests at various constant temperatures

ii. Thermal cycling at constant applied loads of various magnitudes

iii. Combined tension-torsion tests at a constant axial load and various constant temperatures

iv. Combined tension-torsion tests at a constant temperature and various constant axial loads

Tests iii. and iv. were performed to study the response of the SMA wire in a general nonproportional loading. For comparison with experiments, we adopted datasets from an extensive experimental database available at Roundrobin SMA modeling website (Pilch et al., 2009). It is possible to find details of the utilized material and experimental procedures as well as other experimental datasets there. Let us only note the experiments were carried out on trained wires with a stable response.

The first two tests were simulated as simple uniaxial tension tests, with displacement control in i. and load control in ii., with prescribed homogenous (constant or varying) temperature field using one 8-node linear brick element. The simulations of combined tension-torsion tests were performed using four-node axisymmetric bilinear elements with an additional twist degree of freedom. 500

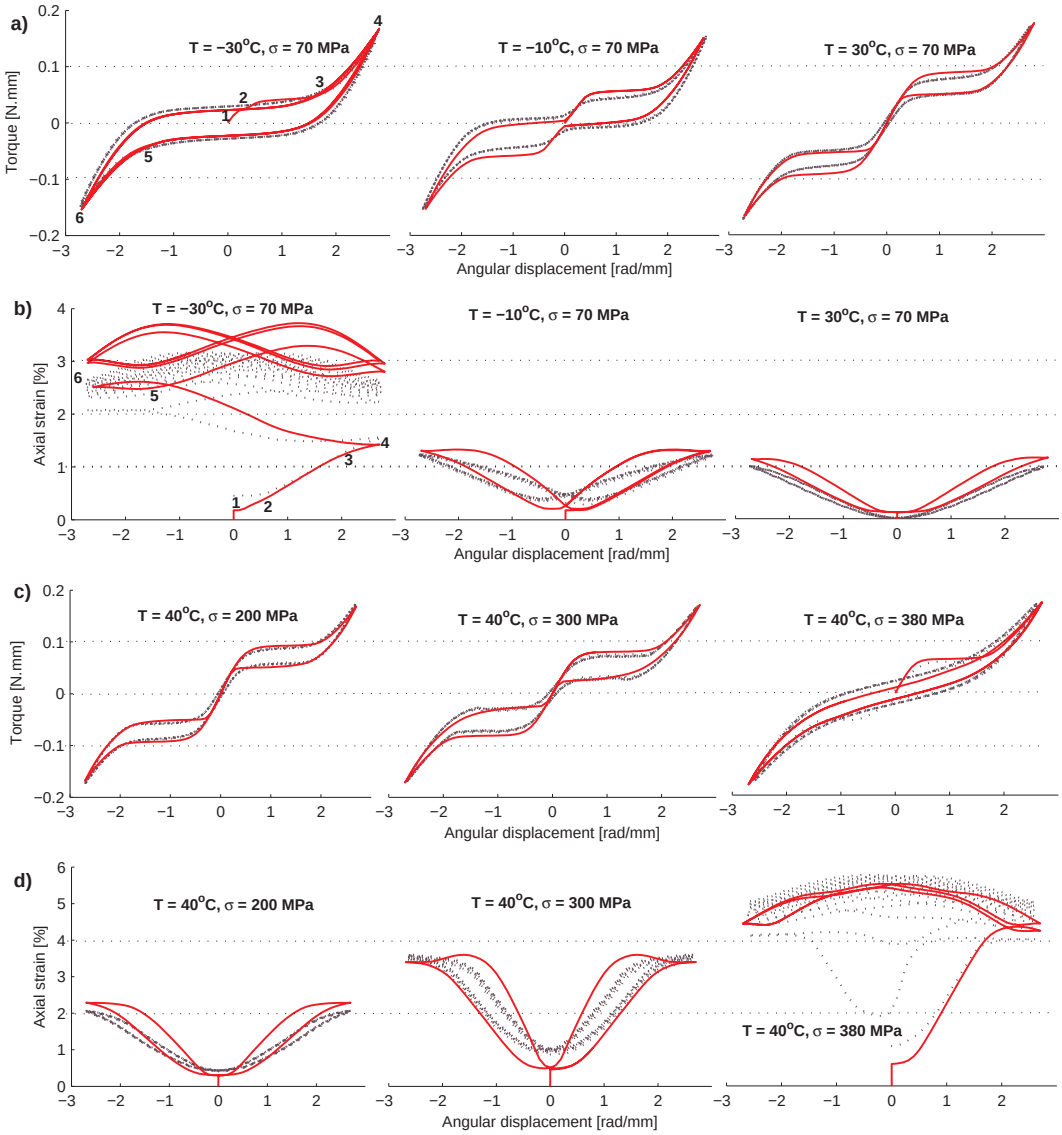

Figure 6.8: Comparison of experiments (dashed line) and simulations (full line). Combined tension-torsion tests at a constant axial preload and various temperatures a) and b), Combined tension-torsion tests at various axial preloads and a constant temperature c) and d).

(50x10) elements were used to represent a 1 mm long segment of the wire. Rotation and axial displacement were fixed at the boundary representing the upper base of the wire segment, whereas prescribed surface load and rotation were applied on the lower base. Homogenous temperature was prescribed. The torque in Fig. 6.8 was obtained by integration of the moment over the lower boundary of the segment, the axial strain was obtained from the averaged value of relative displacement over the lower boundary.

Simulations of stress-strain responses of a NiTi wire in tensile tests at three different temperatures are compared with experimental results in Figure 6.7a). The model captures changes of the behavior from martensite reorientation at low temperatures (−20 °C) to superelastic at higher temperatures (60 °C). A considerable change of the apparent elastic modulus of austenite in experiments, caused by the R-phase transformation occurring at lower temperatures, is well captured

by the model, too. A gradual nonlinear nonhysteretic response in martensite state beyond the end of the plateau is also well reflected owing to the regularization energy term. Instantaneous changes of the response ("steps") in experimental results demonstrate localisation, which is not covered in present simulation.

Simulations of thermal cycling experiments at three different constant tensile loads (300 MPa, 400 MPa and 500 MPa) are shown in figure 6.7b). Although the hysteresis width is slightly overestimated, the general behavior (transition from austenite to twinned or detwinned martensite through R-phase) is successfully captured.

Combined tension-torsion tests performed at different temperatures (30 °C, 0 °C and −30 °C) and at a preload in tension of 70 MPa can be seen in boxes a) and b) of Fig. 6.8. The evolution of the simulated torque-angular displacement behavior exhibits a very good correspondence with experiments – a transition from superelasticity to martensite deformation is again observed. As mentioned in the work of Šittner et al. (2009), due to the strong texture in the NiTi wire isotropic models may fail to properly predict the length of the transformation plateau. This is not the case of the model introduced here since the transformation strain anisotropy was included. The increase of the hysteresis width with decreasing temperature is successfully followed. The values of simulated axial strain in Fig. 6.8b) generally correspond to experimental values, only at the lowest temperature the maximum axial strain seems to be slightly overestimated.

For illustration, the evolution of axial and shear components of the transformation strain at the surface of the wire during this test at −30 °C was plotted to Fig. 6.1; there the numbering of stages in the complex path corresponds to Fig. 6.8. After initial cooling under a preload, a small amount of elastically deformed martensite is produced. Then, between stages 1 and 2 the path corresponds to detwinning of this martensite, path between stages 2 and 3 corresponds to further formation of martensite by stress. From stage 3 onwards, the variation of applied load further reorients the martensite reaching a stable response after several cycles.

Finally, combined tension-torsion tests at constant temperature 40 °C (unloaded sample was fully in austenite) and three different axial preloads (200 MPa, 300 MPa and 400 MPa) were simulated. Again, torque-angular displacement and axial strain-angular displacement responses are presented in Fig. 6.8c) and 6.8d), respectively. In this type of simulations, the core part of the wire is exposed to tension whereas surface layers are exposed to a combination of tension and shear. Besides the correct length of plateaus, the well-captured initial "virgin" loading path at the highest preload should be noted in the left graph. The model quantitatively predicts axial elongation at turnabouts of loading direction at all preloads. The simulation of ratcheting at 400 MPa, when stress induced transformation changes to martensite reorientation processes and vice versa during cycling, is very sensitive to model parametrisation.

6.4.5 Example of finite elements-analysis

To test the model behavior in a more complex geometry, response of a SMA plate with a cylindrical hole, see Fig. 6.9a), subject to tension was simulated. Due to the chosen geometry, a heterogenous stress state is expected to develop in the

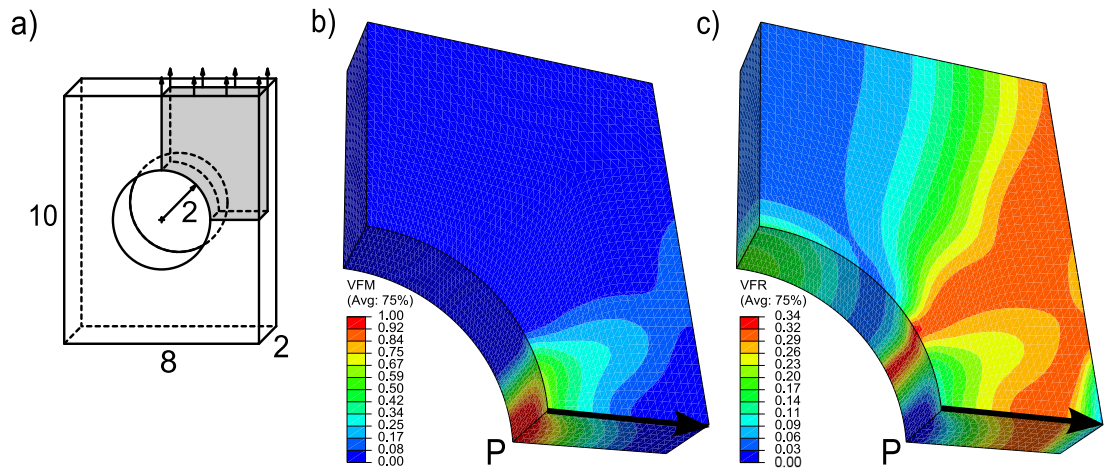

Figure 6.9: Finite elements simulation: a sketch of holed plate with simulated part shaded (dimensions in mm) a), distribution of volume fraction of martensite b) and volume fraction of R-phase c) at the maximum displacement.

body. The material parameters of the plate were adopted from Table 6.1; the anisotropy axis (x-axis) is supposed to be parallel to the loading direction.

Due to the obvious symmetry, only one eight of the plate was simulated (see shaded part in Fig. 6.9a) and appropriate symmetry conditions were prescribed.

The loading was performed at constant temperature $T_{\mathrm{sim}} = 40\,^{\circ}\mathrm{C}$ ($T_{\mathrm{sim}} > R_{\mathrm{s}}$). Initially, the SMA holed plate was stress free and fully in austenite. During the simulation, the displacement in vertical direction was prescribed on the upper face of the plate to reach, incrementally, the value of 0.12 mm at maximum; then the load was incrementally released back to zero displacement – we used approximately 100 load increments for the whole cycle. Other faces for which symmetry boundary conditions do not apply were let free.

The problem was solved using a hexaedral mesh with standard 8-node linear brick elements. To find a suitable mesh density, we performed several calculations with increasing number of elements. According to this tests, a relatively fine mesh with 10591 uniformly distributed elements was used in the presented simulation, even though the dependence of the total force on the displacement was obtained within good accuracy (maximum relative error of order 10^{-3}) using a coarser mesh with only 2525 elements; see the inset of Fig. 6.10. For simplicity, we did not exploit adaptive mesh refinement methods.

The first transformation process occurring in the simulation is the transformation of austenite into R-phase. The transformation starts at the bottom left-hand corner of the simulated part of the plate (point P in Fig. 6.9). When the applied load increases, R-phase transforms into oriented martensite. The conversion of austenite to R-phase and subsequently to martensite is illustrated in Fig. 6.10 that shows the distribution of volume fraction of martensite and R-phase along the thick arrow marked in Fig. 6.9b), c) in three selected points of the forward evolution. In particular, we chose the points when the prescribed displacement reaches one third and two thirds of the maximum displacement as well as the turning point.

Further, the martensite and R-phase volume fraction distribution in the plate at the maximum displacement are shown in Fig. 6.9b) and c), respectively. As

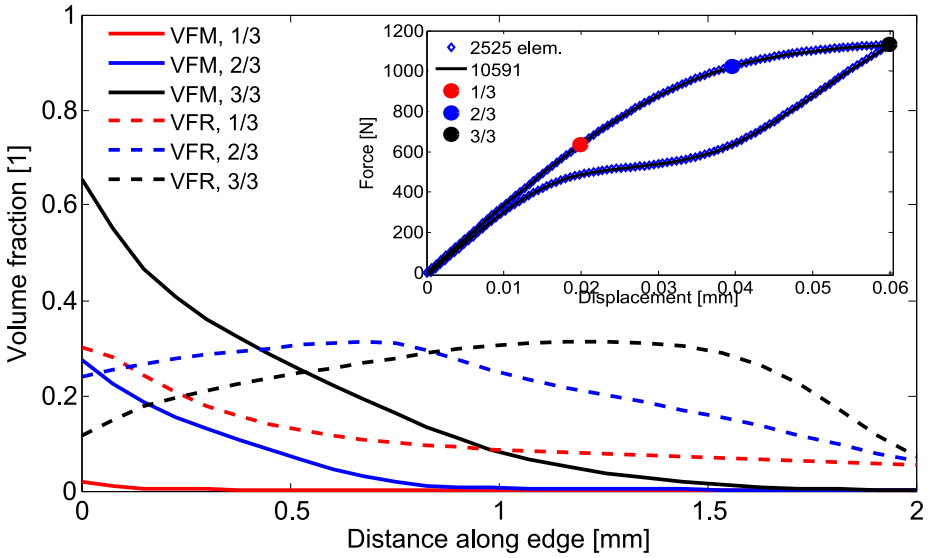

Figure 6.10: Distribution of volume fraction of martensite (VFM; full lines) and R-phase (VFR; dashed lines) along the thick arrow in Fig. 6.9b),c) during loading when one third (1/3), two thirds (2/3) and full maximum displacement (3/3) were reached. Inset: dependence of total force on displacement for 2 different mesh densities.

can be seen there, the region nearby the point P transformed already fully to martensite, whereas the region above the hole is dominated by austenite. Moreover, while on the line from P to the middle of the right edge of the simulated part both martensite and R-phase evolved, in other regions with higher R-phase concentration almost no martensite is present. Finally, after unloading, only austenite was present in the body.

Conclusions

In this thesis, a thermomechanical three-dimensional constitutive model of NiTi-based SMA in small strain setting was developed and implemented into the finite element package ABAQUS.

In the *modeling part* of the thesis, the following results were reached:

- The constitutive model was formulated within the framework of generalised standard materials introducing two dissipative internal variables. Whereas the form of the Helmholz free energy function is rather standard and makes profit form the rule of mixtures, the rate-independent dissipation function has a novel form, which combines contributions stemming from the phase transformation and reorientation of martensite. The formulation of the dissipation function was motivated by the analysis of experimentally determined phase diagrams, but also an alternative approach based on a set of assumption is presented.

- The change in the material response associated with the phase transformation between austenite and R-phase was covered by introducing a further, non-dissipative internal variable. By this way, presence of R-phase influences both elastic and thermal properties of the material.

- The convex set to which is the transformation strain constrained is chosen in a such way, that material anisotropy and tension-compression asymmetry are covered. Both these phenomena as well as the R-phase transformation are usually exhibited in real polycrystalline products, thus, have to be covered in the model.

- The model is able to reliably simulate the major thermomechanical phenomena in SMA as superelasticity, martensite deformation in complex non-proportional loading paths, the one-way shape memory effect, martensite stabilization by deformation or evolution of the transformation hysteresis with temperature.

In the *mathematical part* of the thesis, we obtained the following results:

- Based on the constitutive model, a time-evolutionary problem of a quasistatic mechanical loading of an NiTi SMA body with prescribed temperature evolution was formulated within the framework of energetic solutions Francfort and Mielke (2006). It was proved that there exists a solution of the problem, i.e. a time-dependent quadruplet of state variables satisfying the energetic balance and the stability condition. The standard approach by Francfort and Mielke (2006) was slightly modified since the dissipation

function depends on temperature. Only natural restrictions on the basic physical parameters of the model were needed in the proof.

- A time-incremental minimization problem corresponding to the evolutionary problem was formulated and it was shown to have a solution. This discrete formulation provided a conceptual algorithm utilized in the numerical treatment.

In the *numerical part* of the thesis, the following was presented:

- The constitutive model was implemented to the finite element package Abaqus, which allows to solve problems with general boundary conditions and complex geometries. It is easy to modify the set of material parameters of the model, hence adapt it to a particular NiTi-based alloy.

- The Nelder-Mead minimization procedure was utilized in a script which numerically solves a part of the time-incremental minimization problem and provides the results to the main routine, which completes the computation. The script was written in the C++ programming language and provides also the so-called mechanical tangent operator to accelerate convergence of the main routine.

- In order to demonstrate the performance of the implemented model, experimental results from a set of thermomechanical tests on thin NiTi wires were checked against simulation results. The considerable agreement between them confirms very good predictive abilities of the model. A finite element structural analysis of a NiTi bulk component was also presented.

Appendix A

Elements of Convex Analysis

In this part, we will introduce some basic concepts of convex analysis (see e.g. Barbu and Precupanu, 2012).

Definition A.0.1 (Convex set)**.** Let X be a vector space. A set $K \subseteq X$ is called *convex* if for any $x_1, x_2 \in K$ and $t \in [0,1]$ it holds

$$tx_1 + (1-t)x_2 \in K. \tag{A.1}$$

Definition A.0.2 (Convex function)**.** Let V be a normed vector space and f a function such that $f : V \to \mathbb{R} \cup \{+\infty\}$. The function is said to be *convex* if for any $x_1, x_2 \in V$ and $t \in [0,1]$ it holds

$$f(tx_1 + (1-t)x_2) \leq tf(x_1) + (1-t)f(x_2). \tag{A.2}$$

The convex function is called *proper*, if there is at least one $x \in V$ such that $f(x) < +\infty$.

Definition A.0.3 (Indicator function)**.** Let A be a subset of a set X. We define *indicator function* $\mathcal{I}(x) : A \to \{0, +\infty\}$ by

$$\mathcal{I}(x) = \begin{cases} 0 & \text{if } x \in A, \\ +\infty & \text{if } x \notin A. \end{cases} \tag{A.3}$$

Definition A.0.4 (Subdifferential)**.** Let V be a normed vector space, V^* be the dual space of V and f a function such that $f : V \to \mathbb{R} \cup \{+\infty\}$. A subset ∂f of V^* such that

$$\partial f(x) := \{z \in V^* \ : \ f(y) - f(x) \geq \langle z, y - x\rangle \quad \forall\, y \in V\}, \tag{A.4}$$

is called the *subdifferential* of function f at point x and any member of the set is called a *subderivative* of f at x.

The notion of subderivative is a generalization of the notion of derivative to a convex, non differentiable function.

Example A.0.5. Let K be a convex set in V. Then

$$\partial \mathcal{I}_K(x) = \begin{cases} \emptyset & \text{if } x \notin K, \\ N_K(x) & \text{if } x \in \partial K, \\ \{0\} & \text{if } x \in K^{\text{int}}, \end{cases} \tag{A.5}$$

where we define a cone of outer normals to K at a point $x \in \partial K$, also called *normal cone* of K at x, as

$$N_K(x) := \{z \in V^* \ : \ \langle z, y - x\rangle \leq 0 \quad \forall\, y \in K\}. \tag{A.6}$$

Let us show the claim. The definition of the subdifferential of $\mathcal{I}_K$ for any $x \in K$, i.e. $\mathcal{I}_K(x) = 0$, gives

$$0 \geq \langle z, y - x\rangle \quad \forall\, y \in K, \tag{A.7}$$

where z is any subderivative of $\mathcal{I}_K$ at x. If x is inside K, i.e. $x \in K^{\text{int}}$, then $\{0\} \subseteq \partial\mathcal{I}_K(x)$. Next, we can find $0 < \epsilon \in \mathbb{R}$ such that $\forall\, u \in B_\epsilon := \{w \in V \ : \|w\| \leq \epsilon\}$ it holds $x + u \in K$. Then take any $w \in B_\epsilon$. Since also $-w \in B_\epsilon(x)$, we may apply (A.7) both to $y_1 := x + w$ and to $y_2 := x - w$ and obtain $\langle z, w\rangle = 0$. For any $z \neq 0$ we now define $\tilde{z} := \epsilon z/\|z\|$, and since $\|\tilde{z}\| = \epsilon$, i.e. $\tilde{z} \in B_\epsilon(x)$, it is $\langle z, \tilde{z}\rangle = 0$, hence $\langle z, z\rangle = 0$, which is in a contradiction to $z \neq 0$. Thus, $\{0\} = \partial\mathcal{I}_K(x)$.

If $x \in \partial K$, then the definition of the subbdifferential of $\mathcal{I}_K$ at x and the definition of the normal cone at x, (A.6), are equivalent.

For $x \notin K$, (A.4) may rewritten for any $y \in K$ as $0 \geq \langle z, y - x\rangle + \infty$ and the rest is clear.

Remark A.0.6. If f is as in Definition (A.0.4) and convex, then $0 \in \partial f(x)$ is obviously a necessary and sufficient condition for x to be a minimizer of f at V.

Definition A.0.7 (Legendre-Fenchel transformation, also convex conjugation)**.** Let V be a normed vector space with the dual V^*. Let f be a convex function on V. Its *Legendre-Fenchel transform*, f^*, also called *convex conjugate*, is defined by

$$f^*(z) := \sup_{x \in V}\{\langle x, z\rangle - f(x)\}, \quad \forall\, z \in V^*. \tag{A.8}$$

Remark A.0.8. Let us note that the just defined convex conjugate, $f^*(z)$, is a weak lower semicontinuous convex function in V^*.

The convex conjugate of the convex conjugate, $(f^*)^*$, is often called biconjugate. If f is a proper, weak lower semi-continuous convex function, then $(f^*)^* = f$ due to Fenchel-Morau theorem. In that case, moreover,

$$z \in f(x) \Leftrightarrow x \in f^*(z) \Leftrightarrow f(x) + f^*(z) = \langle x, z\rangle \tag{A.9}$$

for $x \in V, z \in V^*$.

Definition A.0.9. (Positive homogeneity) A function $g(x) : V \to \mathbb{R}$ is called *positive k-homogenous*, $k \in \mathbb{N}$, if for any real $\lambda > 0$ and any $x \in V$ it holds

$$g(\lambda x) = \lambda^k g(x). \tag{A.10}$$

Lemma A.0.10. *Let g be a positive 1-homogeneous convex function defined on a normed vector space V. Then there exists a closed convex set K such that $g^*(x) = \mathcal{I}_K(x)$ for all $x \in V$.*

Proof. According to the definition of Legendre-Fenchel conjugate,

$$g^*(x) = \sup_{z \in V^*} \{\langle x, z\rangle - g(z)\}. \tag{A.11}$$

If there exists $z_0 \in V^*$ such that

$$\langle x, z_0\rangle - g(z_0) =: C > 0, \tag{A.12}$$

then, thanks to positive 1-homogeneity of g,

$$g^*(x) \geq \sup_{\lambda>0}\{\langle x, \lambda z_0\rangle - g(\lambda z_0)\} = \sup_{\lambda>0} \lambda\{\langle x, z_0\rangle - g(z_0)\} = \sup_{\lambda>0} \lambda C = +\infty. \tag{A.13}$$

If it is not the case, then, necessarily, for all $z \in V^*$ it holds

$$\langle x, z\rangle - g(z) \leq 0, \tag{A.14}$$

thus, obviously, $g^*(x) \leq 0$. Furthermore, continuity (due to convexity) and positive 1-homogeneity of g even implies $g(0) = 0$, hence $g^*(x) = 0$.

Comparing with the definition of indicator function, (A.3), it remains to show that the set $K := \{x : \langle x, z\rangle - g(z) \leq 0 \quad \forall\, z \in V^*\}$ is convex, i.e. for any $x_1, x_2 \in K$ and any $t \in [0, 1]$ it holds $\tilde{x} := tx_1 + (1-t)x_2 \in K$. In our setting, we need to show, that $\langle \tilde{x}, z\rangle - g(z) \leq 0$ for all $z \in V^*$. But this is true, since we observe

$$\begin{aligned}\langle \tilde{x}, z\rangle - g(z) &= \langle tx_1 + (1-t)x_2, z\rangle - g(z)\\ &= t\langle x_1, z\rangle + (1-t)\langle x_2, z\rangle - tg(z) - (1-t)g(z)\\ &= t[\langle x_1, z\rangle - g(z)] + (1-t)[\langle x_2, z\rangle - g(z)] \leq 0.\end{aligned} \tag{A.15}$$

□

Nomenclature

$[0, \mathcal{T}]$	a time-interval on which the evolutionary problem is set
$\mathbb{R}^n$	the Euclidean space with the norm $\|x\| = (\sum_{i=1}^n x_i^2)^{1/2}$
$\mathbb{R}^{3\times 3}_{\mathrm{sym},0}$	the Euclidean space of symmetric tensors $\boldsymbol{x}$ in $\mathbb{R}^{3\times 3}$ with zero trace, i.e. $\sum_{i=1}^3 x_{ii} = 0$
Ω	an open bounded domain in $\mathbb{R}^3$ with Lipschitz boundary; the reference configuration
Γ_{D}	the part of the boundary of the domain Ω where Dirichlet boundary condition is considered
Γ_{N}	the part of the boundary of the domain Ω where Neumann boundary condition is considered
C	a *generic* constant; if it is dependent on some variables, it is explicitly stated
$\mathcal{I}_K$	the indicator function (in the sense of convex analysis) to the set K
$\|\cdot\|_V$	a norm on a Banach space V; the subscript is omitted for the Euclidean norm on $\mathbb{R}^n$
$\mathrm{B}([0, \mathcal{T}], V)$	the spaces of bounded *not necessarily measurable* functions on $[0, T]$ with values in the Banach space V
$\mathrm{BV}([0, \mathcal{T}], V)$	the space of function with bounded variation with values in the Banach space V equipped with the norm $\|u\|_{\mathrm{BV}([0,\mathcal{T}],V)} = \sup\{\sum_{i=1}^N \|u(t_{i+1}) - u(t_i)\|_V;$ over all partitions $0 \le t_1 \le \ldots \le t_N \le \mathcal{T}\}$
$\mathrm{C}^1([0, T], V)$	the space of functions on $[0, \mathcal{T}]$ with values in some Banach space V with continuous first derivative equipped with the norm $\|u\|_{\mathrm{C}^1([0,T],V)} = \sup_{t\in[0,\mathcal{T}]} \|u(t)\|_V + \sup_{t\in[0,\mathcal{T}]} \|\dot{u}(t)\|_V$
$\mathrm{L}^p(\Omega, V)$	the space of p-integrable functions ($p \in [1, \infty)$) on Ω with values in some Banach space V equipped with the norm $\|u\|_{\mathrm{L}^p(\Omega)} = \left(\int_\Omega \|u(x)\|_V^p \mathrm{d}x\right)^{1/p}$
$\mathrm{L}^\infty(\Omega, V)$	the space of measurable functions on Ω with values in some Banach space V such that the norm $\|u\|_{\mathrm{L}^\infty(\Omega)} = \operatorname{ess\,sup}_{x\in\Omega} \|u(x)\|_V < \infty$
$\mathrm{L}^p([0, \mathcal{T}], V)$	the space of p-integrable functions ($p \in [1, \infty)$) on $[0, T]$ with values in some Banach space V equipped with the norm $\|u\|_{\mathrm{L}^p([0,\mathcal{T}],V)} = (\int_0^T \|u(t)\|_V^p \mathrm{d}x)^{1/p}$,
$\mathrm{L}^\infty([0, \mathcal{T}], V)$	the space of measurable functions on $[0, T]$ with values in some Banach space V such that the norm $\|u\|_{\mathrm{L}^\infty([0,\mathcal{T}],V)} = \operatorname{ess\,sup}_{t\in[0,\mathcal{T}]} \|u(t)\|_V < \infty$

$\mathrm{W}^{1,p}(\Omega, V)$	the Sobolev space of p-integrable functions ($p \in [1, \infty)$) on Ω whose distributional derivatives are also p-integrable with values in a Banach space V equipped with the norm $\|u\|_{\mathrm{W}^{1,p}(\Omega)} = (\int_\Omega \|u(x)\|_V^p + \|\nabla u(x)\|_V^p \mathrm{d}x)^{1/p}$
$\mathrm{W}_0^{1,p}(\Omega, V)$	the Sobolev space of functions from $W^{1,p}(\Omega, V)$ whose traces on Γ_D vanish
^{A,M,R}	superscripts denoting the type of phase: austenite, martensite or R-phase
α	vector of internal variables
d	dissipation function
δ	dissipation distance
$\mathcal{D}$	integrated dissipation distance, see (5.43)
$\mathcal{E}$	regularized energy functional, see (5.42)
$\boldsymbol{\varepsilon}$	strain tensor
$\boldsymbol{\varepsilon}^{\mathrm{in}}$	inelastic strain tensor, see (4.2)
$\boldsymbol{\varepsilon}^{\mathrm{tr}}$	transformation strain tensor
η	volume fraction of R-phase
ξ	volume fraction of martensite
f	Helmholtz free energy function
F_{vol}	volume force vector acting in Ω
F_{surf}	surface force vector prescribed on Γ_N
q	heat flux vector
s	entropy per unit volume
$\boldsymbol{\sigma}$	stress tensor
t	time
T	temperature
u^X	internal energy per unit volume
u	displacement vector
U	displacement vector prescribed on Γ_D
x	vector of spatial coordinates

Bibliography

ABAQUS (2010), *Abaqus reference manuals*, SIMULIA Inc, USA.

Airoldi, G. and Rivolta, B. (1988), "Thermal cycling and intermediate R-phase in NiTi system", *Phys. Scr.* , Vol. 37, pp. 891–893.

Arghavani, J., Auricchio, F., Naghdabadi, R., Reali, A. and Sohrabpour, S. (2010), "A 3-D phenomenological constitutive model for shape memory alloys under multiaxial loadings", *Int. J. Plast.* , Vol. 26, pp. 976–991.

Auricchio, F., Mielke, A. and Stefanelli, U. (2008), "A rate-independent model for the isothermal quasi-static evolution of shape-memory materials", *Math. Models Meth. Appl. Sci.* , Vol. 18, pp. 125–164.

Auricchio, F. and Petrini, L. (2002), "Improvements and algorithmical considerations on a recent three-dimensional model describing stress-induced solid phase transformations", *Int. J. Numer. Meth. Engng.* , Vol. 55, pp. 1255–1284.

Auricchio, F. and Petrini, L. (2004), "A three-dimensional model describing stress-temperature induced solid phase transformations: solution algorithm and boundary value problems", *Int. J. Numer. Meth. Engng* , Vol. 61, pp. 807–836.

Auricchio, F., Reali, A. and Stefanelli, U. (2007), "A three-dimensional model describing stress-induced solid phase transformation with permanent inelasticity", *Int. J. Plast.* , Vol. 23, pp. 207–226.

Auricchio, F. and Sacco, E. (1997), "A one-dimensional model for superelastic shape memory alloys with different elastic properties between austenite and martensite", *Int. J. NonLin. Mech.* , Vol. 32, pp. 1101–1114.

Ball, J. and James, R. (1987), "Fine phase mixtures as minimizers of energy.", *Arch. Ration. Mech. An.* , Vol. 100, pp. 13–52.

Ball, J., Koumatos, K. and Seiner, H. (2011), "Nucleation of austenite in mechanically stabilized martensite by localized heating", *J. Alloy. Compd.* .

Barbu, V. and Precupanu, T. (2012), *Convexity and Optimization in Banach Spaces*, Springer, New York.

Bartels, S., Mielke, A. and Roubíček, T. (2012), "Quasistatic small-strain plasticity in the limit of vanishing hardening and its numerical approximation.", *SIAM J. Numer. Anal.* , Vol. 50, pp. 951–976.

Bekker, A. and Brinson, L. C. (1997), "Temperature-induced phase transformation in a shape memory alloy: phase diagram based kinetics approach", *J. Mech. Phys. Solids* , Vol. 45, pp. 949–988.

Benešová, B. (2012), Mathematical and computational modeling of shape-memory alloys, PhD thesis, Charles University in Prague.

Bernardini, D. and Pence, T. J. (2002), "Models for one-variant shape memory materials based on dissipation functions", *Int. J. NonLin. Mech.* , Vol. 37, pp. 1299—-317.

Bhattacharya, K. (2003), *Microstructure of martensite. Why it forms and how give rise to the shape-memory effect.*, Oxford: Oxford University Press.

Bigoni, D. and Piccolroaz, A. (2004), "Yield criteria for quasibrittle and frictional materials", *Int. J. Solids Struct.* , Vol. 41, pp. 2855–2878.

Bouchitté, G., Mielke, A. and Roubíček, T. (2009), "A complete-damage problem at small strains.", *Z. Angew. Math. Phys.* , Vol. 60, pp. 205–236.

Bouvet, C., Calloch, S. and Lexcellent, C. (2004), "A phenomenological model for pseudoelasticity of shape memory alloys under multiaxial proportional and nonproportional loading", *Eur. J. Mech. A* , Vol. 23, pp. 37–61.

Boyd and Lagoudas, D. C. (1996), "A thermodynamical constitutive model for shape memory materials. part i. the monolithic shape memory alloy", *Int. J. Plast.* , Vol. 12, pp. 805–842.

Brinson, L. C., Schmidt, I. and Lammering, R. (2004), "Stress-induced transformation behavior of a polycrystalline NiTi shape memory alloy: micro and macromechanical investigations via in situ optical microscopy", *J. Mech. Phys. Solids* , Vol. 52, pp. 1549–71.

Chan, C. W., Chan, S. H. J., Man, H. C. and Ji, P. (2012), "1-D constitutive model for evolution of stress-induced R-phase and localized Lüders-like stress-induced martensitic transformation of super-elastic NiTi wires", *Int. J. Plast.* , Vol. 32–33, pp. 85–105.

Chemisky, Y., Duval, A., Patoor, E. and Ben Zineb, T. (2011), "Constitutive model for shape memory alloys including phase transformation, martensitic reorientation and twins accommodation", *Mech. Mater.* , Vol. 43, pp. 361–376.

Coleman, B. and Noll, W. (1963), "The thermodynamics of elastic materials with heat conduction and viscosity.", *Arch. Ration. Mech. An.* , Vol. 13, pp. 167–178.

Collins, I. F. and Houlsby, G. T. (1997), "Application of thermomechanical principles to the modelling of geotechnical materials", *Proc. R. Soc. Lond. A* , Vol. 453, pp. 1975–2001.

Dacorogna, B. (2008), *Direct Methods in the Calculus of Variations*, Vol. 78 of *Applied Mathematical Sciences*, 2nd edn, Springer-Verlag, New York.

Dal Maso, G., Francfort, G. A. and Toader, R. (2005), "Quasistatic crack growth in nonlinear elasticity.", *Arch. Ration. Mech. An.* , Vol. 176, pp. 165–225.

Delville, R ans Malard, B., Pilch, J., Šittner, P. and Schryvers, D. (2010), "Microstructure changes during non-conventional heat treatment of thin Ni–Ti wires by pulsed electric current studied by transmission electron microscopy", *Acta Mater.* , Vol. 58, pp. 4503–4515.

Entel, P., Meyer, R. and Kadau, K. (2000), "Molecular dynamics simulations of martensitic transitions", *Philos. Mag. B* , Vol. 80, pp. 183–194.

Evangelista, V., Marfia, S. and Sacco, E. (2009), "Phenomenological 3D and 1D consistent models for shape-memory alloy materials", *Comput. Mech.* , Vol. 44, pp. 405–421.

Francfort, G. and Mielke, A. (2006), "Existence results for a class of rate-independent material models with nonconvex elastic energies", *J. Reine Angew. Math.* , Vol. 595, pp. 55–91.

Frost, M. (2007), Elastic properties of blood veins with a scaffold, Master's thesis, Charles University in Prague, Faculty of Mathematics and Physics.

Frost, M. and Rudajevová, A. (2009), "Strain release from pre-deformed $Ni_{53.6}Mn_{27.1}Ga_{19.3}$ shape memory alloy during thermal cycling", *Int. J. Mater. Research* , Vol. 100, pp. 898–900.

Frost, M. and Sedlák, P. (2009), Modeling of two-dimensional thermomechanical loading of NiTi wires, *in* 'ESOMAT 2009 - The 8th European Symposium on Martensitic Transformations'.

Frost, M., Sedlák, P., Sippola, M. and Šittner, P. (2010), "Thermomechanical model for NiTi shape memory wires", *Smart Mater. Struct.* , Vol. 19, p. 094010.

Funakubo, H. and Kennedy, J. B. (1987), *Shape Memory Alloys*, Gordon and Breach.

Gall, K., Sehitoglu, H., Chumlyakov, Y. I. and Kireeva, I. V. (1999), "Tension-compression asymmetry of the stress-strain response in aged single crystal and polycrystalline NiTi", *Acta Mater.* , Vol. 43, pp. 1203–17.

Gao, X., Qiao, R. and Brinson, L. C. (2007), "Phase diagram kinetics for shape memory alloys: a robust finite element implementation", *Smart Mater. Struct.* , Vol. 16, pp. 2102–2115.

Grabe, C. and Bruhns, O. T. (2008), "On the viscous and strain rate dependent behavior of polycrystalline NiTi", *Int. J. Solids Struct.* , Vol. 45, pp. 1876–1895.

Grolleau, V., Louche, H., Delobelle, V., Penin, A., Rio, G., Liu, Y. and Favier, D. (2011), "Assessment of tension–compression asymmetry of NiTi using circular bulge testing of thin plates", *Scr. Mater.* , Vol. 65, pp. 347–350.

Hackl, K. and Fischer, F. D. (2008), "On the relation between the principle of maximum dissipation and inelastic evolution given by dissipation potentials", *Proc. R. Soc. A* , Vol. 464, pp. 117–132.

Halphen, B. and Nguyen, Q. S. (1975), "Sur les matériaux standard généralisés", *J. Mecanique* , Vol. 14, pp. 39–63.

Hartl, D. J., Chatzigeorgiou, G. and Lagoudas, D. C. (2010), "Three-dimensional modeling and numerical analysis of rate-dependent irrecoverable deformation in shape memory alloys", *Int. J. Plast.* , Vol. 26, pp. 1485–1507.

Hartl, D. J. and Lagoudas, D. C. (2009), "Constitutive modeling and structural analysis considering simultaneous phase transformation and plastic yield in shape memory alloys", *Smart Mater. Struct.* , Vol. 18, p. 104017.

Hartl, D. J., Lagoudas, D. C., Calkins, F. T. and Mabe, J. H. (2009), "Use of a Ni60Ti shape memory alloy for active jet engine chevron application: I. Thermomechanical characterization", *Smart Mater. Struct.* , Vol. 19, p. 015020.

Hartl, D. J. and Mooney, J. T. (2010), "Use of a Ni60Ti shape memory alloy for active jet engine chevron application: II. Experimentally validated numerical analysis", *Smart Mater. Struct.* , Vol. 19, p. 015021. and Lagoudas, D C and Calkins, F T and Mabe, J H.

Helm, D. and Haupt, P. (2003), "Shape memory behaviour: modelling within continuum thermomechanics", *Int. J. Solids Struct.* , Vol. 40, pp. 827–849.

Houlsby, G. T. and Puzrin, A. M. (1999), An approach to plasticity based on generalised thermodynamics, *in* '3rd European Conference on Constitutive Modeling of Granular Materials', pp. 319–332.

Houlsby, G. T. and Puzrin, A. M. (2000), "A thermomechanical framework for constitutive models for rate-independent dissipative materials", *Int. J. Plast.* , Vol. 16, pp. 1017–47.

Houlsby, G. T. and Puzrin, A. M. (2001), "A thermomechanical framework for rate-independent dissipative materials with internal functions", *Int. J. Plast.* , Vol. 17, pp. 1147–1165.

Jacobus, K., Sehitoglu, H. and Balzer, M. (1996), "Effect of stress state on the stress-induced martensitic transformation in polycrystalline Ni-Ti alloy", *Metall* , Vol. 27, pp. 3066–3073.

Juhasz, L., Schnack, E., Hesebeck, O. and Andra, H. (2002), "Macroscopic modeling of shape memory alloys under non-proportional thermo-mechanical loadings", *J. Intell. Mater. Systems Struct.* , Vol. 13, pp. 825–836.

Khandelwal, A. and Buravalla, V. (2009), "Models for shape memory alloy behavior: An overview of modeling approaches", *Int. J. Struct. Changes* , Vol. 1, pp. 111–148.

Lagoudas, D. C. and Bo, Z. (1999), "Thermomechanical modeling of polycrystalline smas under cyclic loading, Part II: material characterization and experimental results for a stable transformation cycle", *Int. J. Eng. Sci.* , Vol. 37, pp. 1141–1173.

Lagoudas, D. C., Entchev, P. B., Popov, P., Patoor, E., Brinson, L. C. and Gao, X. (2006), "Shape memory alloys, Part II: Modeling of polycrystals", *Mech. Mater.* , Vol. 38, pp. 430–62.

Lagoudas, D. C., Hartl, D. J., Chemisky, Y., Machado, L. G. and Popov, P. (2012), "Constitutive model for the numerical analysis of phase transformation in polycrystalline shape memory alloys", *Int. J. Plast.* , Vol. 32–33, pp. 155–183.

Langelaar, M. and van Keulen, F. (2004), "A simple R-phase transformation model for engineering purposes", *Materials Science and Engineering A* , Vol. 378, pp. 507–512.

Leclercq, S. and Lexcellent, C. (1996), "A general macroscopic description of the thermomechanical behavior of shape memory alloys", *J. Mech. Phys. Solids* , Vol. 44, pp. 953–980.

Lexcellent, C., Boubakar, M. L., Bouvet, C. and Calloch, S. (2006), "About modelling the shape memory alloy behaviour based on the phase transformation surface identification under proportional loading and anisothermal conditions", *Int. J. Solids Struct.* , Vol. 48, pp. 613—-26.

Lexcellent, C., Tobushi, H., Ziolkowski, A. and Tanaka, K. (1994), "Thermodynamical model of reversible R-phase transformation in TiNi shape memory alloy", *Int. J. Pres. Ves. & Piping* , Vol. 58, pp. 51–57.

Liang, C. and Rogers, C. A. (1990), "One-dimensional thermomechanical constitutive relations for shape memory materials", *J. Intel. Mat. Syst. Str.* , Vol. 1, pp. 207–234.

Liu, Y. and Favier, D. (2000), "Stabilisation of martensite due to shear deformation via variant reorientation in polycrystalline NiTi", *Acta Mater.* , Vol. 48, pp. 3489–3499.

Liu, Y., Mahmuda, A., Kursawea, F. and Nam, T. H. (2008), "Effect of pseudoelastic cycling on the Clausius–Clapeyron relation for stress-induced martensitic transformation in NiTi", *J. Alloys Compd.* , Vol. 449, pp. 82–87.

Liu, Y. and Tan, G. S. (2000), "Effect of deformation by stress-induced martensitic transformation on the transformation behaviour of NiTi", *Intermetallics* , Vol. 8, pp. 67–75.

Liu, Y., Xie, Z. and Van Humbeeck, J. (1998), "Asymmetry of stress–strain curves under tension and compression for niti shape memory alloys", *Acta Mater.* , Vol. 46, pp. 4325–4338.

Liu, Y., Xie, Z., Van Humbeeck, J. and Delaey, L. (1999), "Deformation of shape memory alloys associated with twinned domain re-configurations", *Mat. Sci. Eng. A* , Vol. 273–275, pp. 679–684.

Machado, L. G. and Savi, M. A. (2003), "Medical applications of shape memory alloys", *Braz. J. Med. Biol. Res.* , Vol. 36, pp. 683–691.

Mao, S. C., Luo, J. F., Z, Z., Wub, M. H., Liu, Y. and Han, X. D. (2010), "EBSD studies of the stress-induced B2–B190 martensitic transformation in NiTi tubes under uniaxial tension and compression", *Acta Mater.* , Vol. 58, pp. 3357–3366.

Mielke, A. (2003), "Energetic formulation of multiplicative elasto-plasticity using dissipation distances.", *Continuum Mech. Therm.* , Vol. 15, pp. 351–382.

Mielke, A. (2006), A mathematical framework for standard generalized materials in the rate-independent case, *in* B. W. R. Helmig, A. Mielke, ed., 'Multifield problems in Fluid and Solid Mechanics', lecture notes in applied and computational mechanics edn, Vol. 28, Springer, Berlin.

Mielke, A., Paoli, L. and Petrov, A. (2009), "On existence and approximation for a 3D model of thermally induced phase transformations in shape-memory alloys.", *SIAM J. Math. Anal.* , Vol. 41, pp. 1388–1414.

Mielke, A. and Rossi, R. (2007), "Existence and uniqueness results for a class of rate-independent hysteresis problems.", *Math. Mod. Meth. Appl. S.* , Vol. 17, pp. 81–123.

Mielke, A. and Theil, F. (2004), "On rate-independent hysteresis models.", *NODEA-Nonlinear. Diff.* , Vol. 11, pp. 151–189.

Mielke, A., Theil, F. and Levitas, V. I. (2002), "A variational formulation of rate-independent phase transformations using an extremum principle.", *Arch. Ration. Mech. An.* , Vol. 162, pp. 137–177.

Morin, C., Moumni, Z. and Zaki, W. (2011), "A constitutive model for shape memory alloys accounting for thermomechanical coupling", *Int. J. Plast.* , Vol. 27, pp. 748–767.

Moumni, Z., Zaki, W. and Ngu (2008), "Theoretical and numerical modeling of solid–solid phase change: Application to the description of the thermomechanical behavior of shape memory alloys", *Int. J. Plast.* , Vol. 24, pp. 614–645.

Nelder, J. A. and Mead, R. (1965), "A simplex method for function minimization", *Comput. J.* , Vol. 7, pp. 308–313.

Nemat-Nasser, S., Choi, J. Y., Guo, W. G. and Isaacs, J. B. (2005), "High strain-rate, small strain response of a NiTi shape-memory alloy", *J. Eng. Mater. Technol.* , Vol. 127, pp. 83–89.

Nguyen, Q. S. (2000), *Stability and Nonlinear Solid Mechanics*, John Wiley.

Novák, V., Šittner, P., Dayananda, G. N., Braz-Fernandes, F. M. and Mahesh, K. K. (2008), "Electric resistance variation of NiTi shape memory alloy wires in thermomechanical tests: Experiments and simulation", *Mar. Sci. Eng. A* , Vol. 481–482, pp. 127–133.

Olbricht, J., Yawny, A., Pelegrina, J. L., Dlouhý, A. and Eggeler, G. (2011), "On the stress-induced formation of R-phase in ultra-fine-grained Ni-rich NiTi shape memory alloys", *Metall. Mater. Trans. A* , Vol. 42A, pp. 2556–2574.

Orgéas, L. and Favier, D. (1999), "Stress-induced martensitic transformation of a NiTi alloy in isothermal shear, tension and compression", *Acta Mater.* , Vol. 46, pp. 5579–5591.

Ortín, J. and Delaey, L. (2002), "Hysteresis in shape-memory alloys", *Int. J. Nonlinear Mech.* , Vol. 37, pp. 1275–1281.

Otsuka, K. and Ren, X. (2005), "Physical metallurgy of Ti-Ni-based shape memory alloys", *Prog. Mater. Sci.* , Vol. 50, pp. 511–678.

Otsuka, K. and Wayman, C. M. (1998), *Shape Memory Materials*, Cambridge University Press.

Panico, M. and Brinson, L. C. (2007), "A three-dimensional phenomenological model for martensite reorientation in shape memory alloys", *J. Mech. Phys. Solids* , Vol. 55, pp. 2491–2511.

Patoor, E. (2009), 'An overview of different approaches used to model smas and sma structures', keynote lecture at ESOMAT Prague.

Patoor, E., Lagoudas, D. C., Entchev, P. B., Brinson, L. C. and Gao, X. (2006), "Shape memory alloys, Part I: General properties and modeling of single crystals", *Mech. Mater.* , Vol. 38, pp. 391–429.

Petryk, H. and Stupkiewicz, S. (2010), "Interfacial energy and dissipation in martensitic phase transformations. Part I: Theory", *Journal of the Mechanics and Physics of Solids* , Vol. 58, pp. 390–408.

Peultier, B., Ben Zineb, T. and Patoor, E. (2006), "Macroscopic constitutive law for SMA: Application to structure analysis by FEM", *Mech. Mater.* , Vol. 38, pp. 510–524.

Peultier, B., Ben Zineb, T. and Patoor, E. (2008), "A simplified micromechanical constitutive law adapted to the design of shape memory applications by finite element methods", *Mat. Sci. Eng. A-Struct.* , Vol. 481–482, pp. 384–388.

Piao, M., Otsuka, K., Miyazaki, S. and Horikawa, H. (1993), "Mechanism of the A_s temperature increase by pre-deformation in thermoelastic alloys", *Materials Transactions* , Vol. 34, pp. 919–929.

Pilch, J., Heller, L. and Šittner, P. (2009), 'Roundrobin web page'.
URL: *http://department.fzu.cz/ofm/roundrobin/*

Popov, P. and Lagoudas, D. C. (2007), "A 3-D constitutive model for shape memory alloys incorporating pseudoelasticity and detwinning of self-accommodated martensite", *Int. J. Plast.* , Vol. 23, pp. 1679—-720.

Qidwai, M. A. and Lagoudas, D. C. (2000*a*), "Numerical implementation of a shape memory alloy thermomechanical constitutive model using return mapping algorithms", *Int. J. Numer. Meth. Engng.* , Vol. 47, pp. 1123–1168.

Qidwai, M. A. and Lagoudas, D. C. (2000*b*), "On thermomechanics and transformation surfaces of polycrystalline NiTi shape memory alloy material", *Int. J. Plast.* , Vol. 16, pp. 1309–1343.

Qiu, S., Clausen, B andPadula, S. A., Noebe, R. D. and Vaidyanathan, R. (2011), "On elastic moduli and elastic anisotropy in polycrystalline martensitic NiTi", *Acta Mater.* , Vol. 59, pp. 5055–5066.

Rajagopal, K. R. and Srinivasa, A. R. (1999), "On the thermomechanics of shape memory wires", *Z. angew. Math. Phys.* , Vol. 50, pp. 459–496.

Raniecki, B. and Lexcellent, C. (1998), "Thermodynamics of isotropic pseudoelasticity in shape memory alloys", *Eur. J. Much., A/Solids* , Vol. 2, pp. 185–205.

Ren, X. and Otsuka, K. (1998), "The role of softening in elastic constant c_{44} in martensitic tran", *Scr* , Vol. 38, pp. 1669–1675.

Roubíček, T. (2004), *Nonlinear Homogenization and its Application to Composites, Polycrystals and Smart Materials*, NATO Sci.Ser.**II/170**, Kluwer, Dordrecht, chapter Models of microstructure evolution in shape memory materials, pp. 269–304.

Sadjadpour, A. and Bhattacharya, K. (2007*a*), "A micromechanics-inspired constitutive model for shape-memory alloys", *Smart Mater. Struct.* , Vol. 16, pp. 1751–1765.

Sadjadpour, A. and Bhattacharya, K. (2007*b*), "A micromechanics-inspired constitutive model for shape-memory alloys: the one-dimensional case", *Smart Mater. Struct.* , Vol. 16, pp. S51–S62.

Saint-Sulpice, L., Arbab Chirani, S. and Calloch, S. (2009), "A 3D super-elastic model for shape memory alloys taking into account progressive strain under cyclic loadings", *Mech. Mater.* , Vol. 41, pp. 12—26.

Saleeb, A. F., Padula, S. A. and Kumar, A. (2011), "A multi-axial, multimechanism based constitutive model for the comprehensive representation of the evolutionary response of SMAs under general thermomechanical loading conditions", *Int. J. Plast.* , Vol. ěý, pp. 655–687.

Sedlák, P. and Frost, M. (2009), Two-dimensional thermomechanical model for combined loading of NiTi wire structures, *in* 'Proceedings of the ASME 2009 Conference on Smart Materials, Adaptive Structures and Intelligent Systems'.

Sedlák, P., Frost, M., Ben Zineb, T. and Šittner, P. (2010), Thermomechanical models for NiTi shape memory alloys and their applications, *in* 'Proceedings of the ASME 2010 Conference on Smart Materials, Adaptive Structures and Intelligent Systems'.

Sedlák, P., Frost, M., Benešová, B., Šittner, P. and Ben Zineb, T. (2012), "Thermomechanical model for NiTi-based shape memory alloys including R-phase and material anisotropy under multi-axial loadings", *Int. J. Plast.* , Vol. 39, pp. 132–151.

Sengupta, A. and Papadopoulos, P. (2009), "Constitutive modeling and finite element approximation of B2-R-B19' phase transformations in Nitinol polycrystals", *Comput. Methods Appl. Mech. Engrg.* , Vol. 198, pp. 3214–3227.

Shabalovskaya, S. (1995), "Biological aspects of TiNi alloys surfaces", *Journal de Physique IV* , Vol. 5, pp. 1199–1204.

Shaw, J. A. and Kyriakides, S. (1995), "Thermomechanical aspects of NiTi", *J. Mech. Phys. Solids* , Vol. 43, pp. 1243–1281.

Shu, Y. C. and Bhattacharya, K. (1998), "The influence of texture on the shape-memory effect in polycrystals", *Acta Mater.* , Vol. 46, pp. 5457–5473.

Šittner, P., Heller, L., Pilch, J., Sedlák, P., Frost, M., Chemisky, Y., Duval, A., Piotrowski, B., Ben Zineb, T., Patoor, E., Auricchio, F., Morganti, S., Reali, A., Rio, G., Favier, D., Liu, Y., Gibeau, E., Lexcellent, C., Boubakar, L., Hartl, D. J., Oehler, S., Lagoudas, D. C. and Van Humbeeck, J. (2009), Roundrobin SMA modeling, *in* P. Šittner, L. Heller and V. Paidar, eds, 'ESOMAT 2009 - The 8th European Symposium on Martensitic Transformations', EDP Sciences, p. 08001.

Šittner, P., Landa, M., Lukáš, P. and Novák, V. (2006), "R-phase transformation phenomena in thermomechanically loaded NiTi polycrystals", *Mech. Mater.* , Vol. 38, pp. 475–492.

Šittner, P. and Novák, V. (2000), "Anisotropy of martensitic transformations in modeling of shape memory alloy polycrystals", *Int. J. Plast.* , Vol. 16, pp. 1243–1268.

Šittner, P., Vokoun, D., Dayananda, G. N. and Stalmans, R. (2000), "Recovery stress generation in shape memory Ti50Ni45Cu5 thin wires", *Mat. Sci. Eng. A* , Vol. 286, pp. 298–311.

Souza, A. C., Mamiya, E. N. and Zouain, N. (1998), "Three-dimensional model for solids undergoing stress-induced phase transformations", *Eur. J. Mech. A* , Vol. 17, pp. 789–806.

Straka, L., Heczko, O., Seiner, H., Lanska, N., Drahokoupil, J., Soroka, A., Fähler, S., Hänninen, H. and Sozinov, A. (2011), "Highly mobile twinned interface in 10 M modulated Ni-Mn-Ga martensite: Analysis beyond the tetragonal approximation of lattice", *Acta Mater.* , Vol. 59, pp. 7450–7463.

Stupkiewicz, S. and Petryk, H. (2010), "Grain-size effect in micromechanical modelling of hysteresis in shape memory alloys.", *ZAMM, Z. Angew. Math. Me.* , Vol. 90, pp. 783–795.

Sun, Q. P. and He, Y. J. (2008), "A multiscale continuum model of the grain-size dependence of the stress hysteresis in shape memory alloy polycrystals", *Int. J. Solids Struct.* , Vol. 45, pp. 3868–3896.

Sun, Q. P. and Li, Z. Q. (2002), "Phase transformation in superelastic NiTi polycrystalline micro-tubes under tension and torsion – from localization to homogeneous deformation", *Int. J. Solids Struct.* , Vol. 39, pp. 3797–3809.

Svoboda, J., Turek, I. and Fischer, F. D. (2005), "Application of the thermodynamic extremal principle to modeling of thermodynamic processes in material sciences", *Philos. Mag.* , Vol. 85, pp. 3699–3707.

Taillard, K., Arbab Chirani, S., S, C. and Lexcellent, C. (2008), "Equivalent transformation strain and its relation with martensite volume fraction for isotropic and anisotropic shape memory alloys", *Mech. Mater.* , Vol. 40, pp. 151–170.

Thiebaud, F., Lexcellent, C., Collet, M. and Foltete, E. (2007), "Implementation of a model taking into account the asymmetry between tension and compression, the temperature effects in a finite element code for shape memory alloys structures calculations", *Comp. Mater. Sci.* , Vol. 41, pp. 208–221.

Uchil, J., Mohanchandra, K. P., Ganesh Kumara, K., Mahesh, K. K. and Murali, T. P. (1999), "Thermal expansion in various phases of Nitinol using TMA", *Physica B* , Vol. 270, pp. 289–297.

Vokoun, D., Majtás, D., Frost, M., Sedlák, P. and Šittner, P. (2009), "Shape memory hooks employed in fasteners", *J. Mater. Eng. Perform.* , Vol. 18, pp. 706–710.

Vokoun, D., Sedlák, P., Frost, M., Pilch, J., Majtás, D. and Šittner, P. (2011), "Velcro-like fasteners based on NiTi micro-hook arrays", *Smart Mater. Struct.* , Vol. 20, p. 085027.

Wagner, M. F.-X. and Windl, W. (2008), "Lattice stability, elastic constants and macroscopic moduli of NiTi martensites from first principles", *Acta Mater.* , Vol. 56, pp. 6232–6245.

Williams, E. and Elahinia, M. H. (2008), "An automotive SMA mirror actuator: Modeling, design and experimental evaluation", *J. Intell. Mater. Systems Struct.* , Vol. 19, pp. 1425–1434.

Wilson, J. and Wesolowsky, M. (2005), "Shape memory alloys for seismic response modification: A state-of-the-art review", *Earthquake Spectra* , Vol. 21, pp. 569–601.

Zaki, W. (2010), "An approach to modeling tensile–compressive asymmetry for martensitic shape memory alloys", *Smart* , Vol. 19, p. 025009.

Zaki, W. and Moumni, Z. (2007*a*), "A 3D model of the cyclic thermomechanical behavior of shape memory alloys", *J. Mech. Phys. Solids* , Vol. 55, pp. 2427–2454.

Zaki, W. and Moumni, Z. (2007*b*), "A three-dimensional model of the thermomechanical behavior of shape memory alloys", *J. Mech. Phys. Solids* , Vol. 55, pp. 2455–2490.

Zaki, W., Zamfir, S. and Moumni, Z. (2010), "An extension of the ZM model for shape memory alloys accounting for plastic deformation", *Mech. Mater.* , Vol. 42, pp. 266–274.

Zanotti, C., Giuliani, P., Bassani, P., Zhang, Z. and Chrysanthou, A. (2010), "Comparison between the thermal properties of fully dense and porous NiTi SMAs", *Intermetallics* , Vol. 18, pp. 14–21.

Zhou, B. and Yoon, S. H. (2006), "A new phase transformation constitutive model of shape memory alloys", *Smart Mater. Struct.* , Vol. 15, pp. 1967–1973.

Ziegler, H. (1983), *An Introduction to Thermodynamics*, North-Holland Series in Applied Mathematics and Mechanics, 1st edition edn, North-Holland, Amsterdam.